ADDRESSING THE DOWNSTREAM PROCESSING CHALLENGES WITHIN MANUFACTURING OF ONCOLYTIC RHABDOVIRUSES

ADDRESSING THE DOWNSTREAM PROCESSING CHALLENGES WITHIN MANUFACTURING OF ONCOLYTIC RHABDOVIRUSES

By SHABNAM SHOAEBARGH, M.A.Sc.

A Thesis Submitted to the School of Graduate Studies in Partial Fulfillment of the Requirements for the Degree Doctor of Philosophy

McMaster University Ph.D. of Engineering (2019) Hamilton, Ontario (Chemical Engineering)

DOCTOR OF PHILOSOPHY (2019) McMaster University

(Chemical Engineering) Hamilton, Ontario

TITLE: **Addressing the Downstream Processing Challenges Within Manufacturing of Oncolytic Rhabdoviruses**

AUTHOR: SHABNAM SHOAEBARGH, M.A.Sc. (University of Tabriz),

B.ASc. (University of Tabriz)

SUPERVISOR: Dr. David R. Latulippe

NUMBER OF PAGES: xxix, 236

Lay Abstract

There is considerable interest in the development of oncolytic viruses for cancer immunotherapy. Indeed, at the time of this thesis' writing, a Canadian team of researchers is conducting the world's first clinical trial using a combination of two viruses to kill cancer cells and stimulate an immune response. The process of manufacturing oncolytic viruses is generally divided into two major steps: upstream processing and downstream processing. While upstream processing focuses on virus propagation, downstream processing aims at removing process-related and product-related impurities. However, research into downstream process design and optimization has largely been neglected in favour of a focus on upstream processing, aimed at increasing bioreactor yields and achieving high viral titers. Consequently, downstream processing has become the main bottleneck in virus manufacturing processes, accounting for as much as 70% production costs. This thesis aims to identify and develop a fundamental understanding of the main challenges associated with the downstream processing of oncolytic viruses and to investigate methods for addressing them. Specifically, the present work focuses on the purification and final sterile filtration steps in the manufacturing of oncolytic Rhabdoviral vectors.

Abstract

Oncolytic viruses (OVs) are a class of cancer therapy that is currently undergoing clinical trials on its way to full regulatory approval. At present, the downstream processing of OVs relies on a combination of chromatography and membrane-based processes to remove process-related (e.g. host-cell proteins and nucleic acids) and product-related impurities (e.g. aggregated virus particles). This thesis explores various methods that can potentially be used to address the challenges associated with downstream processing during the production of OVs. To this end, the Rhabdoviral vector, which is currently undergoing clinical trials (phase I/II) for use in treating advanced or metastatic solid tumors, was selected as a promising oncolytic virus.

One potential improvement in the downstream process that was investigated was the use of monolithic column chromatography for Rhabdovirus purification. Two monolithic anion-exchange columns (2 and 6 µm pore size) and one hydrophobic interaction column (6 µm pore size) were used to examine how column pore size affects virus recovery and contaminant removal. This investigation ultimately inspired the development of a purification process based on monolithic hydrophobic interaction column chromatography. Furthermore, this work is also the first to investigate how additives, namely glycerol, impact the hydrophobic interaction chromatography of virus particles. The developed process could be readily implemented for the scaled-up purification of the Rhabdoviral vector.

Another challenge associated with the downstream processing of OVs is membrane fouling, which is characterized by a dramatic rise in transmembrane pressure (TMP)

and low virus recovery. Indeed, membrane fouling poses a significant challenge, as some recent studies have reported that it can result in viral vector titer losses of over 80%. One critical use of membranes in downstream processing is for the sterile filtration of OVs, which is a required final step that is conducted right before vialing and involves passing the virus particles through a validated sterile filter. One of the main objectives of this thesis was to develop a fundamental understanding of the sterile filtration process and to optimize it in order to achieve higher throughputs and lower losses, which are both essential to the large-scale production of OVs. To this end, a dead-end sterile filtration setup was designed, and various commercially available filters were evaluated to examine how membrane morphology affects fouling and product recovery. The results of these tests showed that double-layered composite filters enabled higher virus recovery and filtration capacity compared to single-layered sterile filters.

Another cause of membrane fouling is the aggregation of virus particles, which is mediated by various interactions in the solution. To study this, the above-described setup was re-designed to create an effective procedure that utilizes minimal volumes of virus solution, while also enabling the rapid assessment of microscale filtration performance and a comprehensive understanding of virus-virus and virus-membrane interactions. This setup was used to study how different additives, including various proteins (bovine serum albumin and α-lactalbumin) and polymers (polyethylene glycol and polyvinylpyrrolidone), affect the microfiltration of the Rhabdoviral vector and, consequently, the TMP profile. Furthermore, the correlation between the membrane fouling rate (via TMP profiles) and virus recovery was also investigated. This

investigation revealed that proteins significantly increase virus transmission and that polymers are incapable of mimicking the effects of the proteins.

To explain this phenomenon, a theory based on the biophysical structure of proteins, mainly heterogenicity in charge distribution, was proposed. Moreover, membrane surface modification tests were conducted using bovine serum albumin, with the results indicating that this approach has considerable potential for enhancing virus transmission. Due to the similarities between the test setup and actual downstream processing unit operations, the results from this part of the thesis could be easily and accurately applied to process optimization.

Acknowledgments

I would like to express my sincerest gratitude to my supervisor, Dr. David Latulippe, for all his encouragement and continuous support during my Ph.D. studies at McMaster University, as well as for the opportunity to work on this project and to attend national/international conferences. Without his support, mentorship, and inspiration, it would have been impossible to complete this research. I would also like to acknowledge my supervisory committee members, Drs. Carlos Filipe and Leyla Soleymani, for their insightful comments and valuable suggestions, which have been indispensable in helping me to strengthen this research project.

I would like to express my deepest appreciation to Drs. Brian Lichty and Maria Fe Medina for giving me access to the research facility at McMaster Immunology Research Center, where I had the opportunity to work on this thesis and other projects. I am extremely grateful for sharing their priceless experience and accepting me as a member of the lab. Special thanks to Mses. Natasha Kazhdan and Uma Sankar from this research facility for their kind support during these years.

I would like to thank Drs. John Bell and Joris van der Heijden, and Mr. Adam Smith from Biotherapeutic Manufacturing Center at Ottawa Hospital Research Institute, and Dr. Julia Pomoransky from Turnstone Biologics for providing invaluable insight and guidance on the virus manufacturing process.

From the Department of Chemical Engineering, I gratefully acknowledge Drs. Raja Ghosh and Todd Hoare for their helpful advice and guidance throughout this thesis. Many thanks to Mr. Paul Gatt for fabrication of customized parts. Special thanks to Mr.

Michael Clarke, Mses. Kristina Trollip, Michelle Whalen, Linda Ellis, and Joy-Anne Coomber for their technical and administrative assistance.

I am also grateful to Dr. Ales Strancar from 'BIA Separation' for providing invaluable insight on monolithic columns. Thanks to the kind staff of 'Electron Microscopy Facility' at McMaster Children's Hospital and 'Centre for Microbial Chemical Biology' at McMaster University. Special thanks to Ms. Marcia Reid for training me on SEM and TEM apparatus. Many thanks to Dr. Karen Mossman for providing access for qViroX instrument, and Drs. Marta Princz, Linda Luckham, and Danielle Covelli for paving my way to work with BSL II agents at Biointerfaces Institute.

I would also like to acknowledge the "Alliance for Biotherapeutics Manufacturing Innovation," which is supported by the Ontario Research Fund, for providing funding for this research, NSERC Discovery for their provision of partial funding, and BioCanRX for providing HQP Travel Awards, which were used to attend "Summit for Cancer Immunotherapy" conferences.

Thanks to my friends, labmates, and summer students from the Department of Chemical Engineering and McMaster Immunology Research Center for all the fruitful discussions during all those non-ending days of work, and for all the fun we had within the past four years.

Last but not least, I would like to thank my family for their endless love, unceasing encouragement, attention, and support throughout this venture: to my Dad, who has always believed in me and encouraged me to be brave, dream big, and to persistently pursue those dreams; to my Mom, who is the kindest and most thoughtful mother ever

and an angel in my life; and to my sister, who has always been my best friend. Thank you all for always being there in both happy and tough times.

Table of Contents

List of Figures

Chapter I

Chapter II

Chapter III

Chapter IV

Chapter V

List of Tables

Chapter I

Chapter II

Chapter III

Chapter IV

Chapter V

List of Acronyms, Abbreviations and Symbols

AAV	Adeno-associated Virus
AC	Affinity Chromatography
Ad	Adenovirus
AS	Ammonium Sulfate
A(z)	Cross-sectional area perpendicular to the pore axis (z)
α-MEM	Alpha-Minimum Essential Medium
α-LA	Alpha-Lactalbumin
BCA	Bicinchoninic Acid
B. diminuta	*Brevundimonas diminuta*
BSA	Bovine Serum Albumin
CCD	Charged Coupled Device
CIM	Convective Interaction Media
CPE	Cytopathic Effect
CV	Column Volume
DEAE	Diethylaminoethanol
D_h	Hydrodynamic Diameter

D_L	Largest membrane pore size
D_m	Diameter of membrane pore size
d_p	Diameter of particle
DLVO	Derjaguin, Landau, Verwey, and Overbeek
DLS	Dynamic Light Scattering
D_s	Smallest membrane pore size
DSP	Downstream Processing
ΔR	Blockade
ELISA	Enzyme-linked immunosorbent Assay
EPR	Enhanced Permeability and Retention
FC	Flow Cytometry
FDA	US Food and Drug Administration
GF	Glass Fiber
GFP	Green Fluorescent Protein
GMP	Good Manufacturing Practice
HIC	Hydrophobic Interaction Chromatography
HSV	Herpes Simplex Virus
IEC	Ion-Exchange Chromatography
IEP	Isoelectric Point

JUNV	Junín virus
k	Boltzmann's constant
LLOQ	Lower Limit of Quantification
MALS	Multi-angle Light Scattering
MOI	Multiplicity of Infection
MSC	Mesenchymal Stem Cell
MWCO	Molecular Weight Cut Off
NTA	Nanoparticle Tracking Analysis
η	Viscosity
OV	Oncolytic virus
PCR	Polymerase Chain Reaction
PD-1	Programmed Death-1
PEG	Polyethylene glycol
PES	Polyethersulfone
PFU	Plaque Forming Unit
PVDF	Polyvinylidene fluoride
PVP	Polyvinylpyrrolidone
QA	Quaternary Amine
RBC	Red Blood Cell

REACH	Registration Evaluation Authorisation and Restriction of Chemicals
RT	Room Temperature
ρ	Resistivity
SEC	Size Exclusion Chromatography
SEM	Scanning Electron Microscopy
SFCA	Surfactant Free Cellulose Acetate
SO_3	Sulfuric Anhydride
STR	Stirred Tank Reactors
T	Temperature
$TCID_{50}$	50% Tissue Culture Infectious Dose
TEM	Transmission Electron Microscopy
TMP	Transmembrane Pressure
TMV	Tobacco Mosaic Virus
TRPS	Tunable Resistive Pulse Sensing
VLP	Virus-Like Particle
VP	Virus Particle
VST	Viral Sensitizer Technology
VSV	Vesicular Stomatitis Virus
VV	Vaccinia Virus

Declaration of Academic Achievement

This Ph.D. thesis is organized in a sandwich style based on the following articles:

1. S. Shoaebargh, V. Bardal, M. Fe Medina, B. Lichty, D. R. Latulippe, Developing Monolithic Chromatography Purification Method for Rhabdoviral vector. In preparation for submission in Journal of Chromatography A.
   This article was made into Chapter III.

2. S. Shoaebargh, I. Gough, M. Fe Medina, A. Smith, J. Heijden, B. Lichty, J. Bell, D. R. Latulippe, Sterile filtration of oncolytic viruses: An analysis of effects of membrane morphology on fouling and product recovery, Journal of Membrane Science, 548 (2018) 239–246.
   This article was made into Chapter IV.

3. Shabnam Shoaebargh, Evan Wright, Matthew Csordas, Maria Fe Medina, Brian Lichty, David R. Latulippe, Probing the effect of stabilizers on the aggregation of oncolytic viruses via a microscale filtration process. In preparation for submission in Biotechnology and Bioengineering.
   This article was made into Chapter V.

The majority of the experiments for the listed papers have been planned, performed, analyzed, and written by Shabnam Shoaebargh under supervision of Dr. David Latulippe. The following graduate and undergraduate students have contributed to different parts of this thesis under my co-supervision as explained in below:

- Vitaliya Bardal assisted me with performing chromatography runs described in Chapter III – Summer 2017.
- Ian Gough also helped me with membrane permeability measurements described in Chapter IV – Summer 2016.
- Evan Wright carried out some of the filtration experiments described in Chapter V. Evan also contributed to editing the paper described in this chapter.

- Matthew Csordas also assisted Evan and me in conducting filtration experiments described in Chapter V – Summer 2018.

Drs. Maria Fe Medina, Brian Lichty, John Bell, Joris Van der Heijden and Mr. Adam Smith provided helpful guidance and suggestions and contributed to editing the corresponded papers described above.

Chapter I – Introduction

1.1. Virotherapy in Cancer Treatment

An oncolytic virus (OVs) is a type of virus that preferentially infects cancerous cells without harming normal cells. There are two types of OV: naturally selective OVs, which are relatively small in size, have fast replication cycles, and are non-pathogenic for humans;[1,2] and engineered OVs, which are relatively large in size and cause known diseases in humans.[1,2] As shown in Fig. 1.1., OVs have two main anti-tumor mechanisms. The first mechanism allows the OV to kill cancerous cells directly by taking over their cellular machinery and exploiting their cellular resources for virus replication, which is followed by the cell's destruction via oncolysis.[3] The second mechanism allows the OV to kill cancerous cells indirectly by amplifying the body's antitumor immune responses via the expression of transgene-coded proteins, which destroys tumor's vasculature and may even have *in-situ* vaccination effects in the tumor microenvironment due to the cross-presentation of tumor-associated antigens.[1–4] Although the actual mechanisms and pathways undertaken by OVs have yet to be fully understood, it is believed that OV efficiency is mainly dependent on the efficiency of the targeting cell's receptor and the virus-replication mechanism.[5]

Oncolytic virotherapy has become a promising approach cancer treatment thanks in large part to several features that are intrinsic to OVs such as:

- Selective method of cell destruction

- Localized effects due to *in-situ* virus replication and *in-situ* virus dose increase in tumor microenvironment
- Low probability of resistance
- Fine tuning by adding features to the OVs such as specific immune sensitivity [2]

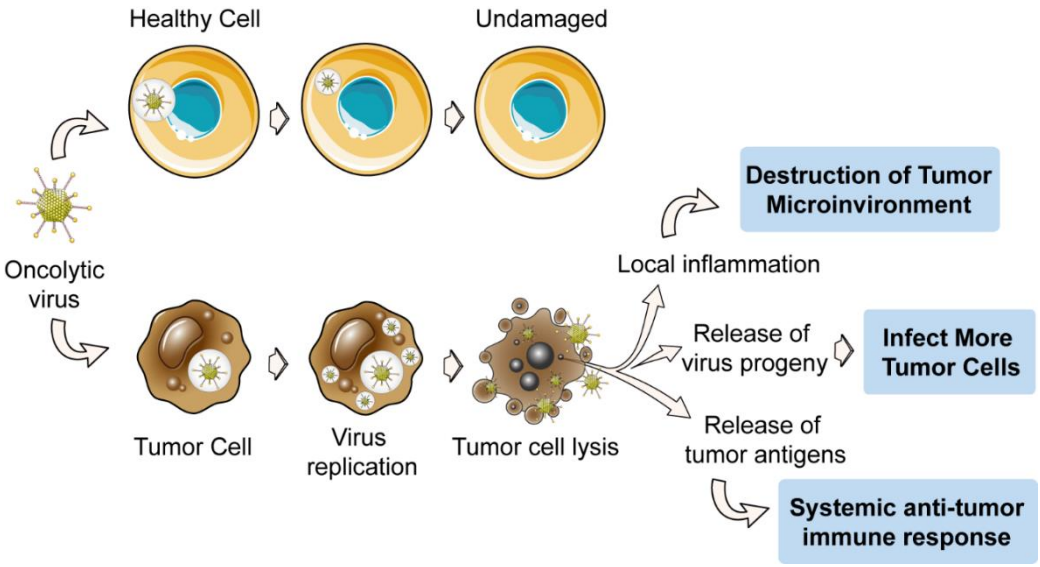

Fig. 1.1. Anti-cancer mechanism of oncolytic viruses for cancer treatment [6]

1.1.1. History and Breakthroughs

Milestones of oncolytic virotherapy are shown in Fig. 1.2. The evidence of oncolytic virus's effects on cancer treatment goes back to 1900s, where regression of tumors was observed by coincided viral infections such as measles, influenza, chickenpox, rabies. In 1950s, several studies were conducted both *in vitro* and *in vivo* studies to identify the best OV candidates. The first clinical trial was conducted by using wild-type hepatitis B. Despite of efforts, tumor responses were low, and the risk of fatal toxicity was high. Therefore, the idea of pre-step animal studies prior to human

clinical trials as a 'proof of principles' was established. [7] By the advent of recombinant DNA technology in the 1980s, oncolytic virotherapy entered a new era of engineered viruses to increase attenuation and decrease immunogenicity.[7,8] In later decades, steps were taken toward enabling oncolytic virotherapy for various cancers, owing to progress in both science and technology.

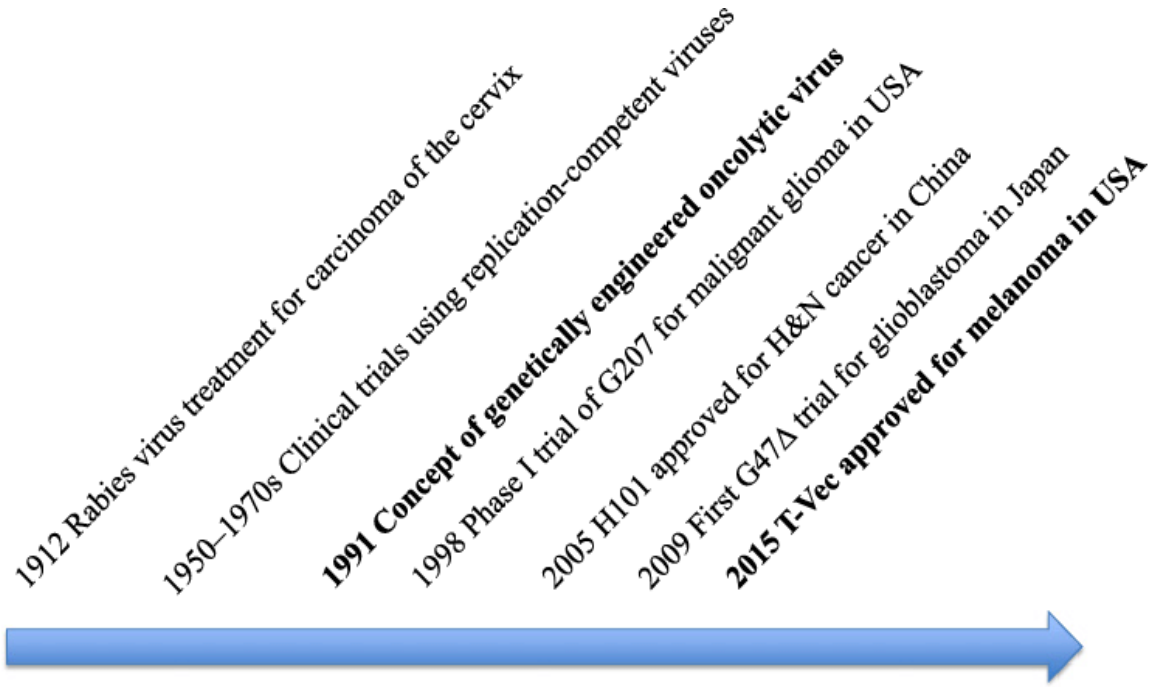

Fig. 1.2. Milestones of clinical development of oncolytic virotherapy;[9] Copyright© 2016 The Authors.

1.1.2. Current Advancement

The current global market demand should be a consequence of the clinical interest in OV-based therapies. In 2017, approximately 77 clinical trials at different phases using various OVs for different cancer types were listed in clinicaltrials.gov, indicating OV-based therapies are becoming an active area of clinical research.[10] Different phases of clinical trials for the human is outlined in Fig. 1.3. Several oncolytic viruses are

currently in clinical trials including Herpesvirus, Adenovirus, Vaccinia virus, Measles virus, Coxsackievirus, Poliovirus, Retrovirus, Reovirus, Parvovirus H1, Vesicular Stomatitis virus, and Newcastle disease virus.[11]

In below, some of the important OVs are selected and explained in more details.

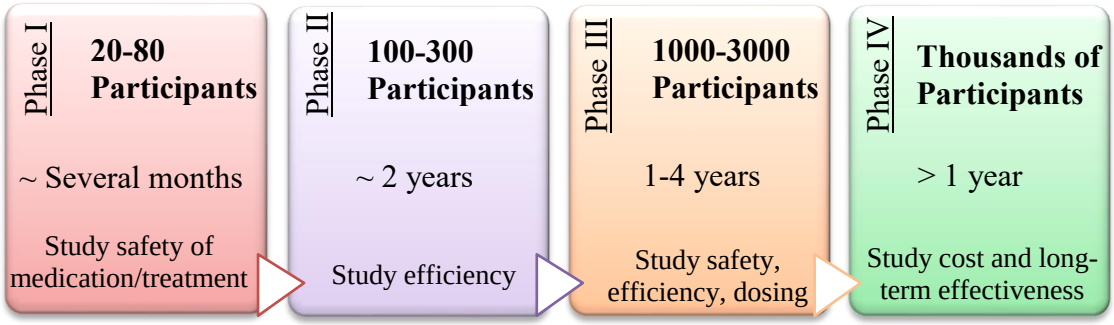

Fig. 1.3. Phases of human clinical trials; reproduced from CERN–Foundation website[12]

Herpes Simplex Virus (HSV)

HSV is an enveloped virus with double-stranded DNA and a spherical shape (~150-200 nm in diameter). In 2015, oncolytic Herpes virus talimogene laherparepvec was the first OV to be approved by US Food and Drug Administration (FDA) for advanced melanoma.[11] This OV was subsequently approved in Europe and Australia in 2016. In addition, phase I trial of oncolytic HSV1, G47Δ, was tested for patients with prostate cancer was completed in 2016.[13] HSV1 is naturally selective toward neural cells but can also be engineered to infect several other cell types.[13] Table 1.1 summarizes the most important Herpes-based OVs in the clinical trials along with the manufacturers and targeted cancer types.

Table 1.1. Summary of the most important HSV-based OVs in the clinical trial;[5] Copyright © 2015, Springer Nature.

Name	Manufacturer	# Clinical Trials			Cancer
		Phase			
		I	II	III	
T-VEC	Amgen	2	3	2	Melanoma, Head and neck, pancreatic cancer
G207	Medigene	3	0	0	Glioblastoma
HF10	Takara Bio	2	1	0	Breast cancer, melanoma, pancreatic
SEPREHVIR	Virttu Biologics	5	1	0	Hepatocellular carcinoma, glioblastoma, mesothelioma, neuroblastoma
OrienX010	OrienGene Biotechnology	1	0	0	Glioblastoma

Adenovirus (Ad)

Ad is a non-enveloped virus with double-stranded DNA and a spherical shape (~70-90 nm in diameter). Two important oncolytic Ads are Oncorine (H101) and ONYX-015 (dl1520), which are having a similar mechanism and interacting with human gene p53.[14] Oncorine was the world's first oncolytic virus that was approved for neck and head treatment by China government in 2005.[14] ONYX-015 has been tested in different clinical trials for patients with prostate cancer.[13] Table 1.2 summarizes the most important Ad-based OVs in the clinical trials along with the manufacturers and targeted cancer types.

Table 1.2. Summary of the most important Ad-based OVs in the clinical trial;[5] Copyright © 2015, Springer Nature.

Name	Manufacturer	# Clinical Trials			Cancer
		Phase			
		I	II	III	
Onyx-015	Onyx Pharmaceuticals	6	6	0	Head and neck cancer, pancreatic cancer, ovarian cancer, colorectal cancer, gliomas, lung metastases, liver metastases
H101	Shanghai Sunwaybio	1	2	1	Squamous cell carcinoma, head and neck cancer
DNX-2401	DNAtrix	4	0	0	Glioblastoma, ovarian cancer
VCN-01	VCN Biosciences	2	0	0	Pancreatic cancer
Colo-Ad1	PsiOxus Therapeutics	1	2	0	Colon cancer, renal cancer, bladder cancer, ovarian cancer
ProstAtak	Advatgagene	4	1	1	Pancreatic cancer, lung cancer, breast cancer, mesothelioma, prostate cancer
Oncos-102	Oncos Therapeutics	1	0	0	Solid tumors
CG0070	Cold genesys	1	1	1	Bladder cancer

Vaccinia Virus (VV)

VV is an enveloped virus with double-stranded DNA and a brick shape (220-450 nm×140-260 nm). The main advantage of VV is that the entire life cycle is in the cytoplasm.[13] This virus has broad cell tropism, rapid replication cycle, and efficient cell-to-cell spread.[15] VV-based clinical trials are recruited for solid tumors, colorectal cancers, renal cell carcinoma, and hepatocellular carcinoma. The most important vaccinia-based OVs in clinical trials are JX-549 and GL-ONC1. Pexa-Vec (JX594) was developed by SillaJen in collaboration with a French biopharmaceutical company Transgene, an engineered Wyeth strain, entered phase III for advanced hepatocellular carcinoma (ClinicalTrials.gov, Identifier: NCT02562755). GL-ONC1 is from

Liverpool strain, in Phase I being tested for advanced cancers such as blood cancer (NCT03420430). Table 1.3 summarizes the most important VV-based OVs in the clinical trials along with the manufacturers and targeted cancer types.

Table 1.3. Summary of the most important VV-based OVs in the clinical trial;[5] Copyright © 2015, Springer Nature.

Name	Manufacturer	# Clinical Trials			Cancer
		Phase			
		I	II	III	
Pexa-vac (JX594)	Jennerex Biotherapeutics	7	6	0	Melanoma, live cancer, colorectal cancer, breast cancer, hepatocellular carcinoma
GL-ONC1	Genelux	4	1	0	Lung cancer, head and neck, mesothelioma

Vesicular Stomatitis Virus (VSV)

VSV is an enveloped virus from Rhabdoviridae family with single-stranded RNA and a bullet shape (~80×170 nm). A schematic of VSV is shown in Fig. 1.4. The mechanism of action is based on the lack of anti-viral defense program due to defective Interferon pathway in cancerous cells.[16] Oncolytic VSV advantages are rapid replication cycle, inherent tumor specificity, cytoplasm life cycle, rarely associated with a disease in human, and induction of a broad range of immune responses to the tumor microenvironment.[17,18] In 2017, a phase I/II clinical trial is initiated to study VSV-IFNβ-NIS (with and without avelumab) for the patients with refractory advanced/metastatic solid tumors (NCT02923466). VSV-hIFNbeta-NIS is another Phase I clinical trial, recruited in 2017, for stage IV Endometrial cancer (NCT03120624).

Maraba virus is from Rhabdoviridae family with the same genus as VSV, showing promising oncolytic features as well. Maraba has the broadest oncotropism, demonstrating oncolysis in broad cell tropism. Attenuated Maraba virus, called MG1, demonstrated remarkable ability to boost adaptive cell immunity.[19] Fig. 1.5 shows MG1 infection in B16-F10 melanoma cells; the infection was noticed within 12 hours and spread over whole cells within 24 hours. Currently, three clinical trials based on Maraba virus have recruited patients started from 2014 for incurable MAGE-A3 expressing solid tumors (Phase I/II), from 2016 for non-small cell lung cancer in combination with Ad-MAGEA3 and Pembrolizumab, and from 2018 for HPV associated cancers in combination with Ad-E6E7 and Atezolizumab (NCT02285816, NCT02879760, NCT03618953).

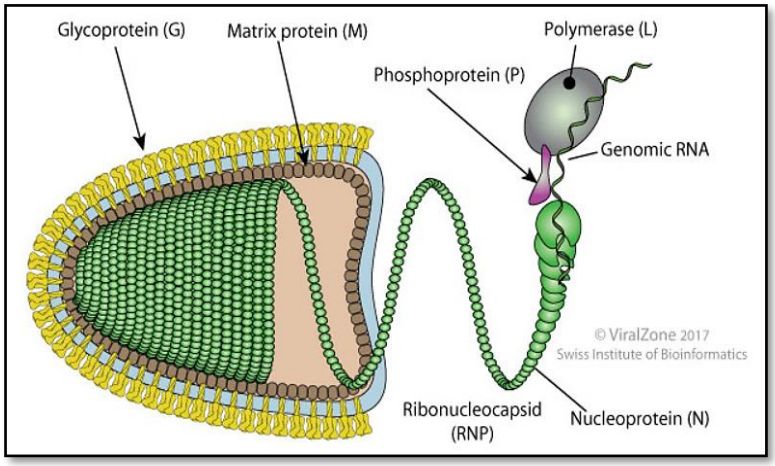

Fig. 1.4. Schematic of VSV [20]

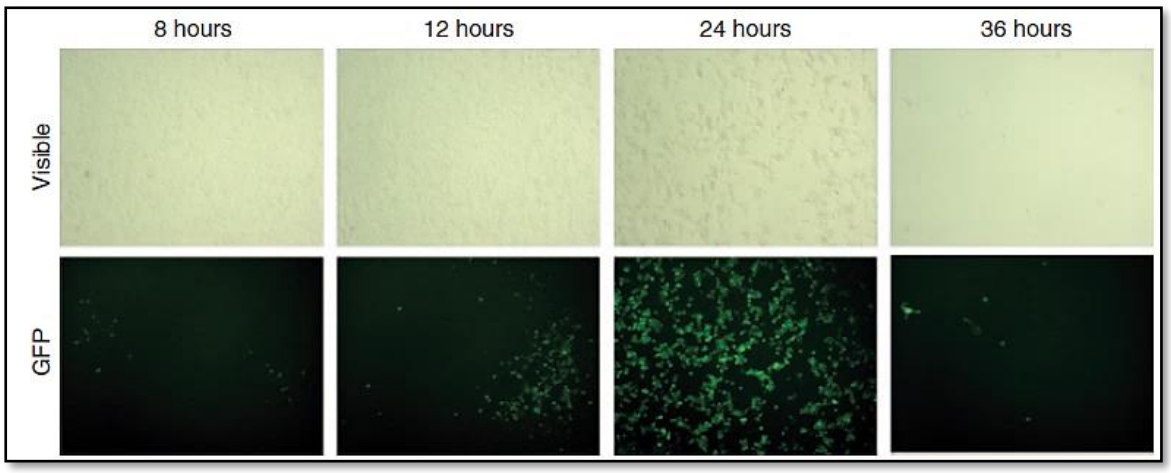

Fig. 1.5. Maraba MG1 infects, replicates in, and kill B16-F10 melanoma cells *in vitro*;[19] Copyright© 2014 Elsevier.

1.1.3. Barriers and Future Direction

Oncolytic virus delivery has been mostly achieved by intratumoral injections; Inadequate and different injected viral doses in tumor environment was observed through intratumoral injections. The latter was reported for the challenging injection to the wall of resection cavity through a hole in the skull in patients with glioblastoma.[8] Thus, a systemic delivery for OV delivery is preferred and sometimes it is required; systemic intravenous delivery is needed for treatment of metastatic cancer. However, the main obstacle to have successful systemic OV delivery is 'sequestration' in liver and spleen.[3] Sequestration refers to the rapid uptake of viruses by splenic macrophages and Kupffer cells, which will result in OV being cleared out from the blood circulation system.

Other main obstacles to having successful systemic OV delivery mainly are pre-existing immunity against viruses, neutralization by antibodies and antiviral cytokines, the difficulty of viral spread in tumor microenvironment due to increased interstitial

fluid pressure, loss of virus infectivity due to chaotic microvasculature, and turbulent distribution of blood (Fig. 1.6).[3,21]

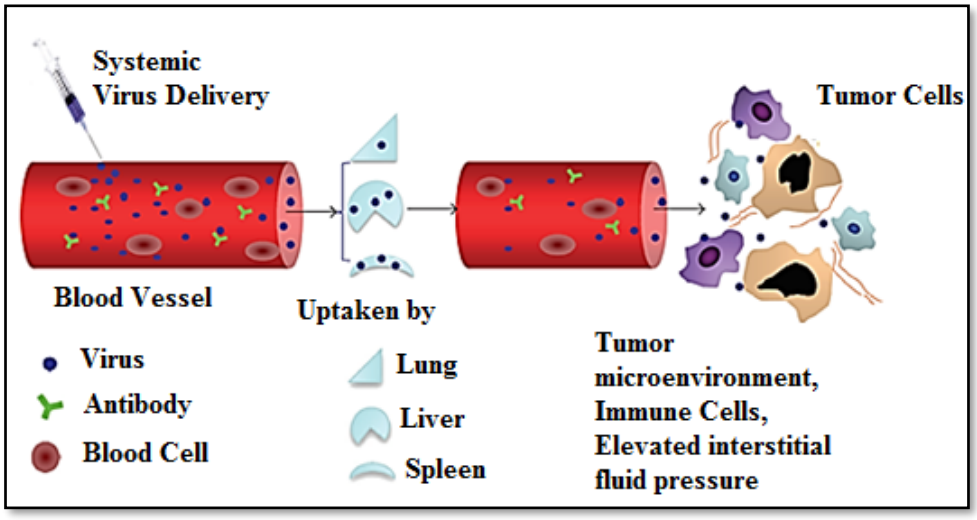

Fig. 1.6. Barriers of oncolytic virotherapy;[21] Copyright© 2012 Elsevier.

Different methods such as 'passive' and 'active' targeting have been examined to improve OV delivery. 'Passive' targeting methods are based on Enhanced Permeability and Retention effect (EPR). EPR is referring to the tendency of macromolecules to accumulate around tumor cells and penetrate into the underdeveloped vessel as a result of gaps in the leaky tumor vasculature and impaired lymphatic drainage.[22] To have a safe 'passive' targeting besides EPR effect, OV should be masked from the immune system to start the journey toward tumor cells.[23] One common method of masking is PEGylation such as PEGylated Ad with prolonged blood circulation.[24] However, polymeric conjugations may decrease virus infectivity due to shielding the receptors. This effect can be restored by 'active targeting' using a high-affinity ligand on the coating polymer to mediates 'passive' targeting such as anti-EGFR.[3,25] One example

for 'active' targeting is the encapsulation of Ad inside positive chitosan nanoparticles via electrostatic interactions.[26] The nanoparticles were targeted with folic acid using PEG as a linker.[26] Unfortunately, 'active' targeting of OVs alone is not ideal and demonstrates only modest yield toward antitumor efficiency; One proposed reason is tumor heterogeneity both in cell morphology and antigen expression.[27]

Current topic in improving systemic OV delivery is using 'stem cells' as Trojan horse delivery system.[10] It was shown that mesenchymal stem cells (MSC) shield OVs from the immune system in the bloodstream; Mader et al. [28] has shown that oncolytic Measles virus was protected from antiviral neutralization in MSCs upon intraperitoneal injection. MSCs as a carrier of oncolytic viruses have been in clinical trials for recurrent ovarian cancer (oncolytic measles virus via intraperitoneal injection, Phase I/II, NCT02068794) and metastatic solid tumors (Oncolytic Ad via IV injection, Phase I & II, NCT01844661).

The other hot topic in oncolytic virotherapy is real-time monitoring of oncolysis. Currently, seven clinical trials are listed to investigate the use of vectors encoding 'sodium iodide symporter'.[10] This symporter facilitates the uptake of iodine and other radiotracers, enabling real-time monitor of oncotropism.[10] Higher uptake of radioiodine also enhances tumor blasting area, which might consequently end up in lower required dose of oncolytic virus.[10]

The future of oncolytic virotherapy is also expected to shift toward more combinational of oncolytic viruses and immunotherapies.[10] One example is the combination of oncolytic virotherapy and checkpoint inhibitors.[10] One of the most important checkpoint proteins is programmed death 1 (PD1). Checkpoint inhibitors are

proteins that blocks either checkpoint recognition sequence (PD-1) on T-cells or checkpoints on cancer cells (programmed death ligand-1: PD-L1), leaving T cells unleashed to engage in the anti-tumor activity (Fig. 1.7). Current FDA approved checkpoint inhibitors are Nivolumab (Opdivo®) for treatment of metastatic melanoma and non-small lung cancer, and Pembrolizumab (Keytruda®) for also metastatic melanoma.

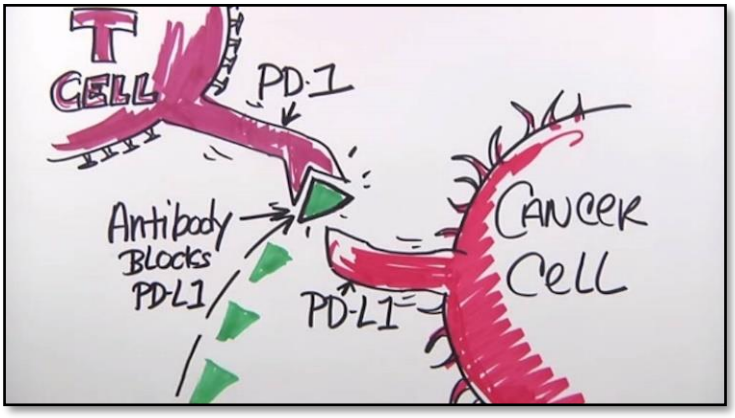

Fig. 1.7. Schematic function of checkpoint inhibitors in recognition of cancer cells by T cells [29]

1.2. Manufacturing of Viruses

The broad spectrum of virus applications and the current expansions of medical markets underline the ongoing efforts to improve gene therapy and vaccine development. Manufacturing of cell culture-derived viruses demands a complex set of unit operations, divided into two main streams as upstream and downstream processing (DSP). The general flow-diagram of virus manufacturing is shown in Fig. 1.8. The use of vectors and immunogenic compositions in clinical applications will require virus samples of adequate purity in order to comply with safety regulations of the various drug safety authorities around the World such as FDA, European Medicines Agency,

and Health Canada's Biologics and Genetic Therapies Directorate. The upstream production is focused on host cell type selection, cultivation in bioreactors, followed by proper virus infection. DSP is directed to the phase after amplification of virus particles in the host cells, where the main goal is to fulfill all the required steps to obtain the final formulated virus product with adequate purity.

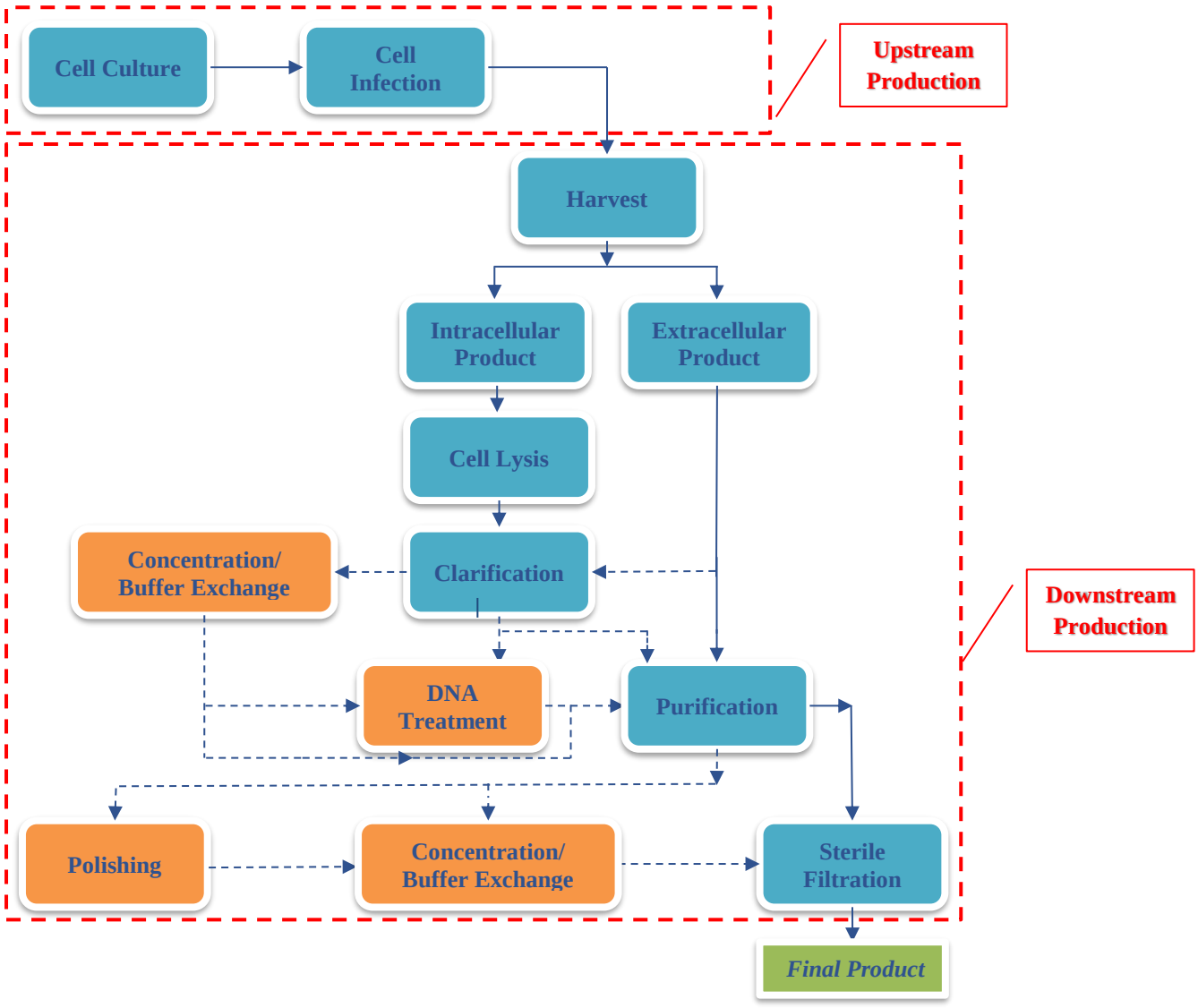

Fig. 1.8. General flow diagram of virus manufacturing including upstream and downstream production; solid lines are related to steps that should be taken (Blue boxes) while dashed line are related to the steps that are recommended to be taken (Orange boxes).

1.2.1. Upstream Processing of Viruses

Cell-line selection is an important aspect of viral-vector production because the cell line determines the viral vector's final titer. For example, production scale and cost can be reduced by using cell lines with higher efficiencies. Furthermore, the culture system is mainly dependent on cell types (suspension or adherent) and requires viral-vector concentration. The cell-culture process is also affected by other factors, such as the use of unit process or multiple parallel process, or the use of serum-free or serum-based media.[30] At the lab scale, cell culturing is performed using T-flasks and adherent or suspension cells. When scaled-up, cell culturing is often done using suspension cells and large spinners or shaker flasks and large stirred-tank reactors (SRT); however, it is generally more difficult to scale-up cell culturing for adherent cells since they need to attach to a surface in order to grow. Thus, the scaling-up of adherent cells is limited by the bioreactor's available surface area. In response to this limitation, some researchers have developed novel, large-scale designs for adherent cells based on the use of roller bottles, plate stacks, microcarriers in suspension, hollow-fiber bioreactors, and rolled membranes[31] (Fig. 1.9). Some examples of commercially available, scalable cell-culture systems include HYPER Stacks, CellCube®, Quantum® Bioreactor, Terumo BCT, and iCELLis® for adherent cells, and Allegro™ STR for suspension cells. The iCELLis® 500 bioreactor, shown in Fig. 1.10, features a surface area of 1,700 cm^2, equivalent to 3,000 roller bottles, the ability to hold a total of 60-70 liters of media.

Over the past decade, upstream titer production has dramatically increased due to optimizations in strain, media, and upstream platform design. However, there remains room for improvement, for example, finding a way to achieve adequate cell

transduction at larger scales, developing stable producer-cell lines, and developing methods for integrating serum-free media for cell cultures, to name just a few areas.

One interesting topic in upstream processing is continuous processing, referred to perfusion. Continuous upstream processing takes place in the stirred tank, where fresh sterile media enters the tank and continuously grown cells withdrawn [32]. For fully continuous upstream processing, continuous cell line is needed. A continuous cell line could divide infinitely. Currently, use of the continuous cell lines in manufacturing of viruses are limited due to stringent regulatory guidelines [33].

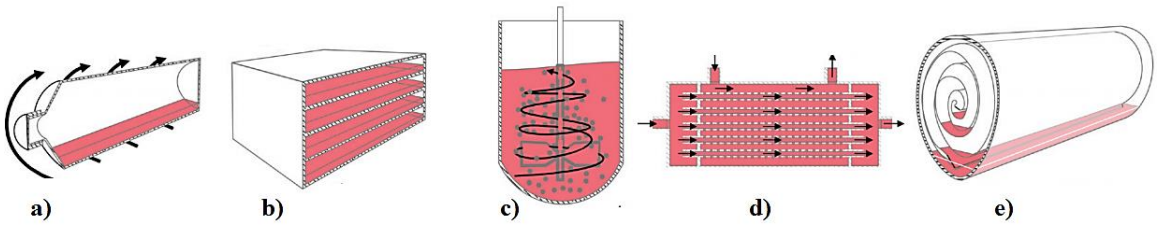

Fig. 1.9. Schematic representation of large-scale cell culture systems for adherent cells; a) roller bottle; b) plate stacks; c) microcarriers; d) hollow-fibre bioreactors; e) rolled membrane. Reprinted from Simon Marcos [31] with an orientation change in the original figure. Copyright©2015 Bioprocess International Magazine.

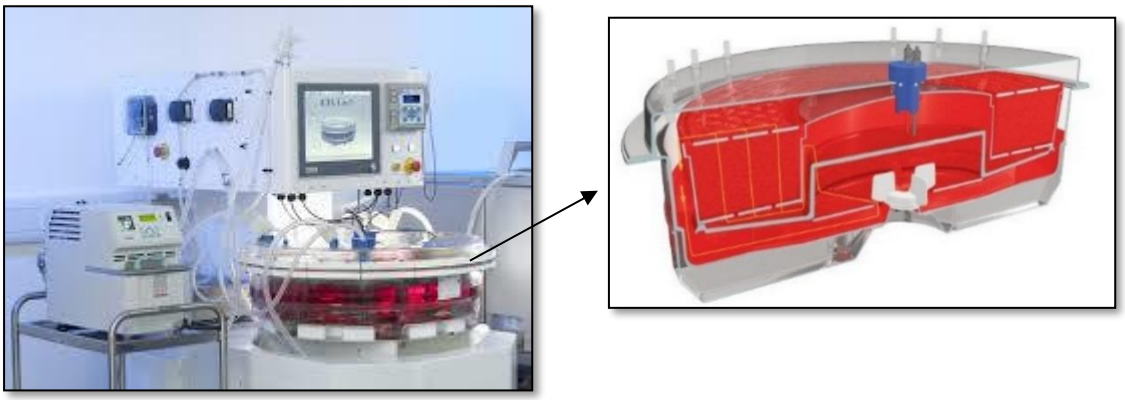

Fig. 1.10. iCELLis® 500 bioreactor system; Reprinted from Pall Biotech Brochure (Biotech.pall.com); Copyright Pall Corporation.

Another hot topic in upstream processing of viral vectors is Viral Sensitizer Technology (VST). VST is a group of compounds that robustly enhance virus amplification in the cells by disrupting cellular antiviral defense [33]. VST resulted in more than 1000-fold increase in activity of oncolytic VSV in different cancer cell lines, shown in Fig. 1.11 [34]. In this study by Diallo et al. [34], VSe1 (3,4-dichloro-5-phenyl-2,5-dihydrofuran-2-one) was recognized as the best sensitizer.

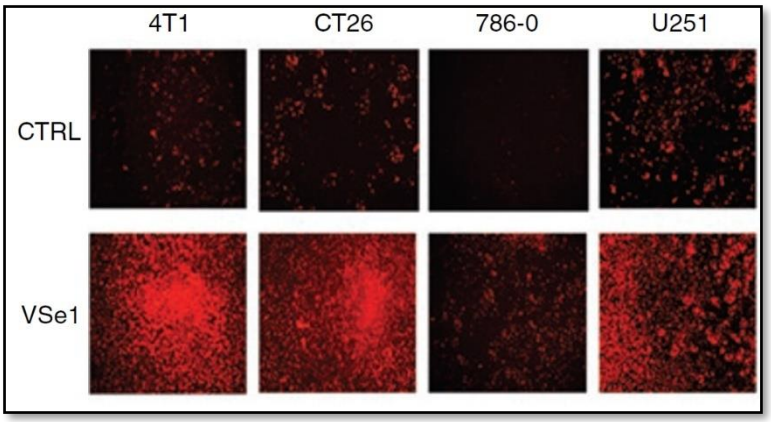

Fig. 1.11 Effects of a potential sensitizer (VSe1) on VSV (expressing Red Fluorescent Protein) activity in 4T1 murine breast, CT26 murine colon, 786-0 human renal, U251 human glioma cancer cell lines [34]; Copyright© 2010 Elsevier.

1.2.2. Downstream processing of Viruses

As Fig. 1.8 illustrates, DSP involves several different steps, including the harvesting of viral vectors from cells, nuclease treatment, clarification, purification (with several buffer-exchange and concentration steps in between), and, when necessary, sterile filtration. DSP aims to remove all process-related impurities (e.g. antibiotic, Benzonase®, host cell proteins and nucleic acids, endotoxin), product-related impurities (e.g. virus aggregates and capsids), and process-related contaminations (e.g. column leaches) in order to ensure the produced viral-based

products adhere to regulatory guidelines.[35] Host cell-related impurities are explained below:

- **Host cell nucleic acids**: guidelines requires high purities in terms of host cell DNA contamination where maximum allowable host cell DNA amount is 10 ng per dose for human vaccines with DNA size lower than 200 bps [36–38]. The concern is the possibility of oncogene being coded by nucleic acid fragments.
- **Host cell proteins**: the set goal for host cell protein is vague; the limit of 10 ng per dose are reported in some papers, while the limit of bovine serum albumin is reported as 50 ng per dose in some other published reports [39]. Residual proteins could cause unwanted immune responses and/or biological reactions due to its nature for being a cytokine, hormone, or antibody [40].
- **Endotoxin**: these substances cause fever in human body [39–41].

There is no one-process-fits-all DSP design strategy, which means that each DSP platform must be specifically designed and optimized for the targeted virus particle. Given this, it is unsurprising that there is currently a strong demand for robust DSP platforms that can improve the speed at which OV products are produced, as well as the amount and purity of the products yielded from these processes.

1.2.2.1. Harvesting and Clarification

The method selected for harvesting viral vectors will depend on whether the targeted virus is intracellular or extracellular. Extracellular viruses are enveloped viruses that are secreted to the media, while intracellular viruses are non-enveloped viruses that stay inside the host cell. Therefore, when working with intracellular viruses,

a cell lysis step is required in order to release the virus particles into the surrounding media (Fig. 1.8). Cell lysis can be performed either mechanically or chemically. Examples of mechanical cell-lysis methods include freeze/thaw cycles, liquid homogenization, and high-frequency sound waves; examples of chemicals commonly used for cell lysis are provided in Table 1.4. Some of these chemicals, such as Triton X-100 that were once commonly used for cell lysis, are currently on the authorization list (Annex XIV) of Registration, Evaluation, Authorization and Restriction, of Chemicals (REACH), effectively banning use of these products. There is a "high risk" for Brij™-35 to be added to the authorization list of REACH and consequently its usage be banned soon. Of the mechanical methods, liquid homogenization via high pressure is particularly adaptable for continuous cell lysis,[32] while chemical lysing methods are also amenable for scaled-up production and continuous processing.

Table 1.4. Summary of common chemicals used for cell lysis; reproduce from GE Technology brochure [42]

Chemical	**Properties**	**Status on REACH***
Brij™-35	Non-ionic	High risk
CHAPS	Zwitterionic	Low risk
Sodium deoxycholate	Negatively charge	Low risk
Tergitol™ NP-40	Non-ionic	On list
Triton X-100	Non-ionic	On list
Tween 20	Non-ionic	Low risk
Tween 80	Non-ionic	Low risk
Zwittergent™ 3-14	Zwitterionic	Low risk

*On list: the chemical is already on the authorization list
High risk: there is a high risk for the chemical to be added to the authorization list
Low risk: there is a high risk for the chemical to be added to the authorization list

Microfiltration, which is generally conducted in dead-end mode with a pore size range of 0.1-10 µm, is frequently used to distinguish virus particles from larger particles, such as cell and cell debris, and as a mid and/or final sterile filtration step. Depth

filtration is another type of dead-end filtration that uses a thick, fibrous, and tortuous membrane material with a relatively large pore size (≥ 0.45 μm). This approach is generally used as a pre-filtering step in crude lysate that is intended to reduce particle load and prevent clogging in subsequent membrane-based processes. In addition, the use of composite microfilters for the DSP of viral vectors has also been garnering considerable interest in recent years. These filters, which consist of multiple membrane layers made from different materials with different pore sizes, offer the main advantage of being able to reduce particle load (similar to depth filter) while maintaining high throughput. One interesting study that dealt with this concept was conducted by Reeves and Cornetta,[43] who compared the performance of a filter with membranes with different pore sizes in series (similar idea to composite filters) to that of a final, single-layer filter. Reeves and Cornetta filtered a retroviral-vector solution through a series of filters with decreasing pore sizes (40/150 μm and 20 μm) and found that this approach enabled a virus-recovery rate of 39%-66% (of initial unfiltered sample) compared to 26%-41% for the single-layer filter with a 0.45 μm pore size.[43]

The harvesting step is often followed by a nuclease treatment step, such as DNA precipitation or the addition of endonuclease (e.g. Benzonase®), in order to digest DNA. Often, other chemical components are also added to the virus solution along with the nuclease treatment in order to prevent aggregation and complex formations.[44]

In order to remove any cell debris, the crude harvest is clarified using centrifugation or microfiltration. This clarification step is followed by a concentration step, wherein ultracentrifugation or ultrafiltration are used to lower the initial volume that will be used for the purification step (as shown in Fig. 1.8).

1.2.2.2. Purification

It is difficult to achieve high-purity viral vectors, especially when dealing with high concentration of virus particles (>10^{12} virus particles). Different methods for purification of viral vector have been reported including: precipitation (using PEG, ammonium sulfate, etc.),[45] two-phase extraction [46] (PEG, dextran, polyvinyl alcohol, etc.), density-gradient ultracentrifugation,[47] membrane-based purifications (microfiltration and ultrafiltration),[43,48] and chromatography-based purifications (using resin-based columns, monoliths, membrane adsorbers).[49] Currently, precipitation and two-phase extraction are not commonly used for purification because they are prone to dramatic losses in virus infectivity, immunogenicity, and transduction efficiency.[35] Instead, viral-vector preparation at the lab scale is often performed via density-gradient ultracentrifugation using sucrose, cesium chloride (CsCl), or iodixanol gradients. Density-gradient ultracentrifugation's main advantage is that it produces a highly purified product that is free from process-related (e.g. host cell impurities) and product-related impurities, such as capsids (empty viral particles), which are often challenging to remove using other methods.[35,50] Despite these advantages, several rounds of ultracentrifugation are required in order to achieve the desired level of purity, which makes this method labor-intensive, time-consuming, scale-limited, and only capable of providing sufficient material up to phase I studies.[35,50] In addition, the shear stress inherent to this method can lead to diminished virus infectivity, specifically for labile virus particles.[51] Other disadvantages associated with density-gradient ultracentrifugation include the necessity for toxic CsCl removal and low yields, often in the range of 1%.[52] Thus, membrane-based and chromatography-based purification methods have become the standard DSP purification methods for manufacturing

scales.[35,53] Fig. 1.12 shows commercially available large-scale chromatography-based platforms for virus purification. These methods would be further discussed in Chapter 2.

Fig. 1.12. Schematic of large-scale commercially available chromatography platforms; a) 8 L monolithic column; reprinted from BIA Separation (www.biaseparations.com); b) Resolute Linear chromatography (Pall) with 350mm-2000mm internal diameter; reprinted from Pall Biotech (biotech.pall.com); Copyright Pall Corporation; c) Membrane adsorber [54]; Copyright Sartorius Stedim Biotech.

1.2.2.3. Concentration and Buffer Exchange

Large-scale processes produce high volumes of starting material; thus, a concentration step is required in order to increase the virus titer in the starting material and to reduce the initial volume of material for DSP.[55] The initial volume of material is critical because it establishes the scale and processing time of DSP. Buffer exchange can be achieved via centrifugation, dialysis, or ultrafiltration; however, virus concentration and buffer exchange can be achieved simultaneously via centrifugation

or ultrafiltration. Among the above-mentioned methods, ultrafiltration offers the best scalability and the most potential for continuous processing.

Ultrafiltration is generally performed in a tangential-flow operation mode, with flow direction being parallel to the membrane surface. Ultrafilters are made of various materials, such as cellulose acetate, polyethersulfone, polysulfone, or polyvinylidene fluoride, and they can have pore sizes ranging between 0.01 µm-0.1 µm, depending on their respective molecular weight cut off (MWCO) sizes. A filter's MWCO size is defined as the molecular weight of the particle that is 90% retained by the membrane.

1.2.2.4. Sterile Filtration

Another frequent membrane-based unit operation in bio-pharmaceuticals is sterile filtration. Sterile filtration is a dead-end microfiltration process aimed at removal of microorganism from the fluid stream without affecting the product. The accepted rating for the sterile filter is 0.2-0.22 µm, for which the filter should be certified to reproducibly retain B. diminuta (ATTC 19146) with a minimum concentration of 10^7 CFU per 1 cm^2 [56]. In the sterile filtration step, we are dealing with the high concentration of the valuable product in the final stream, where the proper membrane performance and consequent product recovery are critical.

Main manufacturers of sterile filters are Pall, Millipore, and Sartorius, producing a broad range of sterile filters from syringe filters to large industrial-scale sterile filters, shown in Fig. 1.13.

Fig. 1.13. Sterile filters at different scales; a) sterile syringe filters (<6.2 cm^2); reprinted from Sartorius (www.sartorius.es) b) Stericup-HV Sterile Vacuum Filtration System (40 cm^2); reprinted from EMD Millipore (www.emdmillipore.com); c) Pall Kleenpak™ Nova Capsules and Cartridge sterile filter (1 m^2); reprinted from Pall (shop.pall.com); Copyright Pall Corporation.

1.3. Motivations and Objectives

Virotherapy is a class of cancer therapy currently undergoing clinical trials in order to eventually attain full approval. Thanks to advances in upstream production with improved yields, DSP has become the main bottleneck in the manufacturing process, negatively impacting overall productivity and costs. At its core, this work is motivated by a desire to identify the main challenges associated with the DSP of viral vectors, and to re-conceptualize these problems as opportunities to develop a deeper understanding of the DSP process and to improve it wherever possible. To this end, this work focuses on oncolytic Rhabdoviral vector, which is a promising OV that is able to directly kill tumor cells and induce tumor-specific immune responses.[19, 59–62]

Existing downstream purification processes use combinations of column chromatography and membrane-based processes to remove impurities. Monolithic columns, which feature a continuous stationary phase with a network of interconnected

pores and high porosity, are one powerful technology that enables the purification of "large" biomolecules. In addition, anion-exchange chromatography has also been commonly reported as a suitable method for the purification of various virus types.[61–69] However, a few studies have found that anion-exchange columns resulted in high virus loss for enveloped viruses,[70,71] which indicates a need for a more detailed understanding of these columns' performance. It is this need that motivates this study's examination of how column characteristics, such as functional groups, and pore size affect the purification of the enveloped Rhabdoviral vector (Chapter III).

Another operational challenge in the DSP of viral vectors is the final sterile filtration step. The primary issue associated with this step is severe membrane fouling, which is characterized by a dramatic and uncontrollable increase in TMP or a significant flux decline, which results in a low viral-vector recovery rate. Indeed, this is a significant problem, as total vector titer losses of up to 80% have been reported.[43] Several studies have used membranes to selectively retain viruses or virus-like particles, while allowing smaller bio-therapeutic molecules (e.g. recombinant proteins) to pass through. These studies are referred to as virus-clearance (or removal) studies, and readers are invited to refer for specific examples of this type of study.[72–75] Conversely, only a few studies have examined the transmission of viruses through membranes. Thus, this gap in the literature motivates the analysis membrane morphology's impact on fouling and product recovery presented in Chapter IV.

In an attempt to increase product recovery through membrane-based processes, researchers have focused on altering the fouling propensity of membranes by modifying their surfaces and improving various surface characteristics, such as hydrophilicity,

charge, and roughness.[76] In addition, beef extract,[77 78] calf or bovine serum,[77,79] and glycine,[78] have been proposed as agents for modifying membrane surfaces in virus applications aimed at recovering intact virus particles. Nevertheless, most of these modified membrane surfaces were only used with water samples that contained very low concentrations ($< 10^4$) of virus particles per liter.[80] On the other hand, the effects of surface modification agents such as serum have been mostly studied in tangential-flow ultrafiltration, where the virus particles were retained.[77] It is also worth noting that most of these studies focused on waterborne viruses, such as enteroviruses.[77,79] Thus, there is a need to study how membrane-surface modification influences the recovery of virus particles when the initial stock is transmitted through the membrane at relatively high concentrations.

The aggregation of virus particles is another possible cause of membrane fouling and consequent virus loss. One potent method that can be used to decrease the membrane fouling rate is to disaggregate virus particles and preventing the formation of virus aggregates during microfiltration through the addition of potential additives such as sugars,[81,82] surfactants,[44] different salts,[83] polymers,[84,85] and etc. It is worth noting that interactions between additives and virus particles, as well as those between virus particles and the environment, are specific. While additives can be used to prevent aggregation and its undesired effects, this phenomenon is often poorly understood.

While membrane surface modification and the use of additives appear to be effective strategies for altering membrane-fouling propensity, the above-cited studies either focused on virus recovery (mostly as a retentate) or controlling membrane fouling. Unfortunately, no systematic studies exist that examine both factors simultaneously,

specifically studies in which virus particles pass through the membrane rather than being retained by it. This gap in the literature provided the motivation for the research presented in Chapter V.

1.4. Thesis Outline

Chapter II provides an in-depth review of this project's background by surveying current viral vector purification technologies and providing an overview of the background of virus aggregation/disaggregation. In addition, this chapter reviews and evaluates methods of virus particle characterization, with a focus on virus particle quantification and size distribution analysis.

Chapter III investigates how monolithic column chemistry and pore size affect the purification of virus particles. Specifically, monolithic columns (CIM, BIA separations) functionalized with anion-exchange (quaternary ammonium) and hydrophobic interaction (hydroxyl) groups are examined for their ability to purify the selected Rhabdoviral vector. This research is the first documented investigation of how different column pore sizes, 2 µm versus 6 µm, impact contaminant removal and virus recovery. In addition, this chapter also documents the development and optimization of monolithic hydrophobic interaction column chromatography for the purification of Rhabdoviral vectors. It is well accepted that hydrophobic interaction column performance is influenced by different factors.[86,87] As such, the optimization of adsorption/desorption conditions of the virus particle to the monolithic hydrophobic interaction column — specifically, salt concentration and pH — are also investigated.

Finally, the research in this chapter also documents the first analysis of how additives, namely glycerol, affect the monolithic hydrophobic interaction column.

Chapter IV investigates how membrane morphology influences fouling behavior and product (i.e. virus) recovery during the sterile filtration of the virus stream, wherein virus particles are transmitting through the membrane. In this chapter, the performance of four commercially available sterile filters (0.2/0.22 μm) — Durapore, Fluorodyne EX EDF, MiniSart NML, and MiniSart Plus — was evaluated using pre-purified batches of the Rhabdoviral vector. Constant-flux filtration tests were conducted, with membrane fouling being determined via online measurements of the transmembrane pressure (TMP). Membrane-fouling severity was evaluated by performing hydraulic-permeability measurements, and a detailed understanding of the fouling process was developed by comparing the measured TMP profiles to the blocking models.

Chapter V builds upon the study in Chapter IV by conducting the first investigation of methods that can be used to probe how stabilizers affect the oncolytic virus solution via a microscale filtration process. In order to develop effective methods of controlling and preventing membrane fouling, it is first necessary to develop a detailed understanding of the fouling mechanisms of virus particles. To this end, a small-scale microfiltration setup was developed that allowed for constant-flux microfiltration using a low volume of the virus solution (< 3 mL) and online transmembrane pressure (TMP) measurement. This setup was used to examine how the use of different additives, including various proteins (bovine serum albumin, alpha-lactalbumin) and polymers

(polyethylene glycol and polyvinylpyrrolidone), impacted Rhabdoviral vector filtration. Furthermore, Chapter V also investigates whether membrane surface modification using proteins effectively mediates virus transmission through the membrane.

1.5. References

1. Zeyaullah, M. *et al.* Oncolytic viruses in the treatment of cancer: a review of current strategies. *Pathol. Oncol. Res.* **18,** 771–781 (2012).

2. Chiocca, E. A. & Rabkin, S. D. Oncolytic viruses and their application to cancer immunotherapy. *Cancer Immunol. Res.* **2,** 295–300 (2014).

3. Russell, S. J., Peng, K.-W. & Bell, J. C. Oncolytic virotherapy. *Nat biotechnol* **30,** 658–670 (2012).

4. Aiuti, A. *et al.* Progress and prospects: gene therapy clinical trials (part 2). *Gene Ther* **14,** 1555–1563 (2007).

5. Kaufman, H. L., Kohlhapp, F. J. & Zloza, A. Oncolytic viruses: a new class of immunotherapy drugs. *Nat. Rev. Drug Discov.* **14,** 642–662 (2015).

6. Creative Biolabs. No Title. Available at: https://www.creative-biolabs.com/car-t/oncolytic-virus-therapy-development.htm.

7. Pikor, L., Bell, J. C. & Kaufman, H. L. Oncolytic viruses. in *Cancer Immunotherapy Principles and Practice* 375 (Springer Publishing Company, 2017).

8. Kerrigan, B. C. P., Shimizu, Y., Andreeff, M. & Lang, F. F. Mesenchymal stromal cells for the delivery of oncolytic viruses in gliomas. *Cytotherapy* **19,** 445–457 (2017).

9. Fukuhara, H., Ino, Y. & Todo, T. Oncolytic virus therapy: a new era of cancer treatment at dawn. *Cancer Sci.* **107,** 1373–1379 (2016).

10. Warner, S. G., O'leary, M. P. & Fong, Y. Therapeutic oncolytic viruses: Clinical advances and future directions. *Curr. Opin. Oncol.* **29,** 359–365 (2017).

11. Lawler, S. E., Speranza, M.-C., Cho, C.-F. & Chiocca, E. A. Oncolytic viruses in cancer treatment: a review. *JAMA Oncol.* **3,** 841–849 (2017).

12. CERN Foundation, Available at https://www.cern-foundation.org/

13. Taguchi, S., Fukuhara, H., Homma, Y. & Todo, T. Current status of clinical trials assessing oncolytic virus therapy for urological cancers. *Int. J. Urol.* **24,** 342–351 (2017).

14. Garber, K. China approves world's first oncolytic virus therapy for cancer treatment. *J. Natl. Cancer Inst.* **98,** 298–300 (2006).

15. Guse, K., Cerullo, V. & Hemminki, A. *Oncolytic vaccinia virus for the treatment of cancer*. *Expert opinion on biological therapy* **11,** (2011).

16. Lichty, B. D., Power, A. T., Stojdl, D. F. & Bell, J. C. Vesicular stomatitis virus:

re-inventing the bullet. *Trends Mol Med* **10,** 210–216 (2004).

17. Melzer, M., Lopez-Martinez, A. & Altomonte, J. Oncolytic vesicular stomatitis virus as a viro-immunotherapy: Defeating cancer with a “Hammer” and “Anvil”. *Biomedicines* **5,** 8 (2017).

18. Brun, J. *et al.* Identification of Genetically Modified Maraba Virus as an Oncolytic Rhabdovirus. *Mol. Ther.* **18,** 1440–1449 (2010).

19. Pol, J. G. *et al.* Maraba Virus as a Potent Oncolytic Vaccine Vector. *Mol Ther* **22,** 420–429 (2014).

20. ViralZone. Available at: https://viralzone.expasy.org/2.

21. Ferguson, M. S., Lemoine, N. R. & Wang, Y. Systemic delivery of oncolytic viruses: hopes and hurdles. *Adv. Virol.* **2012,** (2012).

22. Uthaman, S., Lee, S. J., Cherukula, K., Cho, C.-S. & Park, I.-K. Polysaccharide-coated magnetic nanoparticles for imaging and gene therapy. *Biomed Res. Int.* **2015,** (2015).

23. O’Riordan, C. R. *et al.* PEGylation of adenovirus with retention of infectivity and protection from neutralizing antibody in vitro and in vivo. *Hum. Gene Ther.* **10,** 1349–1358 (1999).

24. Choi, J.-W. *et al.* pH-sensitive oncolytic adenovirus hybrid targeting acidic tumor microenvironment and angiogenesis. *J. Control. Release* **205,** 134–143 (2015).

25. Ulbrich, K. *et al.* Targeted drug delivery with polymers and magnetic nanoparticles: covalent and noncovalent approaches, release control, and clinical studies. *Chem. Rev.* **116,** 5338–5431 (2016).

26. Kwon, O.-J., Kang, E., Choi, J.-W., Kim, S. W. & Yun, C.-O. Therapeutic targeting of chitosan–PEG–folate-complexed oncolytic adenovirus for active and systemic cancer gene therapy. *J. Control. release* **169,** 257–265 (2013).

27. Choi, J.-W., Lee, Y. S., Yun, C.-O. & Kim, S. W. Polymeric oncolytic adenovirus for cancer gene therapy. *J. Control. Release* **219,** 181–191 (2015).

28. Mader, E. K. *et al.* Mesenchymal stem cell carriers protect oncolytic measles viruses from antibody neutralization in an orthotopic ovarian cancer therapy model. *Clin. Cancer Res.* 432–1078 (2009).

29. Dana-Farber. Available at: https://blog.dana-farber.org/insight/2015/09/what-is-a-checkpoint-inhibitor/.

30. Merten, O.-W., Schweizer, M., Chahal, P. & Kamen, A. A. Manufacturing of viral vectors for gene therapy: part I. Upstream processing. *Pharm Bioprocess* **2,** 183–203 (2014).

31. Simón, M. Bioreactor design for adherent cell culture. *Bioprocess Int.* **13,** 1 (2015).

32. Rathore, A. S., Agarwal, H., Sharma, A. K., Pathak, M. & Muthukumar, S. Continuous processing for production of biopharmaceuticals. *Prep Biochem Biotechnol* **45,** 836–849 (2015).

33. Diallo, J.-S. Virus Sensitizer Technology.

34. Diallo, J.-S. *et al.* A high-throughput pharmacoviral approach identifies novel oncolytic virus sensitizers. *Mol. Ther.* **18,** 1123–1129 (2010).

35. Reichl, U. & Wolf, M. W. Downstream processing of cell culture-derived virus particles. *Expert Rev. Vaccines* **10,** 1451–1475 (2011).

36. Knezevic, I., Stacey, G. & Petricciani, J. WHO Study Group on cell substrates for production of biologicals, Geneva, Switzerland, 11–12 June 2007. *Biologicals* **36,** 203–211 (2008).

37. World Health Organization, Guidelines on the Quality, Safety, and Efficacy of Biotherapeutic Protein Products prepared by Recombinant DNA Technology. *Replace. Annex* **3,** (2013).

38. Food and Drug Administration, Vaccines and Related Biological Products Advisory Committee (VRBPAC) adult indication briefing document: Prevnar 13. Silver Spring, MD: US Department of Health and Human Services. *Food Drug Adm.* (2011).

39. Wisher, M. Biosafety and product release testing issues relevant to replication-competent oncolytic viruses. *Cancer Gene Ther.* **9,** 1056 (2002).

40. Briggs, J. & Panfili, P. R. Quantitation of DNA and protein impurities in biopharmaceuticals. *Anal. Chem.* **63,** 850–859 (1991).

41. Ferreira, G. N. M. Chromatographic approaches in the purification of plasmid DNA for therapy and vaccination. *Chem. Eng. Technol. Ind. Chem. Equipment-Process Eng.* **28,** 1285–1294 (2005).

42. GE Healthcare, *Optimization of midstream cell lysis and virus filtration steps in an adenovirus purification process*. Application note, KA875220218AN

43. Reeves, L. & Cornetta, K. Clinical retroviral vector production: step filtration using clinically approved filters improves titers. *Gene Ther* **7,** 1993–1998 (2000).

44. Konz, J. O., Lee, A. L., Lewis, J. A. & Sagar, S. L. Development of a purification process for adenovirus: controlling virus aggregation to improve the clearance of host cell DNA. *Biotechnol Prog* **21,** 466–472 (2005).

45. Ayuso, E. *et al.* High AAV vector purity results in serotype- and tissue-independent enhancement of transduction efficiency. *Gene Ther* **17,** 503–510 (2010).

46. Braas, G. M. F., Walker, S. G. & Lyddiatt, A. Recovery in aqueous two-phase systems of nanoparticulates applied as surrogate mimics for viral gene therapy vectors. *J. Chromatogr. B Biomed. Sci. Appl.* **743,** 409–419 (2000).

47. Smith, R., Yang, L. & Kotin, R. Chromatography-Based Purification of Adeno-Associated Virus. in *Gene Therapy Protocols* (ed. Le Doux, J.) **434,** 37–54 (Humana Press, 2008).

48. Subramanian, S. *et al.* Pilot-scale adenovirus seed production through concurrent virus release and concentration by hollow fiber filtration. *Biotechnol Prog* **21,** 851–859 (2005).

49. Konz, J. O., Pitts, L. R. & Sagar, S. L. Scaleable purification of adenovirus vectors. *Methods Mol Biol* **434,** 13–23 (2008).

50. Morenweiser, R. Downstream processing of viral vectors and vaccines. *Gene Ther.* **12,** S103 (2005).

51. Jungbauer, A. & Hahn, R. Polymethacrylate monoliths for preparative and industrial separation of biomolecular assemblies. *J. Chromatogr. A* **1184,** 62–79 (2008).

52. Chen, G.-Y., Chen, C.-Y., Chang, M. D.-T., Matsuura, Y. & Hu, Y.-C. Concanavalin a affinity chromatography for efficient baculovirus purification. *Biotechnol. Prog.* **25,** 1669–1677 (2009).

53. Rajamanickam, V., Herwig, C. & Spadiut, O. Monoliths in Bioprocess Technology. *Chromatography* **2,** 195 (2015).

54. Fischer-Fruhholz S., Sartobind Membrane Chromatography, Sartorius Stedim Biotech (2012).

55. Nestola, P. *et al.* Evaluation of Novel Large Cut-Off Ultrafiltration Membranes for Adenovirus Serotype 5 (Ad5) Concentration. *PLoS One* **9,** (2014).

56. Food and Drug Administration, Guidance for Industry: Sterile Drug Products Produced by Aseptic Processing—Current Good Manufacturing Practice. *FDA Cent. Drug Eval. Res. Cent. Biol. Eval. Res. Off. Regul. Aff. (ORA), Washington, DC* (2004).

57. Hummel, J. *et al.* Maraba virus-vectored cancer vaccines represent a safe and novel therapeutic option for cats. *Sci. Rep.* **7,** 15738 (2017).

58. Brun, J. *et al.* Identification of genetically modified Maraba virus as an oncolytic rhabdovirus. *Mol Ther* **18,** 1440–1449 (2010).

59. Zhang, J. *et al.* Maraba MG1 virus enhances natural killer cell function via conventional dendritic cells to reduce postoperative metastatic disease. *Mol Ther* **22,** 1320–1332 (2014).

60. Le Boeuf, F. *et al.* Oncolytic Maraba virus MG1 as a treatment for Sarcoma. *Int.*

J. Cancer **141,** 1257–1264 (2017).

61. Urbas, L. *et al.* Purification of recombinant adenovirus type 3 dodecahedric virus-like particles for biomedical applications using short monolithic columns. *J Chromatogr A* **1218,** 2451–2459 (2011).

62. Peterka, M., Strancar, A., Banjac, M., Kramberger, P., Maurer, E. and Muster, T. Method for influenza virus purification. European Patent Application 20060116979, filed January 16, 2008.

63. Bandeira, V. *et al.* Downstream processing of lentiviral vectors: releasing bottlenecks. *Hum Gene Ther Methods* **23,** 255–263 (2012).

64. Venkatachalam, A. R. K., Szyporta, M., Kiener, T. K., Balraj, P. & Kwang, J. Concentration and purification of enterovirus 71 using a weak anion-exchange monolithic column. *Virol. J.* **11,** 99 (2014).

65. Allmaier, G. *et al.* Monolithic anion-exchange chromatography yields rhinovirus of high purity. *J. Virol. Methods* **251,** 15–21 (2018).

66. Forcic, D. *et al.* Concentration and purification of rubella virus using monolithic chromatographic support. *J. Chromatogr. B* **879,** 981–986 (2011).

67. Gerster, P. *et al.* Purification of infective baculoviruses by monoliths. *J. Chromatogr. A* **1290,** 36–45 (2013).

68. Rupar, M. *et al.* Fast purification of the filamentous Potato virus Y using monolithic chromatographic supports. *J. Chromatogr. A* **1272,** 33–40 (2013).

69. Gutiérrez-Aguirre, I. *et al.* Concentrating rotaviruses from water samples using monolithic chromatographic supports. *J. Chromatogr. A* **1216,** 2700–2704 (2009).

70. Sviben, D., Forcic, D., Ivancic-Jelecki, J., Halassy, B. & Brgles, M. Recovery of infective virus particles in ion-exchange and hydrophobic interaction monolith chromatography is influenced by particle charge and total-to-infective particle ratio. *J. Chromatogr. B* **1054,** 10–19 (2017).

71. Kang, Y., Cutler, M. W., Ouattara, A. A. & Syvertsen, K. E. Purification processes for isolating purified vesicular stomatitis virus from cell culture. U.S. Patent 7,875,446, issued January 25, 2011.

72. Bakhshayeshi, M. *et al.* Use of confocal scanning laser microscopy to study virus retention during virus filtration. *J. Memb. Sci.* **379,** 260–267 (2011).

73. Grein, T. A., Kovacs, Z., Ebrahimi, M., Michalsky, R. & Czermak, P. Membrane supported virus separation from biological solutions. *Chemie Ing. Tech.* **85,** 1183–1192 (2013).

74. Pontius, F. W., Amy, G. L. & Hernandez, M. T. Fluorescent microspheres as virion surrogates in low-pressure membrane studies. *J. Memb. Sci.* **335,** 43–50

(2009).

75. Wickramasinghe, S. R., Stump, E. D., Grzenia, D. L., Husson, S. M. & Pellegrino, J. Understanding virus filtration membrane performance. *J. Memb. Sci.* **365,** 160–169 (2010).

76. Rana, D. & Matsuura, T. Surface Modifications for Antifouling Membranes. *Chem. Rev.* **110,** 2448–2471 (2010).

77. Winona, L. J., Ommani, A. W., Olszewski, J., Nuzzo, J. B. & Oshima, K. H. Efficient and predictable recovery of viruses from water by small scale ultrafiltration systems. *Can. J. Microbiol.* **47,** 1033–1041 (2001).

78. Tartera, C., Araujo, R., Michel, T. & Jofre, J. Culture and decontamination methods affecting enumeration of phages infecting Bacteroides fragilis in sewage. *Appl. Environ. Microbiol.* **58,** 2670–2673 (1992).

79. Cliver, D. O. Factors in the membrane filtration of enteroviruses. *Appl. Microbiol.* **13,** 417–425 (1965).

80. Xagoraraki, I., Kuo, D. H.-W., Wong, K., Wong, M. & Rose, J. B. Occurrence of human adenoviruses at two recreational beaches of the great lakes. *Appl. Environ. Microbiol.* **73,** 7874–7881 (2007).

81. Wang, P. *et al.* Glycerol facilitates the disaggregation of recombinant adeno-associated virus serotype 2 on mica surface. *Colloids Surfaces B Biointerfaces* **60,** 264–267 (2007).

82. Xie, Q., Hare, J., Turnigan, J. & Chapman, M. S. Large-scale production, purification and crystallization of wild-type adeno-associated virus-2. *J. Virol. Methods* **122,** 17–27 (2004).

83. Wright, J. F. *et al.* Identification of factors that contribute to recombinant AAV2 particle aggregation and methods to prevent its occurrence during vector purification and formulation. *Mol. Ther.* **12,** 171–178 (2005).

84. Armstrong, J. K., Wenby, R. B., Meiselman, H. J. & Fisher, T. C. The hydrodynamic radii of macromolecules and their effect on red blood cell aggregation. *Biophys. J.* **87,** 4259–4270 (2004).

85. Kissmann, J. *et al.* Physical stabilization of norwalk virus-like particles. *J. Pharm. Sci.* **97,** 4208–4218 (2008).

86. Queiroz, J. A., Tomaz, C. T. & Cabral, J. M. S. Hydrophobic interaction chromatography of proteins. *J. Biotechnol.* **87,** 143–159 (2001).

87. Builder, S. E. *Hydrophobic interaction chromatography, principles and methods, Amersham pharmacia biotech*. (ISBN 91-970490-4-2, edition AB, 1993).

Chapter II – Challenges and Opportunities

2.1. Downstream processing of viral vectors

DSP design is critical for virus manufacturing because it ensures the efficacy and safety of the final product. [1] This chapter presents an overview of the main challenges associated with the DSP of viral vectors.

In general, the DSP of viral vectors has been adapted from recombinant protein production, though some DSPs have also been adapted from vaccine-production processes.[2] Although this adaptive approach seems theoretically feasible, it poses several serious challenges for viral-vector manufacturing, which are largely related to the complex characteristics of virus particles, as well as their large size;[1,3,4]virus particles can exceed molecular weights of 5,000 kDa, while proteins generally have molecular weights ranging from 5 to 150 kDa.[4]

Another main challenge arises from the fact that research into DSP design and optimization has largely been neglected in recent years in favour of a focus on enhancing upstream processing methods in order to increase bioreactor yields and achieve high viral titers.[3] This unbalanced focus has caused DSP to become the main bottleneck in virus-manufacturing processes, accounting for as much as 70% of production costs.[4,5] On the other hand, DSP is greatly impacted by upstream processing, as the types and levels of impurities and contaminants to be removed during DSP are determined during host-cell production in upstream processing.[4] Furthermore, while longer upstream processes increase virus titer, they also increases the impurities

produced by the host cells.[6] It is also worth noting that there is batch-to-batch variation in the composition of the upstream bulk.[5] The main challenge related to processing impurities is that viral-product purity is often inversely related to process recovery, which makes DSP design much more complex.[6]

Another challenge that needs to be addressed is the ability to ensure that viral vectors remain intact and viable (i.e. infectivity) throughout the DSP steps.[1,7] Some researchers have suggested that repeating the purification cycle several times is an effective approach for producing viral products with acceptable purity. However, not only would such an approach lack scalability and repeatability, but it would also result in costly DSP design and lead to virus-titer loss, which would in turn result in low process yield.[7] These limitations have given rise to a strong demand for scalable, fast, simple, robust, and cost-effective DSP methodologies, as such an approach would allow researchers to obtain high-purity infective viral vectors that are ready for use in patients.[4] In developing a DSP methodology that meets these requirements, it is important to consider several factors:

- Chemical, physical, and biological characteristics of virus particle

  Dimensions and hydrodynamic size, isoelectric point, enveloped or non-enveloped, surface hydrophobicity, lability of virus particle, etc.
- Type of final product

  Full intact virus, viral subunits, or inactivated virus
- Market demand and scalability requirements
- Regulation requirements (contamination levels)

One design possibility that has become a hot topic for researchers is the development of a *continuous DSP* wherein the product moves directly from one process to another with no product hold between.[8] Ideally, such a process will be steady-state and will enable increased productivity, improved product quality,[8] reduced costs, and shorter processing times,[9] as well as the constant concentration of the product and impurities. Recently, a few researchers have attempted to adapt some of the steps from the production of bacterial products into a continuous design,[9] with some improvements being observed. Despite these improvements, however, the true potential of a continuous DSP system will only be realized after all of the steps have been adapted and integrated to produce full, continuous production.[9]

2.1.1. Membrane-based Purification Processes

Membrane-based methods are generally preferred in DSP of viral vectors because of simplicity of operation, low cost, and straightforward scale-up. Ultrafilters are commercially available in different formats such as flat sheet, hollow fiber, spiral wound, and tubular membrane.

It is well-accepted that there is a trade-off between process yield and product purity in ultrafiltration of viral stream.[2,5] Virus loss in membrane-based processes could happen because of either inactivation or physical disruption of virus particles,[10] specific or non-specific virus particle adsorption,[11,12] virus particles aggregation and complex formation with impurities,[13] and virus particle entrapment in the membrane pores.[10,14] Therefore, virus recovery from membrane-based processes in either mode of operations

(i.e. dead-end filtration and tangential-flow filtration) and any format is mainly dependent on:[3,4,15,16]

- Membrane properties

  Pore size, material, structure, hydrophobicity and hydrophilicity, surface charge

- Characteristics of feed solution

  pH, salt concentration, virus particle size, virus solution size distribution, shape, surface charge, surface functional groups, virus concentration, virus particle aggregation behavior

- Process parameters

  Flow rate or flux, temperature, transmembrane pressure, shear stress through process and near membrane surface

The key parameters in the ultrafiltration of the virus stream are the membrane's MWCO and TMP, and the fluxes of the permeate and retentate.[3] High shear stress is inherent to the ultrafiltration process and can cause virus infectivity loss and/or virus particle disruption. To avoid virus loss due to shear stress, TMP and fluxes should be optimized so that virus particles are subjected to the lowest possible shear. Furiga et al.[17] provide an interesting example of an attempt to achieve this type of optimization. In their study, they used an ultrafiltration process (hollow fiber, cellulose triacetate, MWCO 100 kDa) to purify MS2 phages and found that the phage particles in PBS were prone to shear stress during filtration. However, while no infectious phages from the PBS sample were detected after just 40 minutes of filtration, there was no significant loss when MS2 phages in tap water were concentrated using the same filter configuration. Furiga et al.'s study clearly shows how solution condition (pH and salt) strongly affects the virus' susceptibility to shear stress.

An ultrafilter's MWCO should be selected based on the molecular weight of the target virus particles and the expected sizes of the impurities such that virus particles will be retained on the membrane surface and smaller particles will be allowed to pass through. Table 2.1 shows how nominal molecular weight (NMW) affects processing time and virus recovery. In this report, the authors use NMW, as it is equivalent to MWCO

Table 2.1. Effect of membrane NMW on Adenovirus recovery through tangential flow filtration;[18] Copyright © 2008 American Institute of Chemical Engineers (AIChE)

NMW (kDa)	Process Time (min)	Infectious Adenoviruses (IP) in Retentate	Infectious Adenoviruses (IP) in Permeate	Recovery* Yield of Infectious Adenoviruses (%)
750	20	3.0×10^9	2.9×10^9	42
500	45	6.0×10^{10}	2.2×10^9	71
300	67	1.5×10^{10}	1.2×10^6	96

Smaller MWCO is preferred to retain virus; however, smaller pore size causes higher TMP readings and lower fluxes, which in turn results in longer operation time and it is not desirable for some sensitive and labile virus particles. On the other hand, larger pore size if not causing the virus to permeate, it might cause the virus to be entrapped on the membrane surface pores and would be a start point for membrane fouling.

Membrane fouling is an undesirable phenomenon happened by adsorption or deposition of particles inside or on membrane.[14,19] Membrane fouling inevitably leads to decrease in the efficiency of filtration processes, a dramatic increase of transmembrane pressure (TMP) or severe decrease of flux, which adversely affect membrane permeability, requires frequent membrane replacements, and lead to

dramatic loss of valuable product.[20,21] For practical applications, investigating the fouling mechanism of the feed solution through the desired membrane-based process is critical. Membrane fouling incident still being reported strongly underlines the lack of knowledge of the filtration unit operation for biologics.

Mechanism of membrane fouling is classified as cake formation, standard blocking, complete blocking, and intermediate blocking.[22] A schematic of different fouling mechanisms is shown in Fig. 2.1.

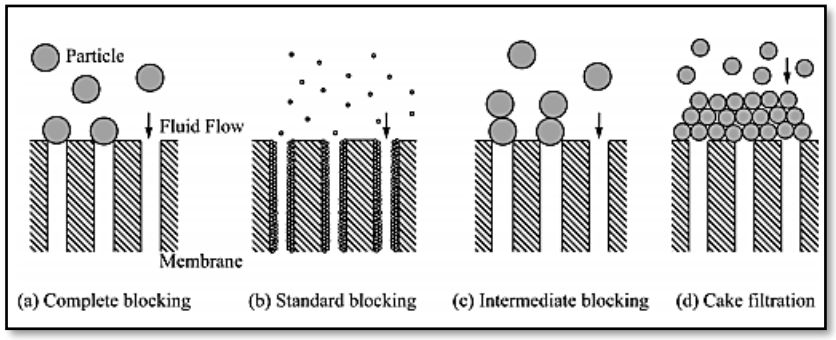

Fig. 2.1. Schematic illustration of different fouling mechanisms;[16] reprinted with permission, Copyright© 2013 Taylor & Francis.

- **Cake formation:** this blocking model assumes that the virus particles will be larger than the membrane's pore size, or that there will be a repulsive interaction between the particles and the membrane surface. The latter condition will lead to the formation of a permeable layer of foulant on membrane surface.[23] In this condition, the particles continue to accumulate on the layer, consequently increasing cake-layer thickness, which in turn causes a dramatic increase in membrane resistance and flux-rate reduction.[22]

- **Standard blocking (pore constriction):** this blocking model assumes particles are much smaller than the membrane pore size or particles are deformable to get into the pores;[22] the particles accumulate on the pore wall (through specific or non-specific interactions), constrict the pores, significantly reduce the available cross-sectional area for flow, and decrease membrane permeability.[16] It was also shown that the membrane fouling is not just because of primary deposition of small particles on pore wall. It is mainly because of secondary deposition, a build-up of small particles on already deposited ones on the pore wall.[24]

- **Complete blocking:** this blocking model assumes that particles size distribution is at the same range of the membrane pore size. As filtering such a solution, particles will deposit on the pore and either partially or totally block the pore. This model assumes total blockage of the pore entrance over time which contributes to cake layer formation due to the accumulation of foulants.[16] The latter leads to severe TMP increase (at constant flux operations) or flux decrease (at constant pressure operations).[22]

- **Intermediate blocking**: this blocking model is similar to complete blocking mechanism; however, it assumes that particles partially blocking the pores. Meanwhile, the other particles are accumulating on already deposited particles [23] which means the first deposited particle acts as a nucleation point for deposition of other particles.

For example, Wickramasinghe et al.[10] reported a rapid drop of permeate flux during the concentration of human Influenza A virus at first cycle using flat sheet microfilter

(flat sheet, polyethersulfone, 0.45 μm). The authors hypothesized that the latter behavior was because of internal fouling of membrane pores due to deposition of virus particles as well as aggregated virus particles. It is worth noting that an individual mechanism or combination of them could happen through the filtration of a specific fluid stream. Mathematical models for individual and combined blocking models under either constant flux or constant transmembrane pressure for both Newtonian and non-Newtonian fluids have been developed.[16,23,25]

2.1.2. Chromatography-Based Purification Processes

Chromatography purification processes are preferred to membrane-based ones due to achieving the desired purity of the product in more consistent and safer ways.[26] Separation by chromatography-based processes is applied based on the differences in interactions of different particles in the liquid phase with stationary phase in the column. Separation mechanisms used in chromatography-based processes are described below and shown in Fig. 2.2.

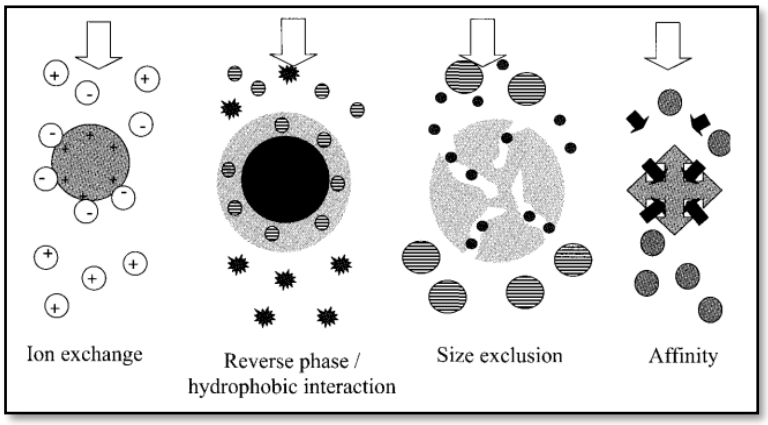

Fig. 2.2. Separation mechanisms in chromatography-based processes;[19] Copyright© 2006 by World Scientific Publishing Co. Pte. Ltd.

Size Exclusion Chromatography (SEC)

The separation mechanism is based on differences in diffusivity of the particles into the pores through the gel. Smaller solute particles, due to their size, can enter pores of solid stationary phase while larger particles are being excluded from these pores. Therefore, smaller particles spend more time inside the column and appeared later. Size exclusion columns are marketed based on the size range of particles that they can resolve. There is a direct relationship between the efficiency of separation and the length of the column, where longer column results in better separation. In addition, SEC is limited to relatively low flow rates to ensure proper separations, which makes the SEC impractical for industrial-scale.[27]

Ion-Exchange Chromatography (IEC)

The separation mechanism in IEC relies on differences in electrostatic interactions of solute particles with the stationary phase. The stationary phase could be functionalized with either positively or negatively charged functional groups, where particles with opposite charge will interact and bind to the stationary phase. Common functional are quaternary amine (QA, positively charged), diethylaminoethanol (DEAE, positively charged), and sulfuric anhydride (SO_3, negatively charged).

Hydrophobic Interaction Chromatography (HIC)

HIC separates particles based on differences in hydrophobicity whereby particles with less hydrophobicity are released from the column first, with higher-hydrophobic particles being eluted later in the process. The functional groups most commonly used

for HIC are the butyl, phenyl, hexyl, octyl groups. Particle binding is mediated by the presence of anti-chaotropic salt, which is composed of anions and cations selected from the well-known Hofmeister series (shown in Fig. 2.3). Since the hydrophobic interaction is considered to be a strong interaction, the ligand type and density should be selected carefully in order to avoid a loss of virus infectivity.[3] In addition, binding conditions with high concentrations of anti-chaotropic salt might be destructive for labile virus particles; thus, it is important to monitor the stability of viral vectors when such conditions are present. For example, hexyl and octyl ligands are strongly hydrophobic, which means their use should be avoided when the production of intact viruses is desired.

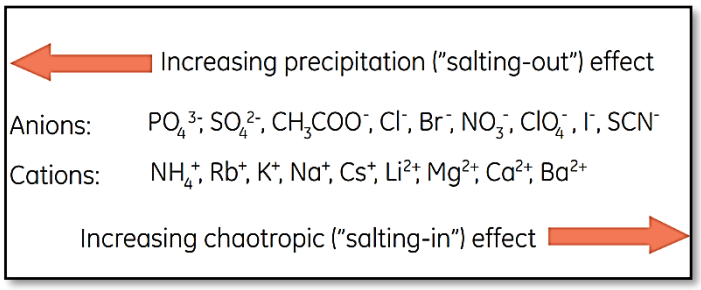

Fig. 2.3. Hofmeister's series [28]

Affinity Chromatography (AC)

The principle is based on a reversible affinity interaction between target virus particle and a specific ligand immobilized on the column matrix. The ligands could be metal-ion affinity, specific antibodies, fragments of antibodies, peptide, etc. Ligands themselves could be cation or anion exchanger.[3] Often, virus recoveries from affinity columns are challenging due to multivariant interactions between the virus particle and the ligand. Having more interactions requires stronger elution condition, which could

result in virus infectivity loss.[29] On the other hand, highly-cost affinity columns exhibit low stability for harsh column sanitizing methods. Thus, affinity chromatography is not an economic option for industrial-scale processes.[30] Examples of commercial affinity columns are Matrex Cellufine Sulfate resin (Millipore) and Heparin-Sepharose resin (GE Healthcare).

Beside different separation mechanisms, different types of columns are also being used for chromatography separations. The most common ones for preparative chromatography are a packed-bed column, membrane adsorber, and monoliths that are shown in Fig. 2.4 and further discussed in detail in upcoming sections.

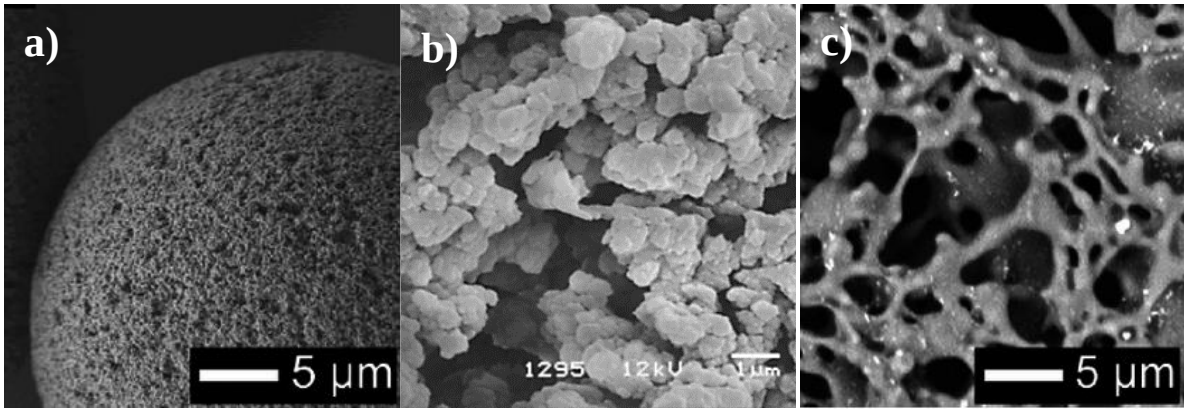

Fig. 2.4. SEM image of a) Fractogel EMD TMAE HiCap packed-bed resin;[31] Copyright© 2014 Elsevier; b) CIM monolithic column,[32] c) Sartobind S cellulose membrane;[31] Copyright© 2014 Elsevier.

2.1.2.1. Packed-Bed Columns

These columns are packed with spherical or non-spherical porous particles with defined size distribution as well as pore size.[33] SEM image of a resin particles is shown in Fig. 2.4a. Resin particle with the mean diameter of <10 µm is being utilized for high-

resolution application whereas mean diameter >50 µm for industrial application in biotechnology.[34] The size range of pores in resins is 10 to 100 nm, although specific resins with larger pores are also available (~ 400 nm). Larger particles cause less pressure drop but also have low binding capacity while smaller particles exhibit higher efficiency but causes higher resistance to mobile phase flow. Table 2.2 shows some examples of virus purification using resin-based column chromatography.

Table 2.2. Examples of resin-based chromatography for purification of viruses

Virus	**Enveloped/ non-enveloped**	**Size (nm)**	**Host**	**Tested Columns (Volume)**	**Ref.**
Ad	Non-enveloped	90	293 & PER.C6	Q Sepharose XL, Source 15 Q, Q Fractogel FF & HP, Fractogel TMAE	[35]
Human Influenza A Virus (H1N1)	Enveloped	80-120	MDCK	Sepharose 4FF (SEC), Q Sepharose XL (IEC)	[27]
Ad	Non-enveloped	90	-	Q Sepharose XL, PL-SAX400nm	[36]
VSV	Enveloped	70×170	293	Poros HQ-50	[37]

The main disadvantage of resin-based columns is that the mass transfer occurs through diffusion. Resin-based columns were mostly designed for small biomolecule's purifications such as proteins (size <10 nm). These columns are impractical for large biomolecules such as viruses due to large particle sizes and complex molecular surfaces, which is resulting in low accessible binding capacities and low particle diffusion rates.[18,38–40] A study by Ljunglöf et al. [41] demonstrated that labeled plasmid DNA (6.3 kbp) adsorbed mainly to the outer surface of Q Sepharose XL resin (45–165 µm) and the interior of the resin particles was remained empty. Similarly, Trilisky and Lenhoff [36]

demonstrated that the binding capacity of Ad 5 on Q Sepharose XL (pore size of 12 nm) was about 50 times lower than bovine serum albumin (BSA), for which the static binding capacity is more than 100 grams per liter. In addition, the static binding capacity of Ad 5 on PL-SAX with the pore size of 400 nm was an order of magnitude lower than BSA on Q Sepharose XL with the pore size of 12 nm.[36] In addition, resin-based chromatography is limited in scaling up by mechanical factors such as bed instability and inherent constraint of low flow rates.[42] Packing columns with resins is also challenging [43] and packed-resins are susceptible to be fouled.[44] Thus, scale-up purification of 'large' biomolecules such as viruses with a high concentration in stocks became challenging for resin-based columns.[34]

"Tentacle" technology is a version of traditional resin-based columns that has been improved via the addition of functional polymeric branches, or "tentacles." In addition to allowing for multipoint target attachment,[45] this technology also enables increased selectivity and binding capacity. The high flexibility of the polymeric branches improves target attachment in the "tentacle" column in terms of uptake amounts and time requirements, which in turn leads to a lower steric hindrance effect and, consequently, improved diffusion.[46] The Fractogel DEAE column is the most extensively used "tentacle" column, with its use having been documented for Ad purification.[47,48] Segura et al.[43] performed hydrophobic interaction chromatography using 'tentacle' Fractogel propyl resin to remove contaminating proteins from Canine Ad vectors with high virus recovery of 88%. Urmann et al. [46] also developed a new 'tentacle' cation exchange column Eshmuno™ S (Particle size of 85 µm, GE Healthcare) and compared its functionality in the binding of monoclonal antibody to 'tentacle' Fractogel S (Particle size of 65 µm, EMD Millipore). Fig. 2.5 demonstrates the confocal

microscopy images of Fractogel EMD uptake compared to Eshumuno™, showing that even among 'tentacle' columns one could show superior performance. Dynamic binding capacity of Eshumuno™ and Fractogel for polyclonal hIgG were reported as 80 mg/mL and 60 mg/mL in 2 minute residence time, respectively.[46]

Commercial resins and pre-packed bed columns are available at different sizes and chemistries by various manufacturers such as GE Healthcare, BioRad, Pall, Sigma Aldrich, Tosoh, Mitsubishi, and Dow.

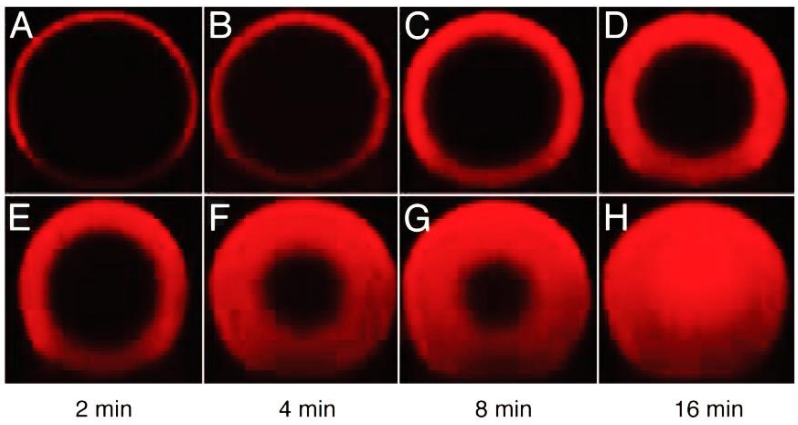

Fig. 2.5. Confocal microscopy image, uptake performance of monoclonal antibody by 'tentacle' Fractogel (A-D) compared to Eshumuno™ (E-H);[46] Copyright© 2010 Landes Bioscience.

2.1.2.2. Monolithic Columns

SEM image of the monolithic matrix is shown in Fig. 2.4b. Monolith features a continuous stationary phase with a network of interconnected large pores.[38,49] Monoliths have two main types of pores called flow-through pores (on average 1.7 µm) and mesopores (2-50 nm).[50] The schematic comparison of the resin-based column with monolithic column was shown in Fig. 2.6. In contrast to the resin-based columns, mass transfer in monoliths are convective, owing to large flow-through pores.[34,51] Monolithic

column enables fast separations (i.e. in short time) with a laminar flow of mobile phase as well as operating with lower back pressure owing to mesopores, even at relatively high flow rates.[38,49] Reducing the chromatography process time could result in higher virus recoveries and less aggregation.[38] Rupar et al. [52] demonstrated that the overall purification procedure of Potato virus Y was reduced by more than half using monolithic columns compared to traditional centrifugation method.

Moreover, Bandeira et al.[53] performed lentiviral vector purification and reduced processing time from 5 days for gradient ultracentrifugation to 3 hours for the monolithic column (CIM® DEAE). Although monoliths have a lower absolute surface area compared to the resin-based column, it has a higher binding capacity for larger biomolecules, owing to the porous structure (as shown in Fig. 2.6).[49] A study by Burden et al. [39] revealed that binding capacity of the monolithic column (CIM® OH) for virus-like particles (VLPs) based on Hepatitis B was about 3-4 times higher than binding capacity of resin (Sepharose FF, Butyl-S 6), shown in Fig. 2.7. The dynamic binding capacity of monolithic CIM® OH column (1 mL, BIA Separations) for the VLPs was reported to be 11 mg/mL. The binding capacity of CIM® columns from BIA is theoretically 2×10^{12} virus particles per mL of the column.

Another advantage of monolithic columns for viral vector manufacturing is ease of scale-up;[49] the monolithic column manufactured by BIA separations are commercially available from 1 mL to 8 L. A further advantage is using monolithic columns eliminate the problems associated with column packing with resins.[43,45]

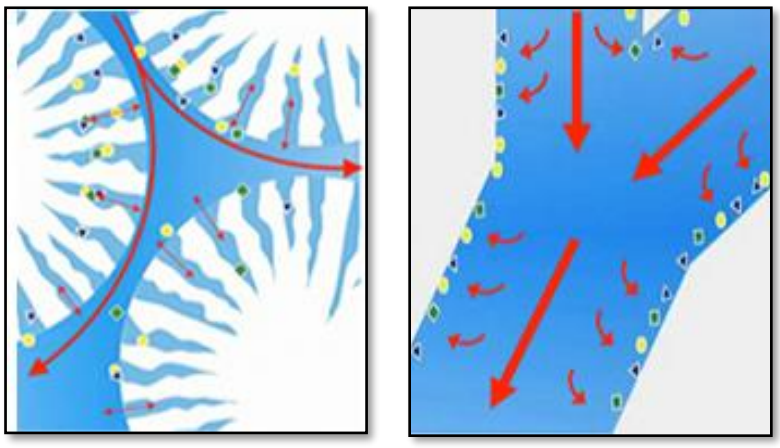

Fig. 2.6 Schematic comparison of a) Resin-based column and b) monolithic; Reprinted from Showa Denko (http://www.sdk.co.jp)

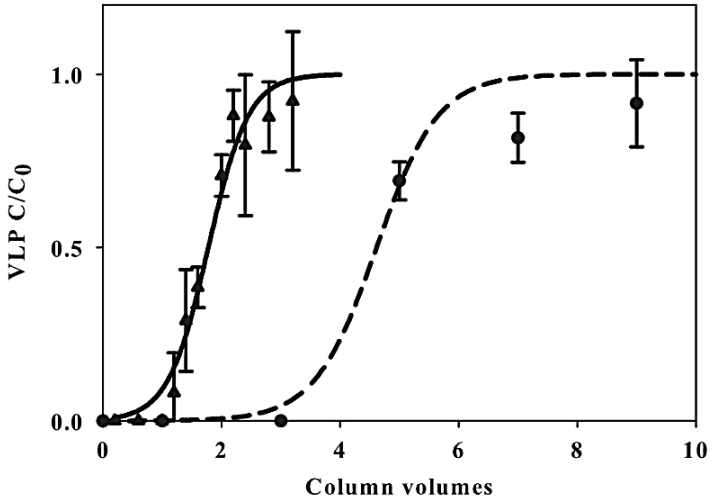

Fig. 2.7 Comparison of dynamic binding capacities of CIM® OH column (BIA Separations, 1 mL, ▲) versus Butyl-S 6 Sepharose S FF (GE Healthcare, 1 mL, ●) for VLPs;[39] Copyright© 2012 Elsevier.

Ion-exchanged and hydrophobic interaction monolithic column chromatography for purification and concentration of virus and VLPs were summarized in Table 2.3 and 2.4, respectively. As shown, monolithic chromatography has been examined for both enveloped and non-enveloped viruses with large sizes such as Vaccinia Virus.[54] As an example from Table 2.3, Gerster et al. [55] purified Baculoviral from cell culture using anion-exchange monolithic column (CIM® QA) with results showing a reduction of

the handled volume by 82-fold and increase in titer by 51-fold, while removing 99% of host cell contaminant.

Monoliths are commercially available in different materials, chemistries, shape, and sizes. It is worth noting that monolithic columns can be applied for any separation mechanism except size exclusion chromatography. Table 2.5 summarizes commercially available monolithic columns. Silica-based columns are mostly designed for HPLC, with analytical and semi-prep working scales, and typical pore size of 2 µm. For example, Onyx® columns from Phenomenex (CA, USA) is available both in 150 mm×0.1 mm (analytical) size as well as 150 mm×10 mm size (semi-prep) with the volume of 1 mL per gram of monolith. However, polymeric-based monoliths are available in analytical, preparative, and industrial scales. For example, monolithic columns from BIA Separations (Ljubljana, Slovenia) is available in the size range of 0.1 mL for analytical purposes (CIMac®) as well as with large volume ranges from 1mL to 8L (CIM®). It is worth noting that Agilent Technologies Inc. (CA, USA) is marketing monolithic columns from BIA Separations under the trade name of Bio-monolith®.

Table 2.3. Monolithic Ion-exchanged column chromatography for purification and concentration of virus and virus-like particles (VLPs)

Virus	**Enveloped/ Non-enveloped**	**Size (nm)**	**Host Cell**	**Tested Columns (Volume)**	**Ref**
Rotavirus	Non-enveloped	80	-	CIM QA, SO_3 (0.34 mL)	56
Rhinovirus	Non-enveloped	30	HeLa-H1	CIM DEAE (1 mL)	57
Lentiviral Vectors	Enveloped	80-100	HEK 293T	CIM DEAE (-)	53
Influenza A and B	Enveloped	80-120	VERO	CIM QA, DEAE, SO_3 (0.34 & 8 mL)	58
AAV 8	Non-enveloped	25	HEK293	CIM QA	59

				(0.34 mL)	
Human Influenza virus A (H1N1)	Enveloped	80-120	MDCK	CIM QA (0.34 mL)	60
Rubella virus	Enveloped	60	MRC-5	CIM QA, SO_3 (0.34 mL)	38
Baculoviruses	Enveloped	21×260	*S. frugiperda*	CIM QA, DEAE (1 mL)	55
TMV	Non-enveloped	18×300	*N. clevelandii*	CIM QA (0.34 mL)	61
Ad 5	Non-enveloped	90	HEK293	Bio-Monolith QA (0.1 mL)	62
Enterovirus 71	Non-enveloped	30	Rhabdomyosarcoma	CIM DEAE (8 L)	40
Flavivirus	Enveloped	50	BHK	CIM QA (0.34 mL)	63
Bacteriophage T4	Non-enveloped	86×120	*E. coli*	CIM QA (0.34 mL)	64
Potato Y virus	Non-enveloped	11×740	*N. tabacum, S. tuberosum*	CIM QA (0.34 mL)	52
Turnip yellow mosaic virus	Non-enveloped	30	*Brassica rapa*	CIM QA, DEAE (0.34 mL)	65
Tomato bushy stunt virus		24-34			
TMV		18×300			
VLPs (Ad 3)	Non-enveloped	~90	*S. frugiperda* Sf21	CIMac QA, DEAE, EDA, SO_3	66

Table 2.4. Monolithic hydrophobic Interaction column chromatography for purification of virus and VLPs

Virus	**Enveloped/ Non-enveloped**	**Size (nm)**	**Host**	**Tested Columns (Volume)**	**Ref**
VLP (HBsAg)	Enveloped	30-35	Recombinant *S. cerevisiae*	CIM OH, C4 (0.34 mL)	39
Mumps virus, Measles virus	Enveloped	150	VERO	CIM QA, SO_3, DEAE, OH (0.34 mL)	67
Orthopoxvirus vaccinia virus Lister strain	Enveloped	200×250	CV-1	CIM QA, SO_3, DEAE, OH (1 mL)	54

Table 2.5 Summary of commercially available monolithic columns

Monolith	Material	Manufacturer/Supplier	Trade Name	Available Chemistry
Inorganic	Silica	Phenomenex	Onyx®	HIC
		Millipore	Chromolith®	HIC
Organic	Polymethacrylate	BIA separation	CIM®	IEX HIC Affinity
		Agilent Technology Inc.	Bio-monolith®	IEX Affinity
	Polystyrene	Dionex	PepSwift® & ProSwift®	IEX HIC Affinity
	Polyacrylamide	BioRad	Uno®	IEX

2.1.2.3. Membrane Adsorbers

SEM image of a membrane adsorber is shown in Fig. 2.4c. Membrane chromatography is a combination of features of membrane filtration with column chromatography, benefiting from high throughput while performing the separation. Membrane adsorber possesses similar characteristics as the monolith, enabling convective mass transfer, high flow rates, and short processing time. Interests in membrane chromatography are growing, owing to the high capacities in manufacturing membranes in any desired formats.[68]

Duffy et al.[69] reported the purification of Ad using Adenopure™ kit, based on membrane chromatography, in about 3 hours whereas CsCl purification requires 1.5 days. The authors also performed AAV purification using ViraKit™ in 2.5 hours compared to iodixanol gradient and heparin affinity column purification method with a duration of 5 hours.[69] Peixoto et al. [18] also purified Ad using Sartobind Q and Sartobind anion direct (both 2.5 mL, Sartorius) with high recoveries up to 62% and high DNA

removal (~97% after optimization). Later, scaled-up purification with Sartobind anion direct (25 mL, 900 cm^2) was conducted with successfully similar infectious Ad recovery.[18] Examples of virus purification using membrane adsorbers were summarized in Table 2.6.

Membrane adsorber suffers from non-uniform axial dispersion, which leads to broad peaks.[3,68] In addition, eddies can be formed in membrane chromatography, which could result in reduced dispersion and consequent lower binding capacities.[3] Eddies could cause infectivity loss for labile virus particles.[3] In a study by Bandeira et al. [53], it was shown that the recovery of infective lentivirus, a well-know fragile virus model, from monolithic column (CIM® DEAE, ~55%) was approximately 2-times higher than membrane adsorber (Sartobind® D, ~28%). The authors obtained 80% lentiviral vector recovery from CIM® DEAE (no information on column volume) after optimization [53], which was reported to be 10% more than the recovery from Mustang® Q capsule.[70]

Membrane adsorbers were traditionally manufactured in the format of a flat sheet, hollow fiber, and radial-flow devices.[44] The advantage of hollow fiber membrane chromatography is high surface area and consequently high binding capacities.[3] The most common format of membrane chromatography is stacking flat sheets of membranes for providing a larger area. Nowadays, it is commercially available in flat-sheet format by Pall Corporation and Sartorius.

Table 2.6. Examples of membrane chromatography for purification of viruses and VLPs

Virus	Enveloped/ Non-enveloped	Size (nm)	Host Cell	Tested Columns (Volume)	Ref
Vesicular Stomatitis Virus	Enveloped	70×170	Vero, HEK 293, CHO, BHK	Sartobind™ Q, Mustang Q	6
Lentivirus	Enveloped	80-100	HEK 293T	Sartobind™ Q	53
Adenovirus	Non-enveloped	~90	HEK293	Sartobind™ Q (2.5 mL), Sartobind™ anion direct (2.5&25mL)	18
Rotavirus VLPs	Enveloped	75-85	*S. frugiperda* Sf9	Sartobind™ D	71
Influenza VLPs	Enveloped	80-120	MDCK.SUS2	*Sulfated cellulose membrane, Sartobind Pico S & Q	72

* Reinforce cellulose membrane was purchased from Sartorius and later modified.

In conclusion, factors that should be considered for a successful chromatography-based purification of viral vectors are:[34,49]

- Viral vector sample

  Virus concentration, virus particles size distribution, virus charge (or isoelectric point), virus particles aggregation tendency, virus particles hydrophobicity, virus stability

- Stationary phase

  Morphology (resin, monoliths, etc.), surface area, pore size, porosity, ligand chemistry, ligand density, mechanical properties, scalability, etc.

- Liquid phase

  Mobile phase composition, pH, salt concentration

- Mode of operation

Isocratic elution, gradient elution, counter-current operation (in simulated moving bed)

- Column and system hardware

  tubing, valves, sampling, flow distribution, pressure, etc.

2.2. Virus Particle Aggregation and Its Impacts on the Downstream Processing of Viral Vectors

Although researchers began studying aggregation in the 1950s, this phenomenon remains poorly understood and continues to be viewed as one of the main challenges in biotherapeutic manufacturing.[73] Aggregated particles can cause complications and inconsistencies in DSP rounds, which can in turn lead to dramatic viral vector loss and reduced yields.[13,74] both in the filtration process and during the virus-purification step [75]. Furthermore, the presence of aggregated virus particles prior to membrane-based processes often causes pore blockage and a consequent rise in transmembrane pressure or a decline in flux, which are obvious signs of membrane fouling. On the other hand, aggregated viral particles affect bio-distribution following *in vivo* administration, which results in unwanted inflammatory immune responses and may even reduce vector-transduction efficiency.[74] Given the broad consensus on the undesirability of virus-particle aggregation, it would be prudent to gain an understanding of the aggregation behavior of virus particles so that methods can be developed that address the challenges associated with viral-vector manufacturing.[76]

It is believed that both electrostatic and hydrophobic interactions play a role in the formation of virus aggregates.[73] The different factors that affect virus aggregation can

be classified into three main groups: biological factors, physicochemical factors, and operational factors. It is worth noting that virus aggregation/disaggregation is not affected/induced/prohibited by any single factor; rather it is the sum of the effects of the interactions between these factors.

2.2.1. Biological Factors

Biological factors refer to cell type that has been used for virus proliferation as well as virus particle characteristics. Each factor is extensively explained in below.

Cell Type and Cell-related Impurities

Viral aggregates may originate from the cells, released as aggregated particles upon cell lysis, which is referred to intercellular virus aggregation.[77] Type of cell line and virus strain are important factors affecting intercellular virus aggregation. In addition, impurities from the host cell such as cell debris [78] and nucleic acid could result in the formation of aggregated virus particles.[13] For example, complex formation of virus particles with nucleic acid and later aggregation formation was reported for Ad,[79] AAV, [74] and VV.[54] Fig. 2.8 shows TEM image of DNA-VV complex.

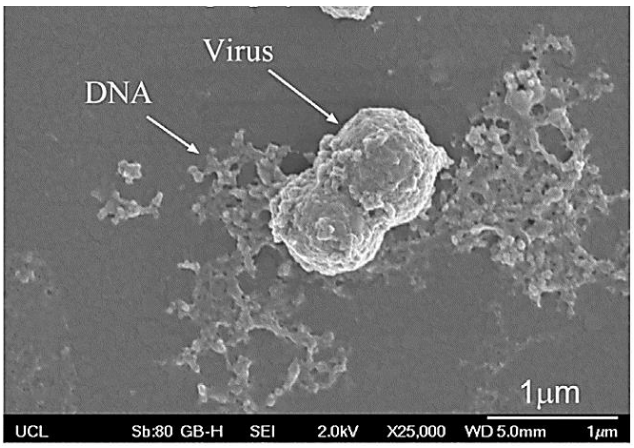

Fig. 2.8. TEM image of VV and DNA residual complex;[54] Reprinted with permission; Copyright© 2017 Elsevier.

Virus Particle

Factors such as virus surface structure,[80] virus hydrophobicity,[81] virus concentration,[82–84] the presence of aggregates,[84] virus size and shape,[85] and virus particle charge [76] could affect the virus aggregation behavior.

Surface structure like fibre prevent aggregation due to the steric hindrance.[80] Virus concentration establishes the collision rate of particles, and the presence of aggregated particles favors more aggregated particles formation, similar to polymerization kinetic.[84]

Isoelectric point (IEP) is the pH value that virus's net charge is zero (i.e. mobility is zero). pH values higher than IEP result in the net negative charge, while pH values lower than IEP cause the net positive charge (shown in Fig. 2.9). IEP of the viruses are most frequently between 3.5 and 7.0.[86] Previously, it was suggested that IEP could be predicted based on external surface proteins on the virus surface; however, more recently, it has been shown that there is a significant difference between experimental

IEP and calculated ones. One reason could be that virus particles are not rigid solid particles, they are soft (i.e. permeable) with multilayered structure; thus, inter-particle structure and chemical contribution (e.g. RNA) is also affecting the net charge, mobility and consequently IEP.[76,87] Viral particle's charge plays a significant role in viral aggregation behavior (Further explanations in Section 2.2.2). Noteworthy, the virus solution conditions such as salt type and concentration could slightly affect the net charge and consequently IEP.[80] Examples of studies on IEP of viruses under different solution conditions were summarized in Table 2.7.

Hydrophobic interactions are strong interactions, which could strongly influence virus solution's size distributions. Virus particles strongly tend to aggregate in the presence of hydrophobic interactions. Langlet et al. [81] demonstrated the effect of hydrophobic interaction on virus aggregation by comparing the aggregation behavior of four different bacteriophages (MS2, Qβ, SP, and GA). MS2 phage aggregation was not observed in pH values higher than IEP (pH > 3.9) at high salt concentrations (100 mM $NaNO_3$). On the other hand, SP and GA aggregated in the whole pH range of 1.5-7.5 and ionic strength of 1-100 mM $NaNO_3$. The authors concluded that SP and GA aggregation behavior is because of their higher surface hydrophobicity compared to MS2 phage.[81] Similarly, it was shown that aggregation of Norwalk VLPs was due to hydrophobic side-chains on the particle surface, for which exposure to polar solvent promoted Norwalk VLPs aggregation to lower interaction of those hydrophobic side-chains with polar solvent.[88]

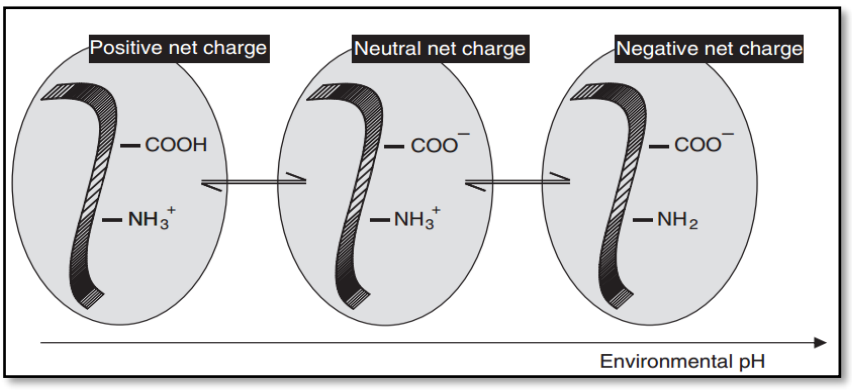

Fig. 2.9. Protonation states of functional group on virus surface as a function of pH;[86] Copyright© 2010 The Society of Applied Microbiology.

Table 2.7. Salt concentration effects on IEP of virus particles

Virus	Salt Type	Tested Salt Conc.	IEP Changes*	Ref.
MS2	$NaNO_3$	1, 100 mM	Elevated	81,87,89
Qβ	$NaNO_3$	1,100 mM	Decreased	81
GA	$NaNO_3$	1, 100 mM	Elevated	81
SP	$NaNO_3$	1,100 mM	Elevated	81
Reovirus III	NaCl	1, 10, 100 mM	Unaffected	90
Ad	NaCl $CaCl_2$	1, 10 mM 1, 3 mM	Elevated	80

*The IEP value was either elevated, decreased, or unaffected by increasing the salt concentration (10 and 100 mM) compared to low salt concentration (1 mM)

2.2.2. Physicochemical Factors

Physicochemical factors are the ones related to virus solution conditions such as salt type (monovalent, divalent, etc.),[83,91] ionic strength,[81,91] pH,[81,83,89,92,93] and additives [74,85] that are affecting virus aggregation/disaggregation behavior. Aggregation behavior of Poliovirus,[94] Reovirus,[94] Human Ad,[80] Ad,[36] MS2 phage,[76,83,95] GA, Qβ, and SP phages,[81] Influenza virus [96] at various solution conditions such as different pH values and/or salt types and concentrations were studied. It was shown that decreasing the pH

to the values close or below the viral IEP results in aggregation.[80,89,91] Often, aggregation is irreversible in the pH values lower than IEP.[83]

Ionic strength is the combinational effects of co-ions and counter-ions in the electrostatic double layer around the virus particles, defining particles mobility and consequently zeta potential (shown in Fig. 2.10). The classic theory of Derjaguin, Landau, Verwey, and Overbeek (DLVO) could be utilized to describe virus particles distribution and adsorption behavior by considering Van der Waals and electrostatic interactions. According to DLVO, higher salt concentration compresses the electrostatic double layer and reduces the zeta potential value and consequently favoring particle aggregation.[89]

It was shown for Qβ phage that increasing salt concentration induces aggregation.[81] In addition, Wong et al. [80] demonstrated that at pH 7.0, the hydrodynamic size of Human Ad was ~100 nm and ~150 nm, measured in either 1 mM or 100 mM NaCl along with the zeta potential values of -24.5 and -7.0 mV, respectively. On the other hand, it was shown for Poliovirus, Reovirus, and Adenovirus that high concentration of salt inhibits their aggregation.[84,92,94] Mattel et al. [83] also demonstrated that high phosphate concentration inhibited MS2 phage aggregation even at low pH values. Moreover, aggregation of AAV was achieved by ionic strength > 200 mM.[74] As discussed, it seems that the effects of salt concentration is not fully understood.

In addition, it was shown that cations are more effective in decreasing aggregation compared to anions regardless of the virus net charge.[91] Furthermore, at pH values higher than IEP, divalent cations could shield virus surface charge more effectively than monovalent cations.[80] Similarly, multivalent ions such as magnesium sulfate require

lower concentrations compared to monovalent ions such as sodium chloride to prevent aggregation of AAV2.[74]

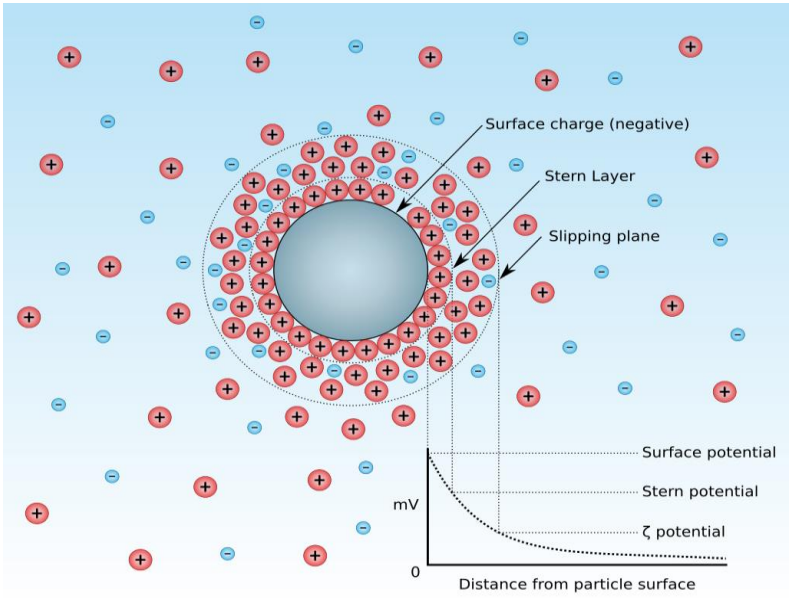

Fig. 2.10. Schematic of charge distribution around negatively charged particle, electrostatic double layer and different potentials;[97] Copyright CC BY-SA 3.0

One interesting topic in the area of virus aggregation is additives, being used with the aim of preventing virus particle aggregation. Konz et al. [13] demonstrated that polysorbate 80 (1% v/v) could reduce the unwanted complex formation between Ad and host cell DNA, and consequently control/prevent aggregation formation. Wright et al. [74,98] also examined a broad range of additives to avoid AAV aggregation. List of some of the examined additives for AAV is shown in Table 2.8. Neither tested sugars nor emulsifiers showed any inhibition of aggregation even at high concentrations. In contrast, amino-acids namely, Lysine, Aspartic acid, Glutamic acid, prevent virus aggregation at higher concentrations (300-320 mOsm).

Table 2.8. Additives examined for AAV2 aggregation prevention; reproduced with selection in the original reported excipients from Reference;[74] Copyright© 2005 Elsevier

Excipient	Maximum tested osmolarity (mOsm)
Arginine	NIA (200 mOsm)
Aspartic Acid	320 mOsm
Glutamic Acid	320 mOsm
Glycine	NIA (200 mOsm)
Histidine	NIA (200 mOsm)
Lysine	300 mOsm
Glycerol	NIA (5% w/v, 543 mOsm)
Iodixanol	NIA (5% w/v, 32 mOsm)
Mannitol	NIA (5% w/v, 275 mOsm)
Sorbitol	NIA (5% w/v, 275 mOsm)
Sucrose	NIA (5% w/v, 146 mOsm)
Trehalose	NIA (5% w/v, 146 mOsm)
Pluronic F68	NIA (10% w/v, 12 mOsm)
Polysorbate 80	NIA (1% w/v)

*NIA: no inhibition of aggregation

In another study, Kissmann et al. [88] examined effects of various additives on stabilizing Norwalk VLPs such as sugars (e.g. sucrose, trehalose, sorbitol, mannitol, lactose, and dextrose) as well as chitosan. It was observed that thermal stability of VLPs were increased in the presence of sucrose (20% w/v), trehalose, and chitosan (0.5% w/v) due to stabilization of secondary and tertiary structural elements; the stabilization most probably related to shielding hydrophobic side-chains from polar solvent.[88]

Glycerol is one of the most common additives for aggregation prevention. For example, for AAV2, it was shown that high concentration (25%) could be effective even at high virus concentrations such as about 10^{14} virus particles per mL [99] while its low concentration such as 5% couldn't prevent aggregation.[74] On the other hand, Wang

et al. [100] reported that low concentration of glycerol (about 3%) is effective on prevention of AAV2 aggregation while depositing on mica. Mesthrige et.al. [85] also reported TMV aggregation while depositing on mica, which was observed to be happened as side-to-side and head-to-head aggregations. The authors demonstrated that BSA molecules could effectively disaggregate TMV particles during deposition, shown in Fig. 2.11.[85] It was shown that BSA was interacting with TMV via hydrophobic patches. The authors hypothesized that the attachment of BSA on TMV resulted in a larger negative charge in total, which resulted in increased electrostatic repulsion between BSA coated TMV particles, and consequent disaggregation of BSA coated TMV particles.

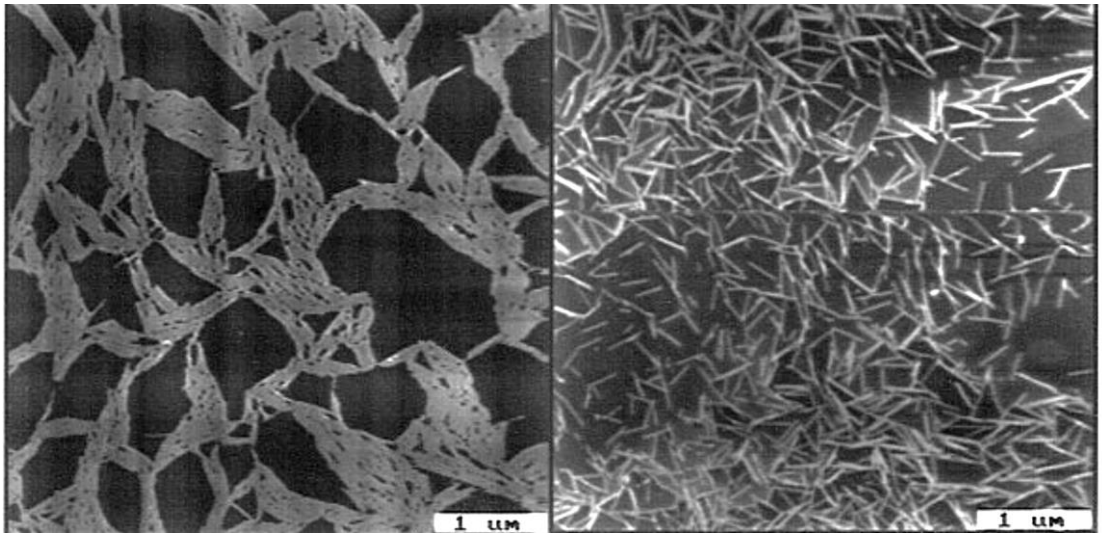

Fig. 2.11. Tobacco Mosaic Virus dispersed on mica; a) aggregation in the absence of BSA b) disaggregation in the presence of BSA;[85] Copyright © 1996 American Chemical Society.

It is worth noting that Armstrong et al. [101] also studied using different polymers such as dextran, polyvinylpyrrolidone, poly(ethylene glycol) over a broad range of

molecular weights (1.5-2000 kDa) as well as albumin and fibrinogen as an additive for studying aggregation/disaggregation of human red blood cells (RBC).[101] It was observed that polymers with hydrodynamic diameter (D_h) < 8 nm inhibited aggregation of RBCs, while polymers with D_h > 8 nm induced aggregation. Interestingly, a similar effect was observed with proteins; addition of proteins such as albumin with D_h ~ 7 nm inhibited aggregation of RBCs, while proteins such as fibrinogen with D_h ~ 22 nm induced strong aggregation in RBCs.[101]

2.2.3. Operational Factors

Operational factors such as purification method,[74,102] temperature,[83,88] contacting materials, flow rates (in case of using pumps), etc. have been shown to influence the viral aggregation state. Dika et.al. [102] demonstrated that MS2 phage purified by method of dialysis aggregated at pH values lower than 4, while MS2 purified by precipitation method (using PEG) demonstrated aggregation at pH values lower than 6. On the other hand, no viral aggregates were observed for the MS2 phage prepared by density-gradient ultracentrifugation. In another study by Wright et al. it was shown that AAV2 purified either by CsCl ultracentrifugation or cation-exchange column chromatography required the same salt condition to prevent/control aggregation.[74] However, AAV2 purified by column chromatography and later subjected to a nuclease digestion step demonstrated lower aggregated particles compared to a case of the purification process with just column chromatography step.[74]

2.3. Characterization of Virus Particles

2.3.1. Virus Particle Quantification

It has been always vital to quantify the number of virus particles. Methods of quantifying virus particles are categorized into two main groups: traditional methods and modern methods. Traditional methods are based on measuring infectivity, while modern methods are based on either measuring viral protein antigens or levels of gene expression, or even directly counting virions. Despite being widely accepted, most traditional methods are time-consuming and labor-intensive, and they are also prone to high levels of variation. On the other hand, modern methods are generally faster and produce more precise results. A discussion of the different viral-counting methods is provided below.

Quantification Based on Infectious Virus Particle

Methods of quantifying infectious virus particles are based on either the tracking of cytopathic effects (CPE)—for example, Plaque Forming Unit (PFU) assays or 50% Tissue Culture Infectious Dose ($TCID_{50}$)—or flow cytometry (FC) methods that detect viral amplification via a reporter gene in the cells. Infectivity assays are the most-trusted methods of viral quantification, but they must be performed by trained personnel. In addition, infectivity assays usually require long incubation times (4-10 days) in order to see CPE effects. On the other hand, PFU and $TCID_{50}$ assays are largely based on the serial dilution of the viral sample, with specific dilutions being selected based on the cell line infection under study.

Quantification Based on Viral Protein and Nucleic Acid

Virus particles can also be quantified by using antibodies, which is an approach that forms the basis of techniques such as enzyme-linked immunosorbent assay (ELISA), immunoblotting, and hemagglutination assays. In contrast, Polymerase Chain Reaction (PCR) assays are based on viral-nucleic-acid detection (RNA and DNA) and can produce quantifications that are either absolute (i.e. copy numbers using a standard curve) or relative. Real-time PCR (i.e. quantitative PCR, which is referred to as qPCR) allows the amplification of DNA to be monitored in real-time during the exponential phase. However, this group of methods faces the drawback of low stringency, which means the detected protein or nucleic acids might not from intact viral particles.[103]

Quantification Based on Physical Number of Virus Particles

The last group of virus-particle quantification methods contains approaches that are based on the physical tracking of virions. These methods are mostly quick and have higher stringency than PCR- and protein-detection-based methods; however, they are still less stringent than CPE-based methods. Most of the methods of this group were adapted from studies on nanoparticles and include approaches such as Transmission Electron Microscopy (TEM), Dynamic Light Scattering (DLS), Nanoparticle Tracking Analysis (NTA), and Tunable Resistive Pulse Sensing (TRPS). These methods are discussed in further detail in the following subsections.

2.3.2. Size Distribution Analysis

Different methods have been reported for studying aggregation of viruses. The most common methods are PFU test [95], Transmission Electron Microscopy (TEM) [76,83,91,94,102,104], and light scattering methods such as DLS [76,80,81,83,102] and Multi-angle Light Scattering (MALS), SDS-PAGE and native electrophoresis, atomic force microscopy, scanning fluorescence correlation spectroscopy [105], turbidity [105], disc centrifuge sedimentation [106], analytical ultracentrifugation [84], SEC, field flow fractionation, and combination of methods such as SEC coupled with MALS were also reported.

Nowadays, with the progress of technology, more precise and promising methods are being introduced to this field such as flow cytometry (FC) [107,108], NTA [109], and TRPS [110,111].

The challenge is to utilize the method capable of tracking the particles without manipulating the virus solution's size distribution, meaning that with no reduction or induction in monomeric or aggregated particles. In below, three important methods of size distribution analysis of virus solution were summarized, and pros and cons of the methods briefly discussed.

2.3.2.1. Dynamic Light Scattering

DLS measures the time-dependent fluctuation of scattered light from particles with Brownian motion. The fluctuation is directly related to the diffusion rate of particle in a solution, which in turn can be used to determine a particle's hydrodynamic radii

via the Stokes-Einstein equation (Eq. 2.1). The principle of size-distribution measurement by means of DLS is shown in Fig. 2.12.

$$r_h = \frac{kT}{6\pi\eta D} \qquad \text{Eq. 2.1}$$

Where k is Boltzmann's constant (1.38×10^{-23} $m^2.kg.s^{-2}.K^{-1}$), T is the temperature (K), η is the solution viscosity.

DLS could measure particles in the size range of ~1 nm to ~10 µm. This technique is the most frequently used method to determine virus aggregation/disaggregation behavior.[76,80,81,83,102] Researchers usually combine the data from DLS with the zeta potential readings to draw a conclusion on factors affecting aggregation/disaggregation of virus particles. To this end, an auto-titrator is coupled with apparatus to change pH condition of solution and measure its effects on size distribution and electrophoretic mobilities.

The well-known apparatus enabling measurement of both size distribution and zeta potential are 'Zetasizer' and 'ZetaPALS' available from Malvern Instruments (Malvern, UK) and Brookhaven (Brookhaven Instruments Corporation), respectively. The sensitivity of 'Zetasizer' apparatus for virus solution was reported to be higher than 10^9 infectious virus particle per mL.[81,93] The required volume is dependent on the cell type, could be ranged from 40 µl to 1 mL. At specific pH, the electrolyte concentration is important due to affecting double-layer thickness (explained in Section 2.2.2) and consequently electrostatic repulsion between virus particles. It is worth noting that electrolyte concentration should be as low as possible while measuring zeta potential

of biologics since interaction and deposition of biologics on electrodes could cause over-heating in the cell.

Although DLS is a very powerful and user-friendly tool, it suffers from several inherent disadvantages. Perhaps one of the largest drawbacks is related to the fact that the intensity of the scattered light is proportional to the sixth power of the particle's diameter; this relationship causes DLS measurements to be very sensitive and biased toward larger particles.[112] As a result, DLS measurements may be prone to tailing towards larger particles in the size distribution.[113] Furthermore, scatters from larger particles might block scatters from smaller ones, thereby causing inaccurate size-distribution measurements.

DLS is mainly designed for single-model size distribution; solutions for multi-model size distributions should have a size-difference factor of 3 between particles. However, it is difficult to obtain a size-distribution with resolved peaks for samples with multi-model sizes, and it is also challenging to obtain reliable and repeatable measurements for virus solutions containing virus particles and impurities (i.e. host cell proteins, nucleic acids, debris, etc.). Sikora et al.[114] were forced to contend with these problems in attempting to accurately measure the size of the nanoparticles dispersed into the serum as a result of dealing with multi-model size distribution.

Moreover, simply reporting the number of particles (i.e. concentration) obtained via DLS measurement is not recommended.[114] Instead, it is more accurate to report intensity data for virus solutions as a function of size; therefore, DLS-based aggregation/disaggregation studies for virus solutions would be qualitative rather than

quantitative, which is another drawback of using DLS for size-distribution analyses of virus solutions.

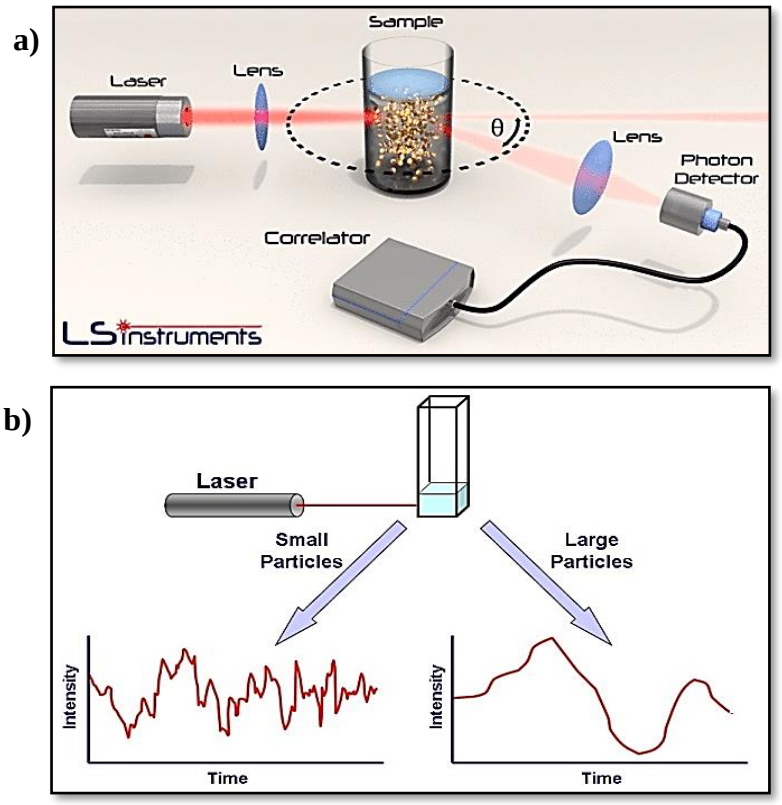

Fig. 2.12. a) DLS instrument; Reprinted from LS Instrument (lsinstruments.ch); b) Principle of particle size distribution analysis using DLS method; Reprinted from AZO Materials (www.azom.com)

2.3.2.2. Nanoparticle Tracking Analysis

This technique was originally developed by NanoSight Ltd., but was later acquired by Malvern Instruments (https://www.malvernpanalytical.com). NTA allows scattered light to be detected from particles when they are irradiated by a light source and the visualization of the particles through a charged coupled device (CCD) camera. The CCD camera operates at 30 frames per second, which allows the particles in the solution to be viewed and recorded.[109] The particles' diffusion coefficient is determined by

tracking the particles at specific time-intervals as defined by the CCD camera's frame rate.[115] Similar to DLS, diffusion coefficient would be converted to hydrodynamic radii using Stokes-Einstein equation (Eq. 2.1). NTA could detect particles in the size range of 30 nm to 1000 nm while particle concentration should be in the range of 1×10^{6}-1×10^{9} virus particles per mL.[109, 54] The required volume for this technique is about 300-500 µl. Fig. 2.13 shows NTA instrument and a frame of video used for size distribution analysis of IgG under heat stress.

Different parameters, such as tracking time, gain, blur, detection limit, camera magnification, and flow rate (in cases that use a pump), should be optimized for particle-size distribution analysis. NTA's performance was thoroughly compared to that of DLS using single-size and multi-size model bead solutions, with the results of this test showing that it outperformed DLS in determining multi-size model distribution.[113] NTA has been used in aggregation studies of viruses such as Ad 5,[109] influenza virus,[109] VV,[54,116] and bacteriophages.[117] However, NTA suffers from two main drawbacks: it can only simultaneous tack down a low number of particles, and it tends to produce large errors in size measurement, especially when using short tracking times.[118] In contrast to DLS, which is highly user-friendly, NTA must be conducted by an expert, and the parameters must be perfectly optimized in order to obtain reproducible results. Another drawback of NTA is that the working concentration range is small and almost always requires sample dilution to meet the range.[103] Furthermore, it was observed that NTA tends to overestimate the number of virus particles, while Vincent et al. [54] reported that NTA also overestimates the VV concentration in the fraction from chromatography purification.

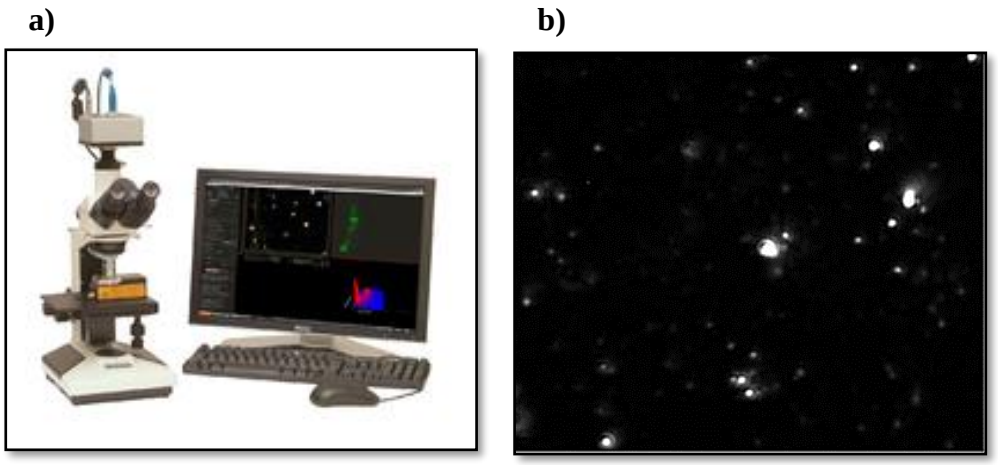

Fig. 2.13. a) Nanosight Instrument; Copyright© to Wikipedia; b) A frame of video obtained by NTA method for size distribution analysis of IgG under heat stress;[113] Copyright© 2010 The Authors.

2.3.2.3. Tunable Resistive Pulse Sensing

This technique utilizes a stretchable membrane that is charged with a specific electrical current in order to measure particle-size distribution and concentration as particles pass through membrane pores. In some configurations of this approach, the measurement of the particle's zeta potential is also enabled (qNano).[114] The key element of this method is the stretchable, polyurethane membrane, as this allows the pores to be adjustment according the needs of the study. Fig. 2.14 shows SEM image of stretchable membrane. Membrane are available at different pore sizes, where each membrane was rated for a specific size range of particles. For example, NP200 is rated for the size range of 80 nm to 500 nm. Stretchable membranes are commercially available from NP40-NP4000, covering size range of 40 nm to 11 µm.

The stretchable membrane is mounted on the fluid cell and electrodes are attached to the upper and lower compartments in order to apply adequate potential difference through the pore.[103] The schematic of the fluid cell and location of the membrane are

shown in Fig 2.15a. As a particle is traversing through the membrane's pore, a resistive pulse event in the current, known as a "blockade event," is detected (Shown in Fig. 2.15b). The blockade (ΔR) is directly related to the particle's volume for cylindrical pores as described by Eq. (2.2). [119,120]

$$\Delta R = \frac{4\rho {d_p}^3}{\pi {D_m}^4} \qquad \text{Eq. 2.2}$$

Where d_p is diameter of particle, ρ is the resistivity of medium filling the pore, D_m is the diameter of membrane. For conical pores, the blockade (ΔR) is calculated by Eq. (2.3).[111,121]

$$\Delta R = \rho \int_0^L \frac{dz}{A(z)} - R \qquad \text{Eq. 2.3}$$

Where A(z) is the cross-sectional area perpendicular to the pore axis (z), and R is defined by Eq. (2.4).

$$R = \frac{4L\rho}{\pi D_L D_S} \qquad \text{Eq. 2.4}$$

Where D_L and D_s are the largest and smallest pore sizes and L is the length of pore.

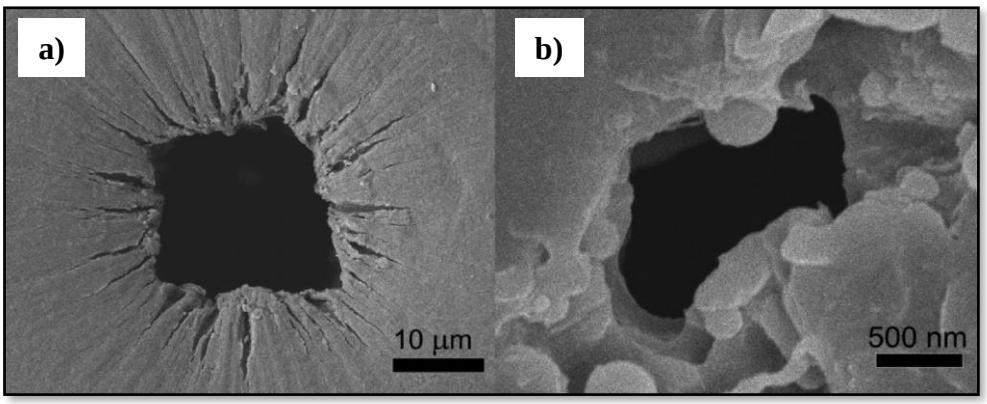

Fig. 2.14. SEM image of a) large and b) small pore size of a stretchable membrane at stretch point of 3 mm;[111] Copyright© 2011, American Chemical Society.

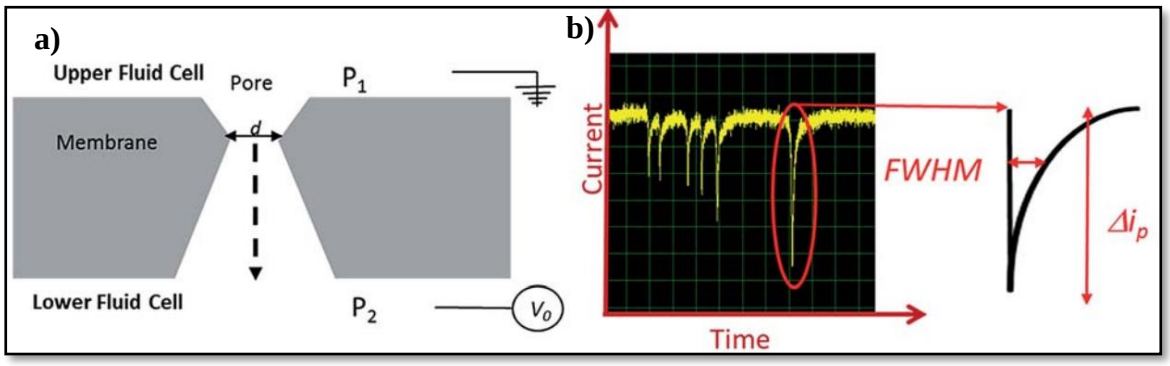

Fig. 2.15. a) Schematic of fluid cell and location of stretchable membrane; b) blockade event while particles passing stretchable membrane's pore;[121] Copyright© 2015 The Royal Society of Chemistry.

The instrument is equipped with a pump to increase the flow of weakly charged particles,[103] and measurements can be tuned by adjusting the stretch of membrane, the voltage, and the applied pressure. Blockade magnitude can be increased by decreasing the membrane stretch or increasing voltage, and it can be decreased by increasing the applied pressure. TRPS requires single-point calibration, which is achieved by examining polystyrene calibration beads under the exact conditions that will be used with the sample. Furthermore, researchers have reported using TRPS for size-

distribution and concentration analyses of Ad,[111] Lentivirus,[103] and VSV.[110] The main advantage of TRPS is that it allows for non-subjective analysis on a particle-by-particle basis.[120] The instrument's detection concentration range is 10^6-10^{13} particles per mL.[103] Obtaining a stable baseline is another main challenge associated with TRPS, as unstable baselines may result from membrane clogging due to using samples with excessively high concentrations (or virus samples with high levels of impurities).

2.3.2.4. Flow Cytometry

FC directly detects light, both scattered and emitted, from excited particles as they pass through a laser. Not all flow cytometers are sensitive enough to detect particles as small as virus particles, with only a few with this ability being available commercially. Indeed, for decades now, researchers have been reporting numerous modifications aimed at improving the detection limits of conventional flow cytometers. However, it wasn't until 1999 that Marie et al.[122] would combine an argon-ion laser with a standard flow cytometer in order to successfully detect viruses stained with SYBR Green I in sea water. Later, in 2000, Brussaard et al.[123] reported using flow cytometry to successfully detect viruses from various families that had been stained with SYBR Green I. Their results showed that flow cytometry could be used to distinguish viruses based on differences in scattered light and the intensity of the emitted green fluorescence.[123] Virus particles are stained with specific dye or combinations of dyes, depending on their proteins or nucleic acids. Several factors, such as the type and concentration of the dye (i.e. stain), fixative, incubation time and temperature, sample solution (e.g. additives, pH, etc.), and sample storage conditions, influence the quality of virus-particle detection via flow cytometer.

In 2003, Brussaard et al. [124] conducted a thorough study on optimizing procedure for counting viruses by FC, summarized in Table 2.9. The proposed optimal method was "fixation with glutaraldehyde (0.5% final concentration, 15 to 30 min), freezing in liquid nitrogen, and storage at -80°C"[124] and later "upon thawing, samples should be diluted in Tris-EDTA buffer (pH 8), stained with SYBR Green I (a 5×10^{-5} dilution of commercial stock), incubated for 10 min in the dark at 80°C, and cooled for 5 min prior to analysis."[124] This method could be a starting point for any other viral sample; however, further optimization and modifications should be implemented based on an individual's need as well as obtained preliminary FC results.

In a later study, Jorio et al. [108] investigated whether FC would be effective for detecting aggregated Baculovirus particles in a sample. The authors demonstrated that the amount of aggregated Baculovirus particles increased during storage time, which was tested for max. 246 days of storage at 4°C.[108] In addition, the authors' examination of particle-size distribution at pHs of 6 and 5.3 demonstrated that the pH of the viral solution affects virus-particle aggregation (Shown in Fig. 2.16). The increased number of events in Gate II indicated that the aggregation of Baculovirus particles had been induced by the lower pH value.

Table 2.9. Tested conditions in order to optimize enumeration of viruses by FC;[124] Copyright © 2004, American Society for Microbiology

Treatment	Levels
Fixative glutaraldehyde (%)	0.1, 0.5, 1, or 2
Fixative formaldehyde (%)	0.4, 0.8, 2, or 4
Storage temp (°C)	4, −20, −80, or −196 (N_2)
Storage time at 4, −20, and −80°C	1 h or 1 mo
Storage time at 4°C	1 h, 2 wk, or 1 or 6 mo
Dye SYBR Green I (10^{-5})	0, 0.5, 1, 5, 10, 15, or 25 (of the commercial stock)
Dye SYBR Gold (10^{-5})	5, 10, or 25 (of the commercial stock)
Incubation temp	20, 40, 60, 80, or 90°C
Incubation time (min)	1, 4, 7, 10, 13, 16, or 19
Dilution solution	TE, Tris, PBS, dH_2O, or seawater
pH of TE buffer	7, 7.4, 7.8, 8, 8.4, or 8.85
Dilution with seawater (%)	0, 1, 2, 5, 10, 20, or 50
Addition of detergents	Triton X-100, Tween 80, NP-40, and SDS at a 0.1% (vol/vol) final concn
Addition of citrate (concn [mM])	0, 1, 2, 5, 10, 20, or 50

[a] Viruses used included four marine phytoplankton viruses (CeV, MpV, PoV, and PpV), one freshwater phytoplankton virus (PBCV), one virus infecting a cyanobacterium (S-PMS2), four characterized bacteriophages (Lambda, T2, T4, and T7), three uncharacterized marine bacteriophages (T-ϕHS1C A, ϕ16, and T-ϕD1B), and two natural marine virus communities. dH_2O, distilled water.

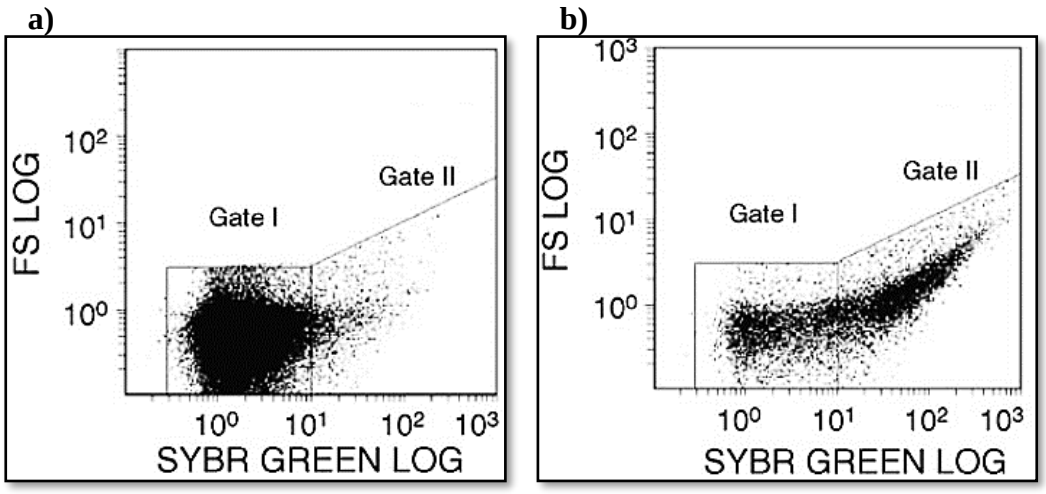

Fig. 2.16 Dot plots of forward scatter versus green fluorescent of Baculovirus freshly produced at pH a) 6.2 b) 5.3;[108] selected panels from the original figure in Reference;[108] reprinted with permission; Copyright 2005 Elsevier.

Moreover, Gaudin et al. [107] developed a technique referred to 'Flow Virometry' to detect and sort Junin virus (JUNV) particles, while retaining infectivity of virus particles. The virus particles were stained with Alexa Fluor 647-conjugated antibody, which specifically interact with envelope of JUNV.[107] The FC was a customized version of FACSAria II Special Order cell sorter (BD Science) with 300 mW 488 nm laser. The

authors utilized the calibration beads with different sizes to determine the size distribution of the virus solution (shown in Fig. 2.17). Remarkably, particles as small as 40 nm were discriminated from background with the aid of fluorescent channel.

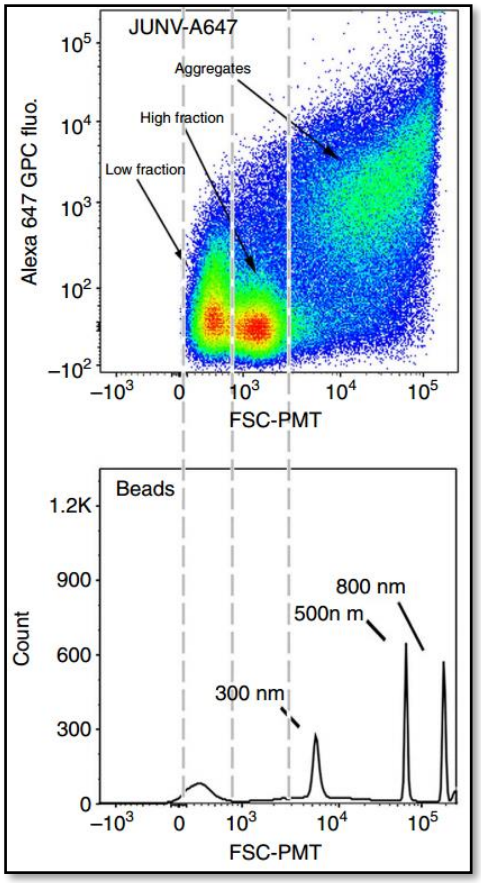

Fig. 2.17. a) Several population discrimination of JUNV labeled with A647 by FC; b) Non-florescent polystyrene beads were detected by forward scatter channel only in larger size (300, 500, and 800 nm);[107] selected panels from the original figure in Reference;[107] Copyright © 2015 Springer Nature.

2.4. References

1. Merten, O.-W., Schweizer, M., Chahal, P. & Kamen, A. Manufacturing of viral vectors: part II. Downstream processing and safety aspects. *Pharm. Bioprocess.* **2,** 237–251 (2014).
2. Kramberger, P., Urbas, L. & Štrancar, A. Downstream processing and chromatography based analytical methods for production of vaccines, gene therapy vectors, and bacteriophages. *Hum. Vaccin. Immunother.* **11,** 1010–1021 (2015).
3. Reichl, U. & Wolf, M. W. Downstream processing of cell culture-derived virus particles. *Expert Rev. Vaccines* **10,** 1451–1475 (2011).
4. Morenweiser, R. Downstream processing of viral vectors and vaccines. *Gene Ther.* **12,** S103 (2005).
5. Grein, T. A., Kovacs, Z., Ebrahimi, M., Michalsky, R. & Czermak, P. Membrane supported virus separation from biological solutions. *Chemie Ing. Tech.* **85,** 1183–1192 (2013).
6. Kang, Y., Cutler, M. W., Ouattara, A. A. & Syvertsen, K. E. Purification processes for isolating purified vesicular stomatitis virus from cell culture. U.S. Patent 7,875,446, issued January 25, 2011.
7. Terova, O., Soltys, S., Hermans, P., De Rooij, J. & Detmers, F. Overcoming downstream purification challenges for viral vector manufacturing: enabling advancement of gene therapies in the clinic. 101-111 (2018).
8. Zydney, A. L. Continuous downstream processing for high value biological products: A Review. *Biotechnol. Bioeng.* **113,** 465–475 (2015).
9. Rathore, A. S., Agarwal, H., Sharma, A. K., Pathak, M. & Muthukumar, S. Continuous processing for production of biopharmaceuticals. *Prep Biochem Biotechnol* **45,** 836–849 (2015).
10. Wickramasinghe, S. R., Kalbfuss, B., Zimmermann, A., Thom, V. & Reichl, U. Tangential flow microfiltration and ultrafiltration for human influenza A virus concentration and purification. *Biotechnol. Bioeng.* **92,** 199–208 (2005).
11. Mocé-Llivina, L., Jofre, J. & Muniesa, M. Comparison of polyvinylidene fluoride and polyether sulfone membranes in filtering viral suspensions. *J. Virol. Methods* **109,** 99–101 (2003).
12. Cliver, D. O. Factors in the membrane filtration of enteroviruses. *Appl. Microbiol.* **13,** 417–425 (1965).
13. Konz, J. O., Lee, A. L., Lewis, J. A. & Sagar, S. L. Development of a purification process for adenovirus: controlling virus aggregation to improve the clearance of host cell DNA. *Biotechnol Prog* **21,** 466–472 (2005).
14. Gesan-Guiziou, G., Wakeman, R. J. & Daufin, G. Stability of latex crossflow filtration: cake properties and critical conditions of deposition. *Chem. Eng. J.* **85,** 27–34 (2002).

15. Kanani, D. M., Sun, X. & Ghosh, R. Reversible and irreversible membrane fouling during in-line microfiltration of concentrated protein solutions. *J. Memb. Sci.* **315,** 1–10 (2008).

16. Iritani, E. A review on modeling of pore-blocking behaviors of membranes during pressurized membrane filtration. *Dry. Technol.* **31,** 146–162 (2013).

17. Furiga, A. *et al.* Effects of Ionic Strength on Bacteriophage MS2 Behavior and Their Implications for the Assessment of Virus Retention by Ultrafiltration Membranes. *Appl. Environ. Microbiol.* **77,** 229 LP-236 (2011).

18. Peixoto, C., Ferreira, T. B., Sousa, M. F. Q., Carrondo, M. J. T. & Alves, P. M. Towards purification of adenoviral vectors based on membrane technology. *Biotechnol. Prog.* **24,** 1290–1296 (2008).

19. Ghosh, R. *Principles of bioseparations engineering*. (World Scientific Publishing company, 2006).

20. Ho, C.-C. & Zydney, A. L. Transmembrane pressure profiles during constant flux microfiltration of bovine serum albumin. *J. Memb. Sci.* **209,** 363–377 (2002).

21. Mulder, M. Polarisation phenomena and membrane fouling. in *Basic Principles of Membrane Technology* 416–464 (Springer, 1996).

22. Rajniak, P. *et al.* Sterilizing filtration—principles and practice for successful scale-up to manufacturing. *J. Memb. Sci.* **325,** 223–237 (2008).

23. Bolton, G., LaCasse, D. & Kuriyel, R. Combined models of membrane fouling: development and application to microfiltration and ultrafiltration of biological fluids. *J. Memb. Sci.* **277,** 75–84 (2006).

24. Bowen, W. R. & Gan, Q. Properties of microfiltration membranes: Flux loss during constant pressure permeation of bovine serum albumin. *Biotechnol. Bioeng.* **38,** 688–696 (1991).

25. Hlavacek, M. & Bouchet, F. Constant flowrate blocking laws and an example of their application to dead-end microfiltration of protein solutions. *J. Memb. Sci.* **82,** 285–295 (1993).

26. Curling, J. Process Chromatography: Five Decades of Innovation. *BioPharm Int.* **5,** 10 (2007).

27. Kalbfuss, B. *et al.* Harvesting and concentration of human influenza A virus produced in serum-free mammalian cell culture for the production of vaccines. *Biotechnol. Bioeng.* **97,** 73–85 (2006).

28. Healthcare, G. E. Hydrophobic interaction and reversed phase chromatography. *GE Healthc. Bio-Sciences AB Uppsala, Sweden* 1–3 (2006).

29. Andreadis, S. T., Roth, C. M., Le Doux, J. M., Morgan, J. R. & Yarmush, M. L. Large-Scale processing of recombinant retroviruses for gene therapy. *Biotechnol. Prog.* **15,** 1–11 (1999).

30. Williams, S. L., Nesbeth, D., Darling, D. C., Farzaneh, F. & Slater, N. K. H. Affinity recovery of Moloney murine leukaemia virus. *J. Chromatogr. B* **820,** 111–119 (2005).

31. Dods, S., Hardick, O., Stevens, B. & Bracewell, D. *Fabricating electrospun cellulose nanofibre adsorbents for ion-exchange chromatography*. *J. Chromatogr. A* **27,** (2014).

32. Svec, F., Tennikova, T. B. & Deyl, Z. *Monolithic materials: preparation, properties and applications*. **67,** (Elsevier, 2003).

33. Barut, M., Podgornik, A., Brne, P. & Štrancar, A. Convective Interaction Media short monolithic columns: Enabling chromatographic supports for the separation and purification of large biomolecules. *J. Sep. Sci.* **28,** 1876–1892 (2005).

34. Jungbauer, A. & Hahn, R. Polymethacrylate monoliths for preparative and industrial separation of biomolecular assemblies. *J. Chromatogr. A* **1184,** 62–79 (2008).

35. Blanche, F. *et al.* An improved anion-exchange HPLC method for the detection and purification of adenoviral particles. *Gene Ther* **7,** 1055–1062 (2000).

36. Trilisky, E. I. & Lenhoff, A. M. Sorption processes in ion-exchange chromatography of viruses. *J. Chromatogr. A* **1142,** 2–12 (2007).

37. Ausubel, L. J. *et al.* current Good Manufacturing Practice production of an oncolytic recombinant vesicular stomatitis viral vector for cancer treatment. *Hum. Gene. Ther.* **22,** 489–497 (2010).

38. Forcic, D. *et al.* Concentration and purification of rubella virus using monolithic chromatographic support. *J. Chromatogr. B* **879,** 981–986 (2011).

39. Burden, C. S., Jin, J., Podgornik, A. & Bracewell, D. G. A monolith purification process for virus-like particles from yeast homogenate. *J. Chromatogr. B* **880,** 82–89 (2012).

40. Venkatachalam, A. R. K., Szyporta, M., Kiener, T. K., Balraj, P. & Kwang, J. Concentration and purification of enterovirus 71 using a weak anion-exchange monolithic column. *Virol. J.* **11,** 99 (2014).

41. Direct visualisation of plasmid DNA in individual chromatography adsorbent particles by confocal scanning laser microscopy. *J. Chromatogr. A* **844,** 129–135 (1999).

42. Champagne, J. *et al.* Pseudoaffinity chromatography using a Convective Interaction Media®-disk monolithic column. *Chromatographia* **65,** 639–648 (2007).

43. Segura, M. M., Puig, M., Monfar, M. & Chillón, M. Chromatography purification of canine adenoviral vectors. *Hum. Gene Ther. Part B Methods* **23,** 182–197 (2012).

44. Ghosh, R. Protein separation using membrane chromatography: opportunities and challenges. *J. Chromatogr. A* **952,** 13–27 (2002).

45. Segura, M., Kamen, A. & Garnier, A. Overview of current scalable methods for purification of viral vectors. in *Viral Vectors for Gene Therapy* (eds. Merten, O.-W. & Al-Rubeai, M.) **737,** 89–116 (Humana Press, 2011).

46. Urmann, M., Graalfs, H., Joehnck, M., Jacob, L. R. & Frech, C. Cation-exchange

chromatography of monoclonal antibodies: Characterisation of a novel stationary phase designed for production-scale purification. in *MAbs* **2,** 395–404 (Taylor & Francis, 2010).

47. Green, A. P. *et al.* A new scalable method for the purification of recombinant adenovirus vectors. *Hum Gene Ther* **13,** 1921–1934 (2002).

48. Kamen, A. & Henry, O. Development and optimization of an adenovirus production process. *J. Gene Med. A cross-disciplinary J. Res. Sci. gene Transf. its Clin. Appl.* **6,** S184–S192 (2004).

49. Rajamanickam, V., Herwig, C. & Spadiut, O. Monoliths in Bioprocess Technology. *Chromatography* **2,** 195 (2015).

50. Sharma, G., Tara, A. & Sharma, V. D. Advances in monolithic silica columns for high-performance liquid chromatography. *J. Anal. Sci. Technol.* **8,** 16 (2017).

51. Wang, P. G. *Monolithic chromatography and its modern applications*. (ILM publications, 2010).

52. Rupar, M. *et al.* Fast purification of the filamentous Potato virus Y using monolithic chromatographic supports. *J. Chromatogr. A* **1272,** 33–40 (2013).

53. Bandeira, V. *et al.* Downstream processing of lentiviral vectors: releasing bottlenecks. *Hum Gene Ther Methods* **23,** 255–263 (2012).

54. Vincent, D. *et al.* The development of a monolith-based purification process for Orthopoxvirus vaccinia virus Lister strain. *J. Chromatogr. A* **1524,** 87–100 (2017).

55. Gerster, P. *et al.* Purification of infective baculoviruses by monoliths. *J. Chromatogr. A* **1290,** 36–45 (2013).

56. Gutiérrez-Aguirre, I. *et al.* Concentrating rotaviruses from water samples using monolithic chromatographic supports. *J. Chromatogr. A* **1216,** 2700–2704 (2009).

57. Allmaier, G. *et al.* Monolithic anion-exchange chromatography yields rhinovirus of high purity. *J. Virol. Methods* **251,** 15–21 (2018).

58. Banjac, M. *et al.* Purification of Vero cell derived live replication deficient influenza A and B virus by ion exchange monolith chromatography. *Vaccine* **32,** 2487–2492 (2014).

59. Lock, M., Alvira, M. R. & Wilson, J. M. Analysis of Particle Content of Recombinant Adeno-Associated Virus Serotype 8 Vectors by Ion-Exchange Chromatography. *Hum. Gene. Ther. Methods* **23,** 56–64 (2012).

60. Fischer, L. M., Wolff, M. W. & Reichl, U. Purification of cell culture-derived influenza A virus via continuous anion exchange chromatography on monoliths. *Vaccine* **36**, 3153-3160 (2018).

61. Kramberger, P., Petrovič, N., Štrancar, A. & Ravnikar, M. Concentration of plant viruses using monolithic chromatographic supports. *J. Virol. Methods* **120,** 51–57 (2004).

62. Whitfield, R. J., Battom, S. E., Barut, M., Gilham, D. E. & Ball, P. D. Rapid high-performance liquid chromatographic analysis of adenovirus type 5 particles with a prototype anion-exchange analytical monolith column. *J. Chromatogr. A* **1216,** 2725–2729 (2009).

63. Mundle, S. T., Giel-Moloney, M., Kleanthous, H., Pugachev, K. V & Anderson, S. F. Preparation of pure, high titer, pseudoinfectious Flavivirus particles by hollow fiber tangential flow filtration and anion exchange chromatography. *Vaccine* **33**, 4255-4260 (2015).

64. Smrekar, F., Ciringer, M., Peterka, M., Podgornik, A. & Štrancar, A. Purification and concentration of bacteriophage T4 using monolithic chromatographic supports. *J. Chromatogr. B* **861,** 177–180 (2008).

65. Ruščić, J. *et al.* A new application of monolithic supports: The separation of viruses from one another. *J. Chromatogr. A* **1388,** 69–78 (2015).

66. Urbas, L. *et al.* Purification of recombinant adenovirus type 3 dodecahedric virus-like particles for biomedical applications using short monolithic columns. *J. Chromatogr. A* **1218,** 2451–2459 (2011).

67. Sviben, D., Forcic, D., Ivancic-Jelecki, J., Halassy, B. & Brgles, M. Recovery of infective virus particles in ion-exchange and hydrophobic interaction monolith chromatography is influenced by particle charge and total-to-infective particle ratio. *J. Chromatogr. B* **1054,** 10–19 (2017).

68. Orr, V., Zhong, L., Moo-Young, M. & Chou, C. P. Recent advances in bioprocessing application of membrane chromatography. *Biotechnol. Adv.* **31,** 450–465 (2013).

69. Duffy, A. M., O'Doherty, A. M., O'Brien, T. & Strappe, P. M. Purification of adenovirus and adeno-associated virus: comparison of novel membrane-based technology to conventional techniques. *Gene Ther.* **12,** S62 (2005).

70. Slepushkin, V. *et al.* Large-scale purification of a lentiviral vector by size exclusion chromatography or Mustang Q ion exchange capsule. *Bioprocess. Sept.* ***2***, 89-95 (2003).

71. Vicente, T. *et al.* Anion-exchange membrane chromatography for purification of rotavirus-like particles. *J. Memb. Sci.* **311,** 270–283 (2008).

72. B Carvalho, S. *et al.* Purification of influenza virus-like particles using sulfated cellulose membrane adsorbers. *J. Chem. Technol. Biotechnol.* **93**, 1988-1996 (2018).

73. Gerba, C. P. & Betancourt, W. Q. Viral Aggregation: Impact on Virus Behavior in the Environment. *Environ. Sci. Technol.* **51,** 7318–7325 (2017).

74. Wright, J. F. *et al.* Identification of factors that contribute to recombinant AAV2 particle aggregation and methods to prevent its occurrence during vector purification and formulation. *Mol. Ther.* **12,** 171–178 (2005).

75. Wright, J. F., Qu, G., Tang, C. & Sommer, J. M. Recombinant adeno-associated virus: formulation challenges and strategies for a gene therapy vector. *Curr.*

Opin. Drug Discov. Devel. **6,** 174–178 (2003).

76. Dika, C., Duval, J. F., Ly-Chatain, H. M., Merlin, C. & Gantzer, C. Impact of internal RNA on aggregation and electrokinetics of viruses: comparison between MS2 phage and corresponding virus-like particles. *Appl Env. Microbiol* **77,** 4939–4948 (2011).

77. Doane, F. W. & Anderson, N. *Electron microscopy in diagnostic virology: a practical guide and atlas*. (CUP Archive, 1987).

78. Williams, F. P. Membrane-associated viral complexes observed in stools and cell culture. *Appl. Environ. Microbiol.* **50,** 523 LP-526 (1985).

79. Goerke, A. R., To, B. C. S., Lee, A. L., Sagar, S. L. & Konz, J. O. Development of a novel adenovirus purification process utilizing selective precipitation of cellular DNA. *Biotechnol. Bioeng.* **91,** 12–21 (2005).

80. Wong, K., Mukherjee, B., Kahler, A. M., Zepp, R. & Molina, M. Influence of inorganic ions on aggregation and adsorption behaviors of human adenovirus. *Environ. Sci. Technol.* **46,** 11145–11153 (2012).

81. Langlet, J., Gaboriaud, F., Duval, J. F. L. & Gantzer, C. Aggregation and surface properties of F-specific RNA phages: Implication for membrane filtration processes. *Water Res.* **42,** 2769–2777 (2008).

82. Croyle, M. A., Gerding, K. & Quick, K. S. Role of the container/closure system and formulation on agitation-induced aggregation phenomena in recombinant adenoviral products. *Bioprocess. J.* **2,** 35 (2003).

83. Mattle, M. J. *et al.* Impact of Virus Aggregation on Inactivation by Peracetic Acid and Implications for Other Disinfectants. *Environ. Sci. Technol.* **45,** 7710–7717 (2011).

84. Galdiero, F. Adenovirus aggregation and preservation in extracellular environment. *Arch Virol* **59,** 99–105 (1979).

85. Wadu-Mesthrige, K., Pati, B., McClain, W. M. & Liu, G.-Y. Disaggregation of Tobacco Mosaic Virus by Bovine Serum Albumin. *Langmuir* **12,** 3511–3515 (1996).

86. Michen, B. & Graule, T. Isoelectric points of viruses. *J. Appl. Microbiol.* **109,** 388–397 (2010).

87. Langlet, J., Gaboriaud, F., Gantzer, C. & Duval, J. F. L. Impact of Chemical and Structural Anisotropy on the Electrophoretic Mobility of Spherical Soft Multilayer Particles: The Case of Bacteriophage MS2. *Biophys J* **94,** 3293–3312 (2008).

88. Kissmann, J. *et al.* Physical stabilization of norwalk virus-like particles. *J. Pharm. Sci.* **97,** 4208–4218 (2008).

89. Dika, C., Duval, J. F. L., Ly, H. M., Merlin, C. & Gantzer, C. Impact of internal RNA on aggregation and electrokinetics of viruses: a comparison between MS2 and corresponding VLPs. *Appl. Environ. Microbiol.* AEM-00407 (2011).

90. Taylor, D. H. & Bosmann, H. B. The electrokinetic properties of reovirus type

3: electrophoretic mobility and zeta potential in dilute electrolytes. *J. Colloid Interface Sci.* **83,** 153–162 (1981).

91. Floyd, R. & Sharp, D. G. Viral aggregation: effects of salts on the aggregation of poliovirus and reovirus at low pH. *Appl Env. Microbiol* **35,** 1084–1094 (1978).

92. Floyd, R. & Sharp, D. G. Aggregation of poliovirus and reovirus by dilution in water. *Appl Env. Microbiol* **33,** 159–167 (1977).

93. Vega-Acosta, J. R., Cadena-Nava, R. D., Gelbar, W. M., Knobler, C. M. & Ruiz-Garcia, J. Electrophoretic Mobilities of a Viral Capsid, Its Capsid Protein, and Their Relation to Viral Assembly. *J. Phys. Chem. B* **118,** 1984–1989 (2014).

94. Floyd, R. & Sharp, D. G. Viral aggregation: buffer effects in the aggregation of poliovirus and reovirus at low and high pH. *Appl. Environ. Microbiol.* **38,** 395–401 (1979).

95. Langlet, J., Gaboriaud, F. & Gantzer, C. Effects of pH on plaque forming unit counts and aggregation of MS2 bacteriophage. *J Appl Microbiol* **103,** 1632–1638 (2007).

96. Pieler, M. M., Heyse, A., Wolff, M. W. & Reichl, U. Specific ion effects on the particle size distributions of cell culture–derived influenza A virus particles within the Hofmeister series. *Eng. Life Sci.* **17,** 470–478 (2017).

97. Zeta Potential. Available at: https://en.wikipedia.org/wiki/Zeta_potential.

98. Wright, J. F. & Qu, G. Compositions and methods to prevent AAV vector aggregation. U.S. Patent 7,704,721, issued April 27, 2010.

99. Xie, Q., Hare, J., Turnigan, J. & Chapman, M. S. Large-scale production, purification and crystallization of wild-type adeno-associated virus-2. *J. Virol. Methods* **122,** 17–27 (2004).

100. Wang, P. *et al.* Glycerol facilitates the disaggregation of recombinant adeno-associated virus serotype 2 on mica surface. *Colloids Surf. B* **60,** 264–267 (2007).

101. Armstrong, J. K., Wenby, R. B., Meiselman, H. J. & Fisher, T. C. The hydrodynamic radii of macromolecules and their effect on red blood cell aggregation. *Biophys. J.* **87,** 4259–4270 (2004).

102. Dika, C., Gantzer, C., Perrin, A. & Duval, J. F. Impact of the virus purification protocol on aggregation and electrokinetics of MS2 phages and corresponding virus-like particles. *Phys. Chem. Chem. Phys.* **15,** 5691–5700 (2013).

103. Heider, S. & Metzner, C. Quantitative real-time single particle analysis of virions. *Virology* **462–463,** 199–206 (2014).

104. Floyd, R. Viral aggregation: mixed suspensions of poliovirus and reovirus. *Appl. Environ. Microbiol.* **38,** 980–986 (1979).

105. Rafikova, E. R. *et al.* A mechanism of macroscopic (amorphous) aggregation of the tobacco mosaic virus coat protein. *Int. J. Biochem. Cell Biol.* **35,** 1452–1460 (2003).

106. Bondoc Jr, L. L. & Fitzpatrick, S. Size distribution analysis of recombinant

adenovirus using disc centrifugation. *J. Ind. Microbiol. Biotechnol.* **20,** 317–322 (1998).

107. Gaudin, R. & Barteneva, N. S. Sorting of small infectious virus particles by flow virometry reveals distinct infectivity profiles. *Nat. Commun.* **6,** 6022 (2015).

108. Jorio, H., Tran, R., Meghrous, J., Bourget, L. & Kamen, A. Analysis of baculovirus aggregates using flow cytometry. *J. Virol. Methods* **134,** 8–14 (2006).

109. Kramberger, P., Ciringer, M., Štrancar, A. & Peterka, M. Evaluation of nanoparticle tracking analysis for total virus particle determination. *Virol. J.* **9,** 265 (2012).

110. Akpinar, F. & Yin, J. Characterization of vesicular stomatitis virus populations by tunable resistive pulse sensing. *J. Virol. Methods* **218,** 71–76 (2015).

111. Vogel, R. *et al.* Quantitative Sizing of Nano/Microparticles with a Tunable Elastomeric Pore Sensor. *Anal. Chem.* **83,** 3499–3506 (2011).

112. Jiskoot, W. & Crommelin, D. *Methods for structural analysis of protein pharmaceuticals*. (Springer Science & Business Media, 2005).

113. Filipe, V., Hawe, A. & Jiskoot, W. Critical evaluation of Nanoparticle Tracking Analysis (NTA) by NanoSight for the measurement of nanoparticles and protein aggregates. *Pharm. Res.* **27,** 796–810 (2010).

114. Sikora, A., Shard, A. G. & Minelli, C. Size and ζ-Potential Measurement of Silica Nanoparticles in Serum Using Tunable Resistive Pulse Sensing. *Langmuir* **32,** 2216–2224 (2016).

115. Boyd, R. D., Pichaimuthu, S. K. & Cuenat, A. New approach to inter-technique comparisons for nanoparticle size measurements; using atomic force microscopy, nanoparticle tracking analysis and dynamic light scattering. *Colloids Surf. A Physicochem. Eng. Asp.* **387,** 35–42 (2011).

116. Mironov, G. G., Chechik, A. V, Ozer, R., Bell, J. C. & Berezovski, M. V. Viral quantitative capillary electrophoresis for counting intact viruses. *Anal. Chem.* **83,** 5431–5435 (2011).

117. Anderson, B. *et al.* Enumeration of bacteriophage particles: comparative analysis of the traditional plaque assay and real-time QPCR-and nanosight-based assays. *Bacteriophage* **1,** 86–93 (2011).

118. Anderson, W., Kozak, D., Coleman, V. A., Jämting, Å. K. & Trau, M. A comparative study of submicron particle sizing platforms: accuracy, precision and resolution analysis of polydisperse particle size distributions. *J. Colloid Interface Sci.* **405,** 322–330 (2013).

119. Coumans, F. A. W. *et al.* Reproducible extracellular vesicle size and concentration determination with tunable resistive pulse sensing. *J. Extracell. Vesicles* **3,** 25922 (2014).

120. Anderson, W., Lane, R., Korbie, D. & Trau, M. Observations of Tunable Resistive Pulse Sensing for Exosome Analysis: Improving System Sensitivity

and Stability. *Langmuir* **31,** 6577–6587 (2015).

121. Blundell, E. L. C. J., Mayne, L. J., Billinge, E. R. & Platt, M. Emergence of tunable resistive pulse sensing as a biosensor. *Anal. Methods* **7,** 7055–7066 (2015).

122. Marie, D., Brussaard, C. P. D., Thyrhaug, R., Bratbak, G. & Vaulot, D. Enumeration of marine viruses in culture and natural samples by flow cytometry. *Appl. Environ. Microbiol.* **65,** 45–52 (1999).

123. Brussaard, C. P. D., Marie, D. & Bratbak, G. Flow cytometric detection of viruses. *J. Virol. Methods* **85,** 175–182 (2000).

124. Brussaard, C. P. D. Optimization of procedures for counting viruses by flow cytometry. *Appl. Environ. Microbiol.* **70,** 1506–1513 (2004).

Chapter III

Developing and Optimizing Monolithic Column Chromatography Purification Process for Oncolytic Rhabdoviral Vectors

Authors: Shabnam Shoaebargh, Vitaliya Bardal, Maria Fe Medina, Brian Lichty, David R. Latulippe

In preparation for submission in the Journal of Chromatography A

3.1. Abstract

Oncolytic virus (OV) therapy is a promising biotherapeutic approach for cancer treatment. Purification of large and complex biomolecules such as OVs with high titers remains a challenge. One powerful purification process alternative would be monolithic column chromatography. In this chapter, monolithic columns with various functional groups, namely anion-exchange and hydrophobic interaction, with different pore sizes (2 and 6 μm) were examined for purification of the oncolytic Rhabdoviral vector. Our detailed study revealed that the recovery of the infectious Rhabdoviral vector from the anion-exchange monolithic column was low (< 20 %). However, higher removal of impurities in the flow-through step were achieved by using the anion-exchange monolithic column with a larger pore size (6 μm). On the other hand, monolithic

hydrophobic interaction column with 6 µm pore size demonstrated a potential application in the purification of Rhabdoviral vectors by achieving both higher virus recovery and impurities removal. Using 2.0 M ammonium sulfate salt in the binding buffer, more than 60% recovery of infectious Rhabdoviral vector particle was obtained, while more than 70% removal of impurities were observed in the flow-through step. The monolithic hydrophobic interaction chromatography process was further optimized by examining various binding and elution conditions as well as additives to achieve a higher yield of the infectious virus. The highest recovery of infectious Rhabdoviral vectors was achieved by performing the elution step mediated by the presence glycerol.

3.2. Introduction

Biotherapeutic manufacturing processes are generally comprised of upstream and downstream processing (DSP), for which DSP remains as the main bottleneck [1]. DSP is the step wherein process-related impurities (i.e. originating from cell culture and additives) as well as product-related impurities (e.g. aggregates and empty capsids) are removed to yield the final purified product.[1] Current technologies with the potential of 'large-scale' production are based on membrane separations, chromatographic separations, or combination of both methods. Conventional resin-based columns that were mostly designed for purification of small biomolecules such as proteins (size < 10 nm) are impractical for larger biomolecules such as viruses. The latter is basically due to complex viral molecular surfaces which, in combination with their large size, lead to low diffusion rates, low binding capacities, and high shearing in resin-based columns.[1–6] For example, in a study by Trilisky et al.,[6] it was shown that binding capacity of

adenovirus type 5 (hydrodynamic size of ~ 100 nm) was at least one order of magnitude lower compared to ovalbumin (hydrodynamic size of ~ 6 nm) on a wide pores of PL-SAX resin (diameter ~400 nm).

One powerful alternative for the purification of 'large' biomolecules is monolithic columns. This technology features a continuous stationary phase with a network of interconnected pores and a high porosity that has been shown to be ideal for the production of 'large' biomolecules such as viruses.[7] In contrast to the resin-based columns, mass transfer in the monoliths are convective, owing to 1 µm to 5 µm pore sizes.[3,8] This feature leads to lower back pressure, increased available surface area for binding and consequent higher productivity for purification of 'large' biomolecules.[3–5,7] In a study by Burden et al.,[4] it was shown that dynamic binding capacity of monolithic column for virus-like particles (VLPs) was three-times higher than resin-based columns. Furthermore, the dynamic binding capacity of monoliths is independent of performing flow rate allowing for ease of scale-up.[4,7] Polymethacrylate-based monoliths are commercially available by BIA Separations (Ljubljana, Slovenia) under the trade name of Convective Interaction Media (CIM®). For several years, ion-exchange chromatography specifically anion-exchange columns have been reported for purification of various enveloped and non-enveloped virus particles.[2,5,9–15] However, a few studies observed high virus loss during anion-exchange chromatography of the enveloped viruses, for which hydrophobic interactions columns were utilized instead.[16,17] One of the first attempts to use hydrophobic interaction columns for viruses was in 1981 by Einarsson et al.,[18] to remove Hepatitis B virus from concentrate of the coagulation factors using octanohydrazide-sepharose 4B resin. More recently, a few studies highlighted the potential of hydrophobic interaction chromatography for the

viral purification such as Vaccinia Ankara virus,[19,20] VLPs based on Hepatitis B surface antigen from clarified yeast homogenate,[4] Canine Adenoviral vector and human Adenovirus,[21] and Orthopoxvirus Vaccinia virus Lister strain.[22]

Although several papers have been reported the use of monolithic column chromatography for virus purification application, a better detailed understanding of monolithic column performance is still required. Of the interest are papers that highlighted the fact that virus particle-virus particle interaction as well as virus particle-environment (membrane, column's matrix, etc.) interactions are complex and could result in dramatic virus loss.[16,17,21,23] This raises the question of how hydrophobicity and virus surface electrostatic charge play a role in virus loss during purification. To this end, an enveloped Rhabdoviral vector was selected to investigate the effectiveness of monolithic columns for virus purification and assess the performance of two columns with different chemistries, namely anion-exchange and hydrophobic interaction. Oncolytic Rhabdoviral vectors have promising therapeutic potential with the combined benefits of direct killing of tumor cells and induction of tumor-specific immune responses.[24–28] Currently, a type of attenuated mutated Rhabdoviral vector is being tested in a clinical trial (phase I/II) given alone or in combination with an Adenoviral vector for advanced or metastatic MAGE-A3 expressing solid tumors (clinicaltrials.gov, NCT02285816). In this chapter, we describe the development of a monolithic hydrophobic interaction chromatography method for purification of Rhabdoviruses. It is well-accepted that different factors such as ligand type and degree of substitution, type of salt and concentration, pH, and additives, etc. affects the hydrophobic interaction column performance.[29,30]

Among the reported additives, glycerol could be an ideal candidate where it was reported to mediate the hydrophobic interaction chromatography of proteins, for which it improves mass recovery and proper refolding of proteins.[31–33] Interestingly, glycerol was also reported to increase the solubility and stability of virus particles.[34–37] To this end, optimization of adsorption/desorption conditions of the virus particle in terms of salt concentration, pH, and additives, namely glycerol, on the monolithic hydrophobic interaction column were explored. To our best knowledge, this is the first study to investigates the effects of additives on hydrophobic interaction chromatography of viruses. In addition, we explored the effects of monolithic column pore size on virus recovery as well as the removal of impurities (i.e. host cell protein and nucleic acids).

3.3. Material and Methods

3.3.1. Vero Cell Growth

Vero cells, African green monkey kidney cells (McMaster Immunology Research Centre, MIRC) were grown in alpha-Minimum Essential Medium (α-MEM) supplemented with 8% fetal bovine serum (FBS, Gibco, Life Technologies) and 1% L-Glutamine (MIRC) in 150 mm plates (Corning®, USA) incubated at 37 °C and 5% CO_2.

3.3.2. Production of Rhabdoviral Vector

Vero cells were plated in 150 mm cell culture dishes (Corning®, USA). After reaching confluence of higher than 90%, the cells were infected with the Rhabdoviral vector, expressing the green fluorescent protein (GFP) protein (kindly provided by Biotherapeutics Manufacturing Centre at the Ottawa Hospital Research Institute). The

multiplicity of infection (MOI) was 0.1 and plates were incubated at 37°C along with rocking every 15 min for a total of 60 minutes, followed by addition of 20 mL of the fresh supplemented α-MEM (with 8% FBS and 1% L-Glutamine) per plate as a last step. The vector with an expression of GFP was selected to simplify the detection of cytopathic effect (CPE) in the cells. After observing CPE, the crude supernatant containing was harvested and centrifuged using Allegra 6R Centrifuge (Beckman Coulter) at 1500 rpm for 12 minutes, wherein the Rhabdoviral vector was recovered in the supernatant. The harvested supernatant was aliquoted into 1.5 mL and stored at -80°C for further use. Three batches were prepared and referred to Batch A, B and C, with Batch C being the largest batch with total harvested volume of 140 mL. Batch A was aliquoted into 130 µl, the virus titer assessed, and then samples from Batch A was used as a Reference Material. The pH values of the virus batches were between 7.6 and 7.8 with a conductivity value of ~ 13 $mS.cm^{-1}$.

3.3.3. Virus Quantification

3.3.3.1. Infectious Titer Quantification

The infectious titer of the virus samples was determined using 50% tissue culture infective dose ($TCID_{50}$) assay and plaque forming unit (PFU) assay. The details for the PFU assay were described in our previous work.[23] Briefly, Vero cells were plated at 8×10^5 cells per 60 mm titer plate; twenty-four hours after seeding, serially diluted virus solution (100 µl) would be added to the cells to measure infectivity of the virus samples. For $TCID_{50}$ assay, Vero cells were plated onto 96 'flat-bottom' well plates (Corning®, USA) with a density of 5×10^4 cells per well to create a monolayer. Next day, a serial

dilution of the samples in α-MEM (supplemented by 8% FBS and 1% L-glutamine), were prepared in round-bottom 96-well plates (Corning®, USA). The assay was conducted in sextuplicate, allocating six wells per sample and two samples per plate. Viral infection was performed by dispensing 100 µl of serially diluted virus sample on Vero cells (in 96 flat-bottom well plates) followed by incubation at 37 °C and 5% CO_2 for 48 hours. CPE caused by Rhabdoviral vector was detected by visualizing GFP expression using Typhoon Trio$^+$ scanner (GE Healthcare) equipped with Blue 488 nm/520 BP 40 laser. In this study, the infectious titer was calculated using Spearman-Karber method according to Eq. (3.1).[38,39] In this chapter, the calculated virus titer from $TCID_{50}$ assay would be expressed in $ID_{50}.mL^{-1}$.

$$\log_{10}^{TCID_{50}} = x_{p=1} + \frac{1}{2}d - d\sum_{x_{p=1}}^{x_{\min}} p_x \qquad \text{Eq. 3.1}$$

Where d is $\left|\log_{10}^{dilution}\right|$, $x_{p=1} = \arg\min_x (p_x = 1)$, and p is proportion of positive wells.

To better capture variations in the assay, an extra step of the calculation was implemented based on making combinations of 4 wells out of 6 infected wells for the $TCID_{50}$ titer calculation which ended up having a total number of 15 different combinations from each sample. The reported $TCID_{50}$ values in this chapter as well as standard deviations were the average and standard deviation of 15 above-mentioned combinations.

Effects of different serial dilutions on the calculated value of $TCID_{50}$ titer for Rhabdoviral vector were tested (Fig. S 3.1) and the method of 5-times dilution in $TCID_{50}$ assay were selected due to causing lower variations. Using 5-times dilution, the infectivity of the virus from Batch A, B and C were $(9.6\pm3.1)\times10^9$ $ID_{50}.mL^{-1}$,

$(5.4\pm0.8)\times10^{9}$ $ID_{50}.mL^{-1}$, and $(3.2\pm0.8)\times10^{9}$ $ID_{50}.mL^{-1}$, respectively. Inherent variability of $TCID_{50}$ assay using 5-time dilution method was found to be lower than 30% in a good agreement with Vincent et al.[22]

To check on the long-term viral stability, the titer of the prepared virus batch A stored at -80°C were tracked down over nine months, with the results indicating stable titer values (Fig. S 3.2). Furthermore, a short-term stability at different temperatures (Room temperature vs. 4°C) were conducted with the results showing no significant change in the virus titer incubated either at RT or on ice for maximum incubation time of 4 hours (Fig. S 3.3). However, the calculated titers of the samples incubated on the ice were slightly higher with lower variations compared to the samples incubated at RT. Thus, any virus sample (either collected from a chromatography run or thawed ones) were incubated on ice for further measurements.

Short-term stability in different buffer conditions were studied by spiking the buffers with the known amount of the Rhabdoviral vector (Section 3.2). Buffer conditions were selected according to the monolithic chromatography conditions. All measurements were performed in parallel with the same dilution ratio of the virus (1:9) in the media as a control.

3.3.3.2. Virus Particle Quantification

Viral RNA in each sample was extracted using a viral RNA QIAamp mini kit (Qiagen) with fast spinning columns. Carrier RNA (Qiagen) was used to enhance RNA recovery. Samples from chromatography were diluted five- and ten-times prior to introducing to spin columns. The extracted RNA samples were used immediately.

Rhabdoviral vector concentration was quantified using real-time quantitative reverse-transcription polymerase chain reaction (real-time RT-PCR). The number of absolute genome copies per mL in the initial sample and eluted fractions were determined based on C_p values and a standard curve. The standard curve was obtained by serial dilution of the Rhabdoviral vector plasmid. The R^2 values for standard curve were > 0.99 and the slope was ranged between 3.0-3.2. The Rhabdoviral vector plasmid was prepared in OneShot Top10 chemically competent E. Coli cells (Invitrogen, Life technologies) followed by plasmid purification using QIAprep Maxiprep kit (Qiagen). The RT-qPCR experiments were conducted using Applied Biosystems StepOnePlus Real-Time PCR system and StepOne software version 2.3.

3.3.4. Virus Characterization

The size distribution of the virus batches was determined by dynamic light scattering (DLS) with Zetasizer Nano ZS (Malvern Instrument, UK). Virus sample preparation for DLS analysis was thoroughly described in our previous work.[23] DLS measurements on the virus solution from Batch A and C were shown in Fig. S 3.4, indicating a similar pattern of size distribution between two batches.

A test was performed using a membrane with MWCO of 300 kDa (BioMax®, Millipore Ultrafiltration discs, Polyethersulfone), aiming at removing the virus particles from the solution; DLS analysis was performed on the permeate, showing one peak spread over in the size range of lower than 100 nm (Data not shown) while no infectious virus was detected (tested by PFU assay). Therefore, the peak at the size range of higher

than 100 nm was attributed to the Rhabdoviral vector particles, in a good agreement with our previous result.[23]

3.3.5. Chromatography Experiments

Flow-diagram of production and purification process of Rhabdoviral vectors was shown in Fig. 3.1. All chromatography runs were conducted at room temperature using NGC Quest Plus chromatography system (BioRad) equipped with UV detector and conductivity meter, connected to a fraction collector (BioRad). All experiments were done in Biosafety Level II (BSL II) lab with having the fraction collector inside a biosafety cabinet to ensure sterility and operator safety.

1 mL monolithic columns, made of polymethacrylate copolymers (poly (glycidyl methacrylate co-ethylene dimethacrylate)) and manufactured by BIA Separations (Ajdovdcina, Slovenia) were examined. The columns have a pore radius of either 950-1150 nm (denoted by average diameter as 2 μm) or 2400-3600 nm (denoted by average diameter as 6 μm), respectively. Dynamic binding capacities of monolithic columns were reported to be theoretically 2×10^{12} virus particles for adenovirus, 2.4×10^{11} PFU for Baculovirus per mL of column bed volume (anion-exchange column),[13] 3.9×10^{9} PFU for vaccinia virus per mL (cation-exchange column),[22] and 5×10^{11} virus particles for Mumps and Measles virus (hydrophobic interaction column).[16] To this point, care was taken to have the virus particle concentration of the loaded sample lower than reported binding capacities; in our case, all the runs had the titer of the initial loaded sample lower than 1×10^{10} ID_{50} per 1 mL.

A flow rate of 4 mL.min^{-1} i.e. 4 column volumes (CVs) per min was used. The flow pattern of the mobile phase in the monolithic columns is radial, from outer space to the center. The monolithic column chromatography steps were:

- Column equilibration with the Binding buffer, 10 CVs
- Sample injection and loading with Binding buffer
- Flow-through wash with Binding buffer, either 12 or 24 CVs
- Either stepwise or linear-gradient elution from 0% to 100% of the Elution buffer, either 4 CVs or 10 CVs, followed by a hold at 100% Elution buffer
- Column equilibration with the Binding buffer, 4 CVs
- Cleaning-in-place (CIP) with the stripping buffer followed by excessive water wash
- Column storage in 20% Ethanol

In initial experiments, a longer flow-through (24 CVs) was conducted to verify whether any virus detachment from the column was occurring.[40] Eleven fractions with the volume of 2 mL per fraction were collected through each chromatography run, six fractions for the flow-through step (12 CVs), followed by five fractions for the elution step (10 CVs) named as Elution1 (E1) to E5. Fractions of the flow-through were pooled in pairs to generate 3 fractions, 4 mL each, and named as Flow-through1 (F1) to F3. The samples were placed on ice for the infectivity analysis and later stored at -80°C (refer to Fig. S 3.3 for virus stability analysis). Virus recovery was defined as the sum of the infectious virus particle in the fractions through the elution step compared to the total initial infectious virus particle that was loaded on the column. To examine

possibility of the virus particle being carried over from one run to another one was performed by a chromatography run with 'virus-free' formulation buffer injection (referred as 'buffer run') and samples from the elution step was collected for later virus infectivity measurement. Each individual chromatography runs were done at least twice. All buffers were sterile filtered through 0.2 µm PES bottle-top filters prior to use (Nalgene™ Rapid-Flow™ Sterile Filter).

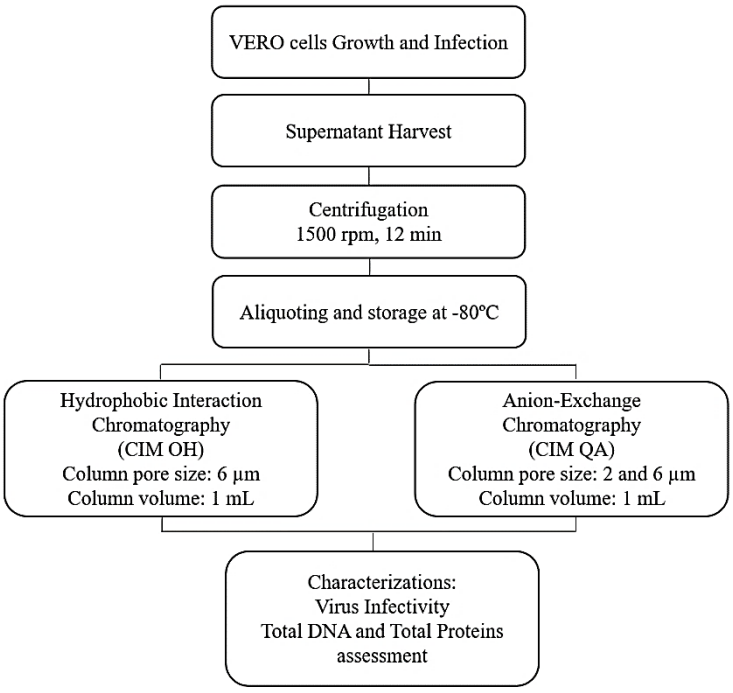

Fig. 3.1. Flow-diagram of production and purification process of Rhabdoviral vectors

3.3.5.1. Monolithic Anion-Exchange Chromatography

In this study, two monolithic columns (referred as CIM) functionalized with quaternary ammonium (QA) group as an anion exchange with either pore size of 2 µm and 6 µm were tested. The Equilibrium/Binding buffer for CIM QA column contained

10 mM HEPES, 4% sucrose, pH 7.4, and the elution buffer was 10 mM HEPES, 4% sucrose, 2 M NaCl at pH 7.4. Monolithic columns could be regenerated with an alkaline solution (up to 1 M NaOH) without any significant loss of functional groups.[41] Therefore, CIP of the anion-exchange monolithic columns was carried out right after the purification run using stripping buffer containing 1 M NaOH and 2 M NaCl for at least 20 CVs. Lower flow rates at CIP is advisable according to Trilisky et al. [42] study in which the large bioparticle entrapment and escape conditions were studied; thus, CIP rounds were conducted at a low flow rate of 1 $mL.min^{-1}$. For enhanced cleaning purpose, columns were detached from the chromatography system and left in the stripping buffer for at least 1 hour but no longer than 3 hours, followed by Milli-Q water washes for 20-30 CVs at higher flow rates and finally stored in 20% Ethanol solution.

3.3.5.2. Monolithic Hydrophobic Interaction Chromatography

In this study, a monolithic hydrophobic interaction column (referred as CIM) with hydroxyl functional groups (OH) and a pore size of 6 µm was examined. The Equilibrium/Binding buffer was 10 mM HEPES, 4% sucrose with varied ammonium sulfate amount (AS, 1.5 to 2 M) and the Elution buffer was 10 mM HEPES, 4% sucrose. The pH values of the buffers tested with the viral sample were adjusted either at 7.4 or 8.0. The virus samples were diluted 1:1 with the corresponding concentrated AS stock solution to match the conductivity of the equilibrium/binding buffer. CIP of the hydrophobic interaction monolithic column was carried out right after the purification run using stripping buffer containing just 1 M NaOH for at least 20 CVs with a low flow rate of 1 $mL.min^{-1}$. The enhanced cleaning method as well as the column storage

condition for monolithic hydrophobic interaction column was like monolithic anion-exchange column (Section 3.3.5.1).

3.3.6. Quantification of Residual Total Protein and DNA

For determination of the total protein, bicinchoninic acid (BCA) assay either microplate or enhanced test tube procedure was performed using a commercial kit by Pierce Biotechnology. The assay was calibrated against bovine serum albumin (BSA, Thermofisher, 2 $mg.mL^{-1}$) as a standard. The microplate format with the validated range of 25-2000 $\mu g.mL^{-1}$ was used for the samples from anion-exchange chromatography. Enhanced test tube format (1:20 sample to reagent ratio) with the validated range of 25-250 $\mu g.mL^{-1}$ was used for the samples from hydrophobic interaction chromatography, for which the samples were diluted 4-times to achieve AS concentration $\leq$ 500 mM. Standard curves were prepared in the buffer conditions matching with the samples. The absorbance of samples was measured at 562 nm using either a plate reader (SpectraMax i3, Molecular devices) for microplate assay or spectrophotometer (Eppendorf Biophotometer) for the enhanced test tube format. The total protein of the virus solution from Batch B and C were 3.9±0.2 $mg.mL^{-1}$ and 3.7±0.3 $mg.mL^{-1}$, indicating that initial virus sample was contaminated with large amount of proteins.

For determination of the DNA, Quant-iT™ PicoGreen® dsDNA kit (Invitrogen, USA) with Lambda DNA (Thermofisher, 0.3 $\mu g.\mu l^{-1}$) as a standard was used. The validated working range was 4-1000 $ng.mL^{-1}$ using the buffer conditions that matches with the samples. Samples were analyzed at excitation and emission wavelength of 480 and 520 nm using the plate reader (SpectraMax i3, Molecular devices), respectively.

The total DNA of the virus from Batch B and C were 329.6±74.3 and 240.2±30.2 $ng.mL^{-1}$.

3.3.7. Statistical Analysis

Every chromatography run as well as any measurement (e.g. virus infectivity, total protein and DNA) were repeated at least two times, and the mean and standard deviation were reported. Error bars were generated using propagation of errors, implemented according to Eq. S 3.1 – Eq. S 3.4 in the supplementary information. The differences between sets of data were examined using the "t-Test" with P-values < 0.05, indicating statistically significant difference.

3.4. Results and Discussion

3.4.1. Anion Exchange Chromatography

Purification of Rhabdoviral vector was firstly conducted using monolithic column chromatography functionalized with positively charged QA. Detailed comparison of the content in the flow-through and elution steps for CIM QA column with 2 and 6 µm pore size were shown in Fig. 3.2. Using QA column with 2 µm pore size, less than 0.1% of the virus particles was detected in the flow-through (12 CVs). Longer flow-through wash (24 CVs) was conducted to check on detachment of the virus particles from the column. No infectious virus particle was detected in the later fractions of the flow-through (12 to 24 CVs). The latter indicated that Rhabdoviral particles at binding condition (pH 7.4) were negatively charged. The results from the monolithic column chromatography using CIM QA 2 µm demonstrated poor virus recovery, where more

than 95% of the virus particles were still on the column even after elution with 2 M NaCl. To ensure no carryover of virus particles from one run to another one, a 'buffer run' on the column was performed and the infectivity assay on the collected samples from the elution step was conducted. The results demonstrated no infectious virus particle in the samples from the 'buffer run'.

In the following, CIM QA 6 µm were tested, where the virus recovery was improved using larger pore size column on average by a factor of 'four', while the recovery of the infectious virus particles was still lower than 20% (Fig. 3.2). Our hypothesis for having a low Rhabdoviral vector recovery from CIM QA 2 µm column was due to restricted movement of materials inside the pores; although the monolithic column pore radius (1 µm on average) was larger than the virus particle size, it also contained pore constrictions such as throats which could restrict the movement of particles;[42] Using CIM QA 6 µm, the virus titer increased presumably due to presence of larger pores in the column that allowed the particles to have relatively an unrestricted passage.[43] Still, the low virus recovery (< 20%) from CIM QA 6 µm revealed that an irreversible interaction (i.e. binding) between the negatively charged virus's envelope and the positively charged QA groups on the column matrix has occurred.

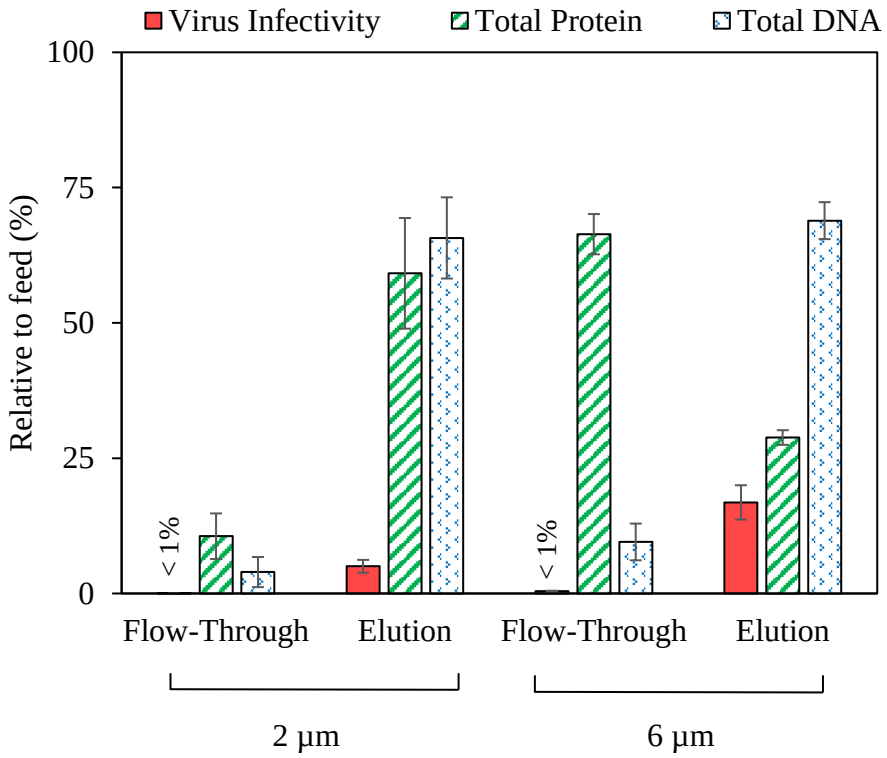

Fig. 3.2 Effects of column pore size on the performance of CIM QA column (1 mL) in purification of the Rhabdoviral vector (Batch B). Column equilibrium and sample loading with 10 mM HEPES, 4% sucrose, pH=7.4, followed by a stepwise elution with 10 mM HEPES, 4% sucrose, pH= 7.4, 2.0 M NaCl buffer. Flow-through: F1 (4 mL). Elution: sum of E2, E3, and E4, each fraction was 2 mL and tested individually. The virus infectivity, total protein and DNA of the loaded sample were $(5.4\pm 0.8)\times10^{9}$ $ID_{50}.mL^{-1}$, 3.9±0.2 $mg.mL^{-1}$ and 329.6±74.3 $ng.mL^{-1}$.

Analysis of the total protein (shown in Fig. 3.2) demonstrated higher protein removal in the flow-through using column with 6 µm pore size (66%±4%) compared to the column with 2 µm pore size (11%±4%). This behavior could have two possible explanations based on protein particles charge. Assuming protein molecules were mainly positively charged, increased protein removal in 6 µm pore size column suggests the pore size effect on the entrapment of the non-adsorbed materials in 2 µm pore size column. On the other hand, if protein molecules were mainly negatively

charged, larger pore size (6 µm) and higher flow rate restricted protein particles from interacting with the column matrix and were consequently washed off the column. The second hypothesis is stronger. In addition, longer flow-through washes (24 CVs) didn't show any improvement on the impurities' removal, where the protein amount in the later fractions were less than lower limit of quantification (< LLOQ). Total DNA amount analysis revealed that DNA content of the flow-through using both 2 and 6 µm pore size columns were similar with slightly higher DNA removal in the flow-through using 6 µm column (Fig. 3.2).

Linear gradient elution was examined for CIM QA 6 µm and the results demonstrated a similar virus recovery as the stepwise elution (Fig. 3.3). This elution method showed a good separation of proteins from the virus particle, where the fraction with the highest virus amount (E3), just had 4% of the contaminating protein, which means that about 96% of the total protein was separated from the eluting virus particles. However, no significant changes were observed on DNA removal from the virus main fraction (E3).

The above results highlighted the importance of selecting the optimal column pore size for both achieving higher virus recovery as well as better removal of impurities, which will consequently affect the column performance in the later runs. The Rhabdoviral vector purifications on CIM QA columns were challenging since the virus particles did not completely detach from the column matrix during the elution step. Presumably, a strong interaction between the negatively charged envelope of the Rhabdoviral vector and positively charged QA functional groups on the matrix prevented the reversible adsorbing/desorbing behavior of the virus particles. Since the

virus recovery from QA column was low, no further optimization on the runs were conducted and alternatives to the anion-exchange chromatography were investigated.

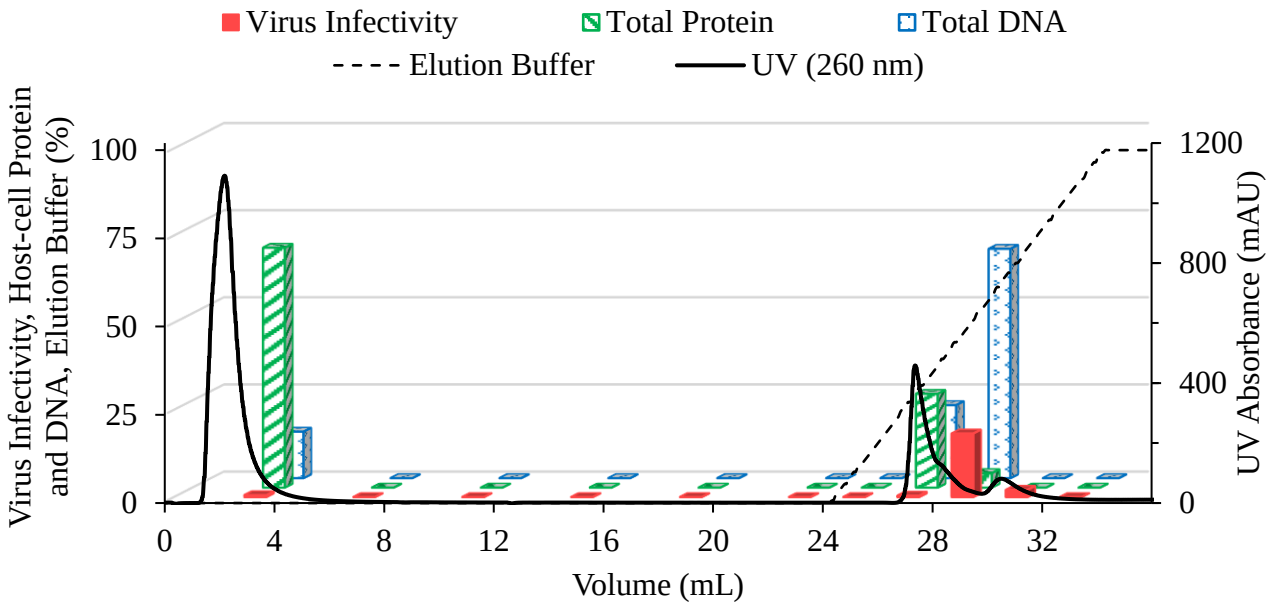

Fig. 3.3. A representative chromatography purification of Rhabdoviral vector (Batch B) using CIM QA with 6 µm pore size. Linear-gradient elution in 10 CVs from 0% to 100% of the Elution buffer. Binding buffer: 10 mM HEPES, 4% sucrose, pH 7.4. Elution buffer: Binding buffer with 2.0 M NaCl. Percentage of virus infectivity (red bar), total protein (green bar), and total DNA (blue bar), all relative to the initial feed sample. The loaded sample contained $(5.4\pm0.8)\times10^{9}$ $ID_{50}.mL^{-1}$ infectious virus, 3.9 ± 0.2 $mg.mL^{-1}$ total protein and 329.6 ± 74.3 $ng.mL^{-1}$ total DNA.

3.4.2. Hydrophobic Interaction Chromatography

Hydrophobic interaction chromatography was performed using a monolithic column with hydroxyl functional groups (CIM OH). The OH column has weak hydrophobicity while exhibiting some hydrophilic properties as well.[4] A pore size of 6 µm was selected based on the results presented in Section 3.4.1. Ammonium sulfate

(AS) was selected from a well-known Hofmeister series as one of the strong anti-chaotropic salt to increase hydrophobicity of the materials and mediate binding of virus particles to the column. The salt concentration in the binding solution is critical to induce sufficient interactions for efficient binding and consequently elution of the Rhabdoviral vector. In fact, hydrophobic interaction between virus particle and the ligand is entropy-driven, where association at high salt condition increases the overall entropy, causing the free energy to decrease.[44] Equilibration and binding conditions were conducted at high concentration of AS, while the elution took place with a sudden one-step drop in the conductivity by applying the elution buffer with no AS salt (100% Elution buffer).

From the results obtained in Section 3.4.1, it was concluded that the virus particles have high surface charge; therefore, relatively high AS salt concentration (1.5 M) was selected as the starting point to conduct hydrophobic interaction chromatography experiments. A set of experiments was designed for the initial screening of the Binding/Elution buffer conditions for hydrophobic interaction chromatography of Rhabdoviral vector (Table 3.1). As shown in Table 3.1, Buffer A with AS concentration of 1.5 M at pH 7.4 result in more than 98% of the virus being captured by the matrix while on average just about 45% of the virus particles were eluted from the column (obtained by $TCID_{50}$ assay). However, increasing the AS concentration to 2.0 M at the same pH value (Buffer C) resulted in no infectious virus particle in the flow-through and on average more than 60% of virus particles were recovered in the elution step (Table 3.1). The infectivity of the virus from Batch C diluted 1:1 with 4 M AS stock solution was $(1.6\pm0.1)\times10^{9}$ $ID_{50}.mL^{-1}$. Infectivity results from PFU assay were also in

good agreement with $TCID_{50}$ assay with 74±31% of the virus recovered using the Binding buffer condition of 2.0 M AS, pH 7.4.

Examining higher pH value, the virus recovery using Buffer D (2.0 M AS at pH 8.0) was increased to average 84±11% (Table 3.1). Effect of pH in hydrophobic interaction chromatography can be complex, where an increase in pH could result in weakening hydrophobic interactions.[45] The latter behavior might be due to increased charged groups on the particles.[29,45] Our hypothesis is that binding of the virus particles by Buffer C (pH 7.4) resulted in a stronger interaction, where consequently on average 30% of the virus particles didn't come off the column during the elution step due to an irreversible hydrophobic interaction. The hydrophobicity of the virus particles in Buffer D (pH 8.0) was still high enough that higher pH didn't affect the virus adsorption to the matrix, since there were no infectious virus particles was detected in the flow-through (Table 3.1). On the other hand, in the elution step, the combination of effects of 'salting-in' and higher pH caused higher recoveries of the virus particles from the column (>80%).

The second fraction from the elution step (E2) in the stepwise elution which always contained the highest amount of virus particles, had a conductivity of ~100 $mS.cm^{-1}$ (~1 M AS). Rhabdoviral vectors incubated in buffer (10 mM HEPES, 4% sucrose) containing 1 M AS were expected to be relatively stable as shown by our short-term stability study with slight titer decrease from 100%±16% to 89%±28% (Fig. S 3.5).

Table 3.1. Effect of AS concentration and pH on Rhabdoviral vector recovery from CIM OH column (6 µm pore size) during stepwise-elution method

Buffer Name	**Buffer Conditions**		**Virus Infectivity (%)**	
	AS (M) in Binding	pH (Binding and Elution)	Flow-through *	Elution $^{\Psi}$
A	1.5	7.4	1.1±0.6 1.0±0.4	62±13 34±15
B		8.0	0.4±0.1 0.3±0.1	66±25 25±8
C	2.0	7.4	N.D.	75±25 60±28
D		8.0	N.D.	84±29 79±21 80±18

* F1 (4 mL)
$^{\Psi}$ Sum of virus infectivity in E2, E3, E4 (2 mL each), tested individually and percentages were relative to the total infectivity of the feed.
N.D: No detection of the infectious virus

Fig. 3.4 demonstrated the effects of AS salt concentration of 1.5 M vs. 2.0 M at pH 8.0 (Buffer B and D) on impurities amount as well as the virus recovery in both flow-through and elution step. The total protein and DNA of the virus solution from Batch C after 1:1 dilution with stock AS solution (4 M) were 1.9±0.1 mg.mL^{-1} and 111.2±9.5 ng.mL^{-1}, indicating that the initial virus sample (i.e. Feed) was contaminated with large amount of proteins. By changing pH from 7.4 to 8.0, no significant change in DNA amount in the flow though was observed, comparing either Buffer A vs. B or Buffer C vs. D (Data not shown); however, the latter pH change caused slightly higher removal of the contaminating proteins in the flow-through; for example, 1.0±0.2 mg removal using Buffer C compared to 1.3±0.3 mg removal using Buffer D.

By increasing AS salt concentration from 1.5 M to 2.0 M (pH 8.0), the total protein amount in the flow-through decreased from 95% to 69%, while there wasn't a significant change in the DNA amount, for which about 85% DNA was removed in the

flow-through (Fig. 3.5). The decrease in the levels of contaminating protein was expected due to the increased amount of anti-chaotropic salt and consequent increase in hydrophobic interaction between proteins and the column. In a study by Hansen et al. [20] , more than 98% protein contents of the loading sample was adsorbed to the hydrophobic resins, while in our case, using monolithic columns with OH functional groups and larger pore size (6 µm), only about 30% (for 2 M AS, pH 8.0) of proteins was adsorbed in the column.

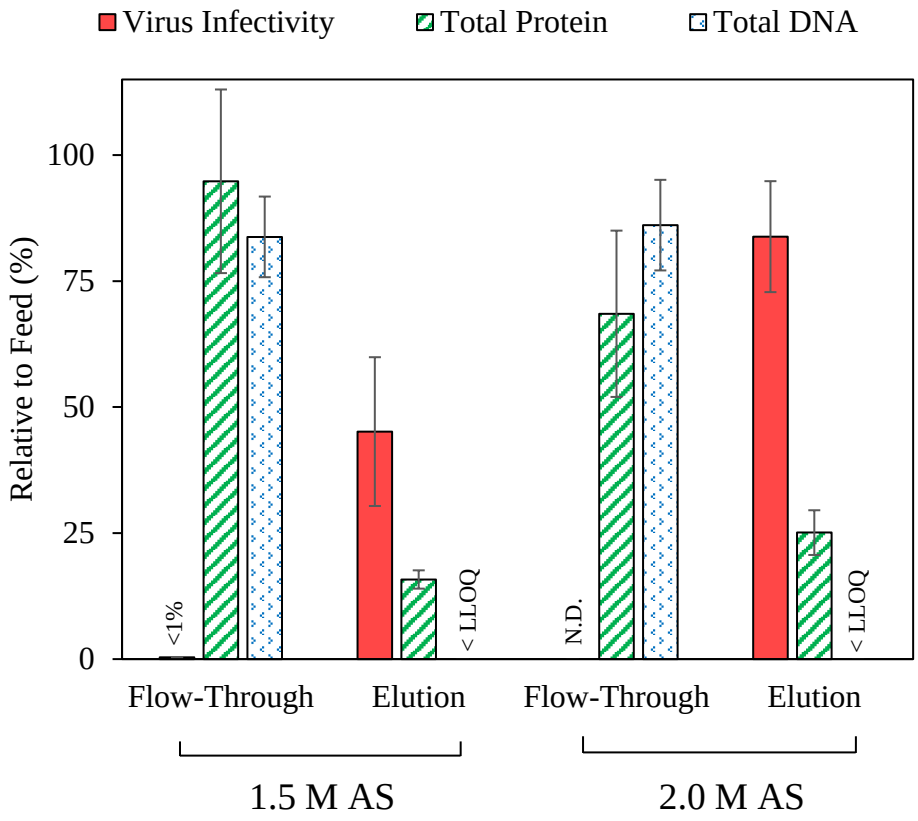

Fig. 3.4. Effect of ammonium sulfate (AS) concentration on virus recovery and removal of impurities during purification of a Rhabdoviral vector with CIM OH column (6 µm pore size). Column equilibrium with 10 mM HEPES, 4% sucrose, pH 8.0 either with 1.5 M AS or 2.0 M AS (Buffer B vs. Buffer D). Sample was loaded with the same Equilibrium buffer followed by a stepwise elution at 100% of the Elution buffer. Flow-through: F1. Elution: sum of the results of E2, E3, and E4, 2 mL per each, tested individually. The virus infectivity, total protein

and DNA were $(1.6\pm0.1)\times10^{9}$ $ID_{50}.mL^{-1}$, 1.9±0.1 $mg.mL^{-1}$ and 111.2±9.5 $ng.mL^{-1}$, respectively. N.D: No detection of the infectious virus particle. LLOQ: lower limit of quantification of the assay.

One main advantage of the monolithic column chromatography using hydrophobic interaction column was more than 85% DNA was removed in the flow-through step without having Benzonase® nuclease treatment step (Fig. 3.5). This is a significant advantage over conventional downstream processing of viruses and vaccines, which mostly includes Benzonase® nuclease treatment step. The DNA and protein content of fraction E2, which had an infectious titer of $(9.5\pm2.3)\times10^{8}$ $ID_{50}.\ mL^{-1}$, was less than LLOQ and 465±78 $\mu g.mL^{-1}$ (25%±4%) using Buffer condition D (2.0 M AS at pH 8.0).

From mechanism of HIC, it could be concluded that additives with "salting-in" effects in the elution buffer could result in weakening hydrophobic interactions and subsequent dissociation of the product-ligand complex.[30] We selected glycerol as an additive since it was reported to mediate the hydrophobic interactions of proteins [31–33] and increases the stability of virus particles.[34–37] Short-term stability test demonstrated that Rhabdovirus is stable in 1.0 M AS on ice for 1-hour in the presence of glycerol (Fig. S 3.5). Addition of glycerol was tested under different pH conditions, shown in Fig. 3.6. The results indicated that the recovery of the infectious Rhabdoviral vector was increased from 67±19% to 77±17% at pH 7.4, and from 84±11% to 97±20% at pH value of 8.0. Recovery results of using Elution buffer with addition of glycerol at pH 8.0 using PFU assay and real-time RT-PCR assay were 95±18% and 86±16%, respectively, in good agreement with the result of $TCID_{50}$ assay.

The protein amount in the main virus fraction (E2) using glycerol as an additive at pH 8.0 was 379±47 µg.mL^{-1} (~20% of the initial loaded sample), whereas DNA amount was still less than LLOQ.

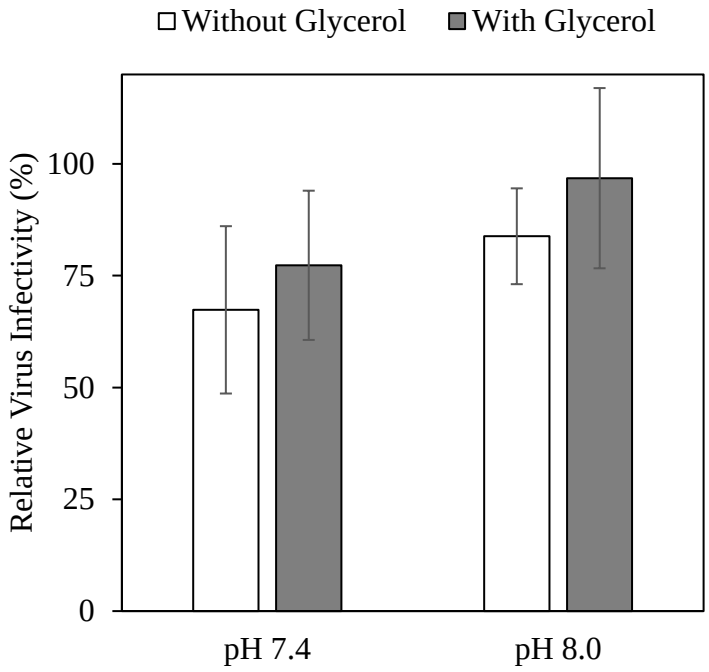

Fig. 3.5. Effect of glycerol addition on the recovery of Rhabdoviral vector (Batch C) from CIM OH column (6 µm pore size) at different pH values (7.4 and 8.0). Column equilibrium with 10 mM HEPES, 4% sucrose with 2.0 M AS at different pH values; Sample was loaded with the same Binding buffer followed by a stepwise elution at 100% of the Elution buffer. Elution buffer 10 mM HEPES, 4% sucrose, pH 7.4 or 8.0, with or without glycerol. The virus infectivity of the loaded sample was (1.6±0.1)×10^{9} ID_{50}.mL^{-1}.

To achieve better separation of the contaminating protein, a linear-gradient elution of the virus was implemented (shown in Fig. 3.6). The linear gradient was defined with a slope of 25% of Elution buffer pumped per CV. Infectivity assays revealed that the virus recovery was 76±14% on average with the total collected infectious virus particle of (1.3±0.3)×10^{9} ID_{50} (Fig. 3.6). Protein quantification assay also demonstrated

separation of a part of the remaining proteins in the fraction just before the main virus fraction. The protein amount of the main virus fraction (E3) was ~14% of the initial sample, 238±69 µg (concentration: 119±34 µg.mL^{-1}). The DNA amount in the fractions from elution step was still LLOQ.

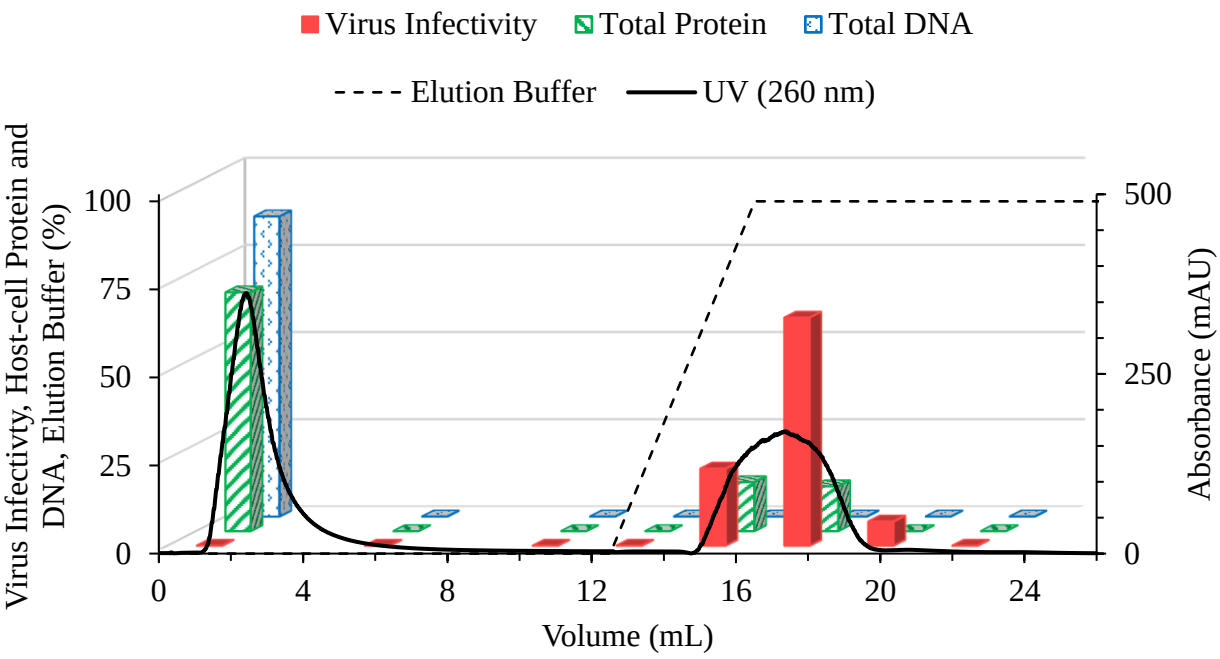

Fig. 3.6. A representative chromatography of Rhabdoviral vector purification (Batch B) using CIM OH (6 µm pore size). Linear-gradient elution was conducted in 4 CVs from 0% to 100% of the Elution buffer. Binding buffer: 10 mM HEPES, 4% sucrose, 2.0 M AS, pH 8.0. Elution buffer: 10 mM HEPES, 4% sucrose, 5% glycerol, pH 8.0. Percentages of virus infectivity (red bars), total protein (green bars), and total DNA (blue bars), all relative to the initial feed sample. The virus infectivity, total protein and DNA of the loaded sample were (1.6±0.1)×10^{9} ID_{50}.mL^{-1}, 1.9±0.1 mg.mL^{-1} and 111.2±9.5 ng.mL^{-1}, respectively.

3.5. Conclusions

The presented results highlight the importance of chromatography column selection in terms of both chemistry of functional group and column matrix pore size for

oncolytic virus purification. Low recovery of Rhabdoviral vector was observed using monolithic anion-exchange column with either 2 µm or 6 µm pore size. We believed that this behavior is mainly due to an irreversible interaction of the negatively charged virus envelope with positively charged functional groups of the column. The column with a larger pore size (6 µm) demonstrated superior removal of the total protein (> 60%) in flow-through. In contrast, the differences in the removal of the total DNA from viral vector solution with both available pore sizes were negligible. Subsequently, the monolithic hydrophobic interaction column with 6 µm pore size was assessed for Rhabdoviral vector purification with significantly higher virus recovery compared to the anion-exchange column. Increasing anti-chaotropic salt concentration as well as pH resulted in higher Rhabdoviral vector recovery from the column. Using a monolithic CIM-OH hydrophobic interaction column with 6 µm pore size, remarkable removal of the total protein (>60%) and DNA (>80%) was observed in flow-through. It is worth noting that this significant amount of DNA removal was achieved without including a nuclease digestion step (e.g. Benzonase treatment).

In several studies of protein and DNA purification with hydrophobic interaction columns, use of specific chemicals was reported mainly to aid elution of the target particle by weakening the hydrophobic interaction ("salting-in" effects) or preserving and stabilizing the target particle while dissociation from the column. We examined glycerol in the hydrophobic interaction chromatography of Rhabdoviral vector and results revealed higher virus recoveries due to combined effects of mediating virus particles elution from the column and increasing virus particle stability.

3.6. Acknowledgments

Funding was provided by the ‘Alliance for Biotherapeutics Manufacturing Innovation’ project that was supported by the Ontario Research Fund – Research Excellence program (RE07-092). The authors thank Adam Smith, Joris van der Heijden, and John Bell from the Biotherapeutics Manufacturing Center at the Ottawa Hospital Research Institute for providing the virus sample and their insight into the work. The authors thank Ales Strancar from BIA Separations for his insightful contribution and Canadian Life Science for kindly providing CIM OH column. From McMaster University, we thank the Biointerfaces Institute for providing access to the DLS equipment.

3.7. References

1. Reichl, U. & Wolf, M. W. Downstream processing of cell culture-derived virus particles. *Expert Rev. Vaccines* **10,** 1451–1475 (2011).
2. Forcic, D. *et al.* Concentration and purification of rubella virus using monolithic chromatographic support. *J. Chromatogr. B* **879,** 981–986 (2011).
3. Jungbauer, A. & Hahn, R. Polymethacrylate monoliths for preparative and industrial separation of biomolecular assemblies. *J. Chromatogr. A* **1184,** 62–79 (2008).
4. Burden, C. S., Jin, J., Podgornik, A. & Bracewell, D. G. A monolith purification process for virus-like particles from yeast homogenate. *J. Chromatogr. B* **880,** 82–89 (2012).
5. Venkatachalam, A. R. K., Szyporta, M., Kiener, T. K., Balraj, P. & Kwang, J. Concentration and purification of enterovirus 71 using a weak anion-exchange monolithic column. *Virol. J.* **11,** 99 (2014).
6. Trilisky, E. I. & Lenhoff, A. M. Sorption processes in ion-exchange chromatography of viruses. *J. Chromatogr. A* **1142,** 2–12 (2007).
7. Rajamanickam, V., Herwig, C. & Spadiut, O. Monoliths in Bioprocess Technology. *Chromatography* **2,** 195 (2015).
8. Wang, P. G. *Monolithic chromatography and its modern applications*. (ILM publications, 2010).
9. Urbas, L. *et al.* Purification of recombinant adenovirus type 3 dodecahedric virus-like particles for biomedical applications using short monolithic columns. *J. Chromatogr. A* **1218,** 2451–2459 (2011).
10. Peterka, Matjaz, Ales Strancar, Marko Banjac, Petra Kramberger, Elisabeth Roethl, and Thomas Muster. "Method for influenza virus purification." U.S. Patent Application 14/791,691, filed January 7, 2016.
11. Bandeira, V. *et al.* Downstream processing of lentiviral vectors: releasing bottlenecks. *Hum. Gene. Ther. Methods* **23,** 255–263 (2012).
12. Allmaier, G. *et al.* Monolithic anion-exchange chromatography yields rhinovirus of high purity. *J. Virol. Methods* **251,** 15–21 (2018).
13. Gerster, P. *et al.* Purification of infective baculoviruses by monoliths. *J. Chromatogr. A* **1290,** 36–45 (2013).
14. Rupar, M. *et al.* Fast purification of the filamentous Potato virus Y using monolithic chromatographic supports. *J. Chromatogr. A* **1272,** 33–40 (2013).
15. Gutiérrez-Aguirre, I. *et al.* Concentrating rotaviruses from water samples using monolithic chromatographic supports. *J. Chromatogr. A* **1216,** 2700–2704 (2009).

16. Sviben, D., Forcic, D., Ivancic-Jelecki, J., Halassy, B. & Brgles, M. Recovery of infective virus particles in ion-exchange and hydrophobic interaction monolith chromatography is influenced by particle charge and total-to-infective particle ratio. *J. Chromatogr. B* **1054,** 10–19 (2017).

17. Kang, Yun, Mark William Cutler, Amadou Affrey Ouattara, and Kristen Elissa Syvertsen. "Purification processes for isolating purified vesicular stomatitis virus from cell culture." U.S. Patent 7,875,446, issued January 25, 2011.

18. Einarsson, M., Kaplan, L., Nordenfelt, E. & Miller, E. Removal of hepatitis B virus from a concentrate of coagulation factors II, VII, IX and X by hydrophobic interaction chromatography. *J. Virol. Methods* **3,** 213–228 (1981).

19. Wolff, M. W., Siewert, C., Hansen, S. P., Faber, R. & Reichl, U. Purification of cell culture-derived modified vaccinia ankara virus by pseudo-affinity membrane adsorbers and hydrophobic interaction chromatography. *Biotechnol. Bioeng.* **107,** 312–320 (2010).

20. Hansen, Sara Post, Rene Faber, Udo Reichl, Michael Wolff, and Anders Peter Gram. "Purification of vaccinia viruses using hydrophobic interaction chromatography." U.S. Patent 8,003,364, issued August 23, 2011.

21. Segura, M. M., Puig, M., Monfar, M. & Chillón, M. Chromatography purification of canine adenoviral vectors. *Hum. Gene Ther. Part B Methods* **23,** 182–197 (2012).

22. Vincent, D. *et al.* The development of a monolith-based purification process for Orthopoxvirus vaccinia virus Lister strain. *J. Chromatogr. A* **1524,** 87–100 (2017).

23. Shoaebargh, S. *et al.* Sterile filtration of oncolytic viruses: An analysis of effects of membrane morphology on fouling and product recovery. *J. Memb. Sci.* **548,** 239–246 (2018).

24. Hummel, J. *et al.* Maraba virus-vectored cancer vaccines represent a safe and novel therapeutic option for cats. *Sci. Rep.* **7,** 15738 (2017).

25. Pol, J. G. *et al.* Maraba Virus as a Potent Oncolytic Vaccine Vector. *Mol. Ther.* **22,** 420–429 (2014).

26. Brun, J. *et al.* Identification of genetically modified Maraba virus as an oncolytic rhabdovirus. *Mol. Ther.* **18,** 1440–1449 (2010).

27. Zhang, J. *et al.* Maraba MG1 virus enhances natural killer cell function via conventional dendritic cells to reduce postoperative metastatic disease. *Mol. Ther.* **22,** 1320–1332 (2014).

28. Le Boeuf, F. *et al.* Oncolytic Maraba virus MG1 as a treatment for Sarcoma. *Int. J. Cancer* **141,** 1257–1264 (2017).

29. Queiroz, J. A., Tomaz, C. T. & Cabral, J. M. S. Hydrophobic interaction chromatography of proteins. *J. Biotechnol.* **87,** 143–159 (2001).

30. Amersham pharmacia biotech, *Hydrophobic interaction chromatography, principles and methods,* (ISBN 91-970490-4-2, edition AB, 1993).

31. Wang, F., Liu, Y., Ma, G. & Su, Z. Glycerol-Assisted Hydrophobic Interaction Chromatography Improving Refolding of Recombinant Human Granulocyte Colony-Stimulating Factor. *Appl. Biochem. Biotechnol.* **159,** 634 (2009).

32. Li, J.-J., Liu, Y.-D., Wang, F.-W., Ma, G.-H. & Su, Z.-G. Hydrophobic interaction chromatography correctly refolding proteins assisted by glycerol and urea gradients. *J. Chromatogr. A* **1061,** 193–199 (2004).

33. Vagenende, V., Yap, M. G. S. & Trout, B. L. Mechanisms of Protein Stabilization and Prevention of Protein Aggregation by Glycerol. *Biochemistry* **48,** 11084–11096 (2009).

34. Xie, Q., Hare, J., Turnigan, J. & Chapman, M. S. Large-scale production, purification and crystallization of wild-type adeno-associated virus-2. *J. Virol. Methods* **122,** 17–27 (2004).

35. Wang, P. *et al.* Glycerol facilitates the disaggregation of recombinant adeno-associated virus serotype 2 on mica surface. *Colloids Surfaces B Biointerfaces* **60,** 264–267 (2007).

36. Jorio, H., Tran, R. & Kamen, A. Stability of serum-free and purified baculovirus stocks under various storage conditions. *Biotechnol. Prog.* **22,** 319–325 (2006).

37. Ugai, H. *et al.* Stability of a recombinant adenoviral vector: optimization of conditions for storage, transport and delivery. *Japanese J. cancer Res.* **93,** 598–603 (2002).

38. SPEARMAN, C. The method of Right and wrong cases ('COnstant Stimuli') without Gauss's Formulae. *Br. J. Psychol. 1904-1920* **2,** 227–242 (2018).

39. Kärber, G. Beitrag zur kollektiven Behandlung pharmakologischer Reihenversuche. *Naunyn. Schmiedebergs. Arch. Exp. Pathol. Pharmakol.* **162,** 480–483 (1931).

40. Gagnon, P., Eric, G. & Torgny, L. Large-Scale Process Development for Hydrophobic Interaction Chromatography, Part I--Gel Selection and Development of Binding Conditions. LC GC Magazine-Magazine of Separation Science-Liquid. in *Chromatography Gas Chromatography* **13,** 318–327 (LC-GC, 1995).

41. Vidič, J. *et al.* Chemical and chromatographic stability of methacrylate-based monolithic columns. *J. Chromatogr. A* **1144,** 63–71 (2007).

42. Trilisky, E. I. & Lenhoff, A. M. Flow-Dependent Entrapment of Large Bioparticles in Porous Process Media. *Biotechnol. Bioeng.* **104,** 127–133 (2009).

43. Podgornik, A., Hamachi, M., Isakari, Y., Yoshimoto, N. & Yamamoto, S. Effect of pore size on performance of monolithic tube chromatography of large biomolecules. *Electrophoresis* **38,** 2892–2899 (2017).

44. Perkins, T. W., Mak, D. S., Root, T. W. & Lightfoot, E. N. Protein retention in hydrophobic interaction chromatography: modeling variation with buffer ionic strength and column hydrophobicity. *J. Chromatogr. A* **766,** 1–14 (1997).

45. Lienqueo, M. E., Mahn, A., Salgado, J. C. & Asenjo, J. A. Current insights on protein behaviour in hydrophobic interaction chromatography. *J. Chromatogr. B* **849,** 53–68 (2007).

3.8. Supplementary Information

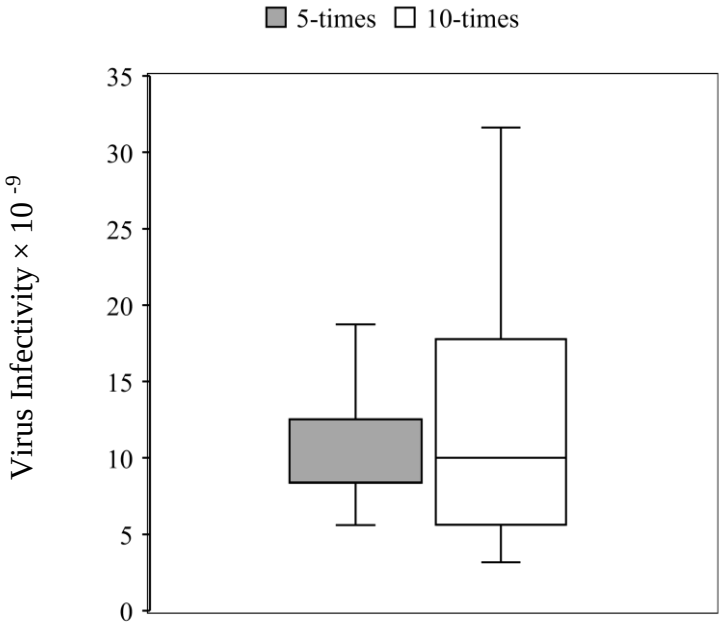

Fig. S 3.1. A box-whisker plot of effect of different serial dilutions (5-times vs 10-times) in $TCID_{50}$ assay for infectivity measurement of Rhabdoviral vector (Batch A). Average infectivity of the virus sample with 5-times and 10-times dilution were $(9.6\pm3.1)\times10^{9}$ $ID_{50}.mL^{-1}$ and $(11.2\pm6.3)\times10^{9}$ $ID_{50}.mL^{-1}$, respectively.

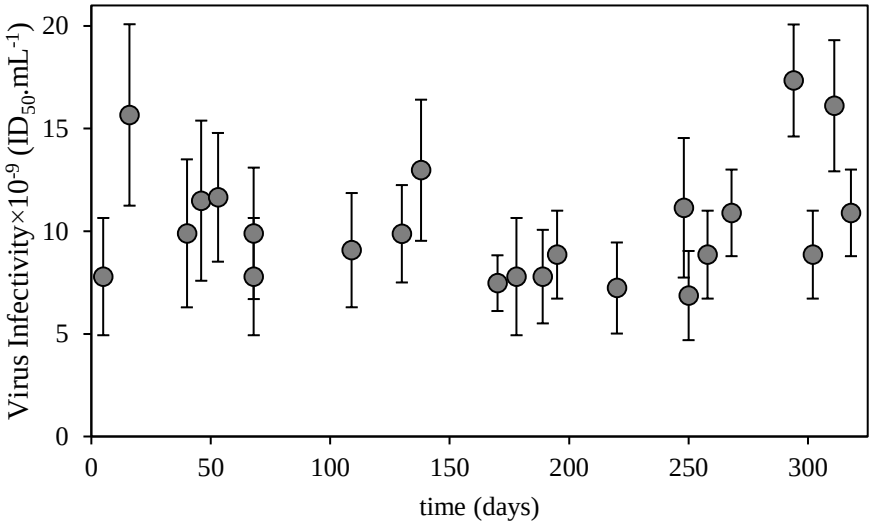

Fig. S 3.2. Long-term stability study of Rhabdoviral vector (Batch A) stored at -80°C. The virus infectivity examined with $TCID_{50}$ assay using 5-times dilution method. Each point and the error bar were average and standard deviation of each conducted $TCID_{50}$ measurement (according to Eq. 3.1).

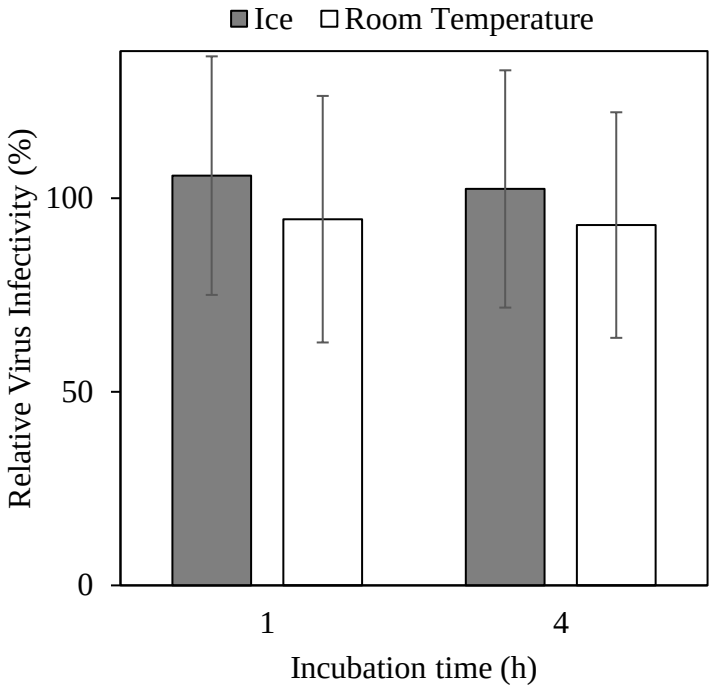

Fig. S 3.3. Short-term stability study of Rhabdoviral vector (Batch C) infectivity after 1-hour and 4-hours incubation either on ice or at room temperature compared to the initial virus infectivity $(3.2\pm0.8)\times10^{8}$ $ID_{50}.mL^{-1}$.

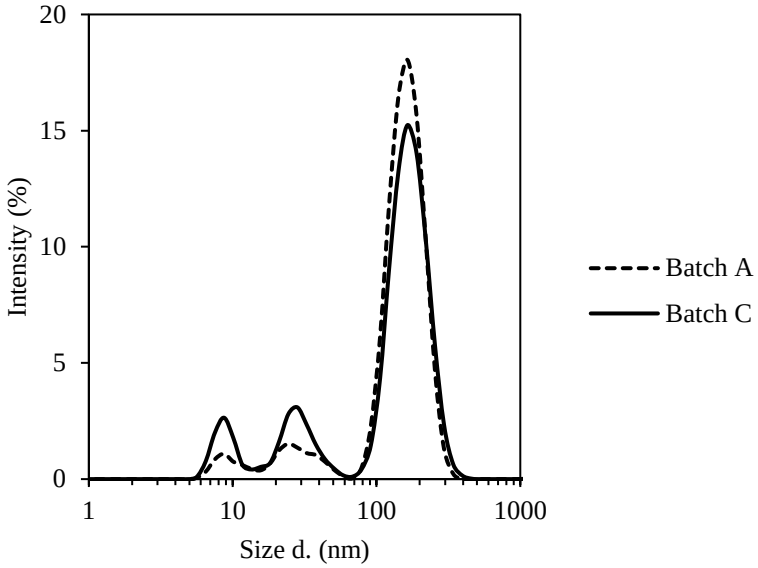

Fig. S 3.4. DLS measurements of the produced Rhabdoviral vector solutions as Batch A and C

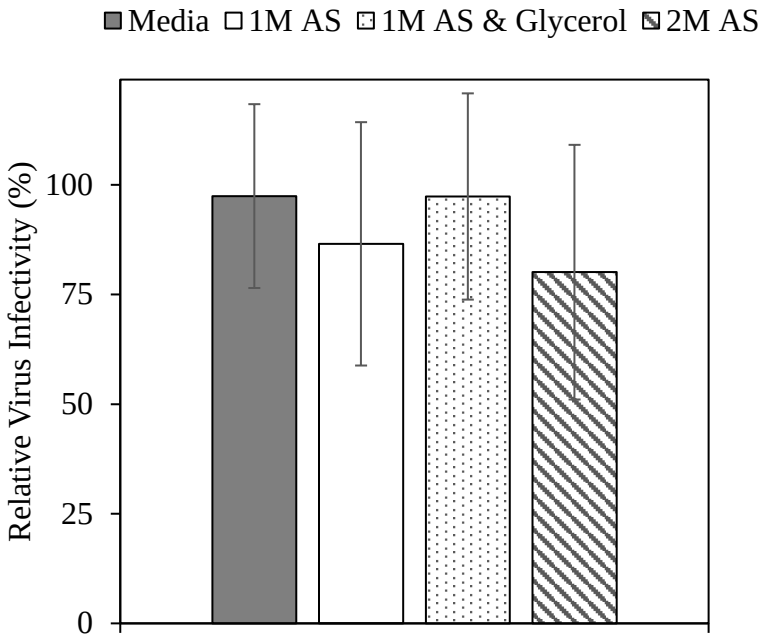

Fig. S 3.5. Short-term stability study of the Rhabdoviral vector (Batch C) infectivity after 1-hour incubation on ice in either media (α-MEM with 5% FBS and 1% L-glutamine, as a negative control) or different buffers; Buffers: 10 mM HEPES, 4% Sucrose, pH=7.4 with either 1.0 M AS, 1.0 M AS with glycerol, or 2.0 M AS. The virus infectivity of the initial sample (i.e. at time 0) was $(3.4\pm0.5)\times10^{8}$ $ID_{50}.mL^{-1}$.

The propagation of the errors was implemented according to Eq. S 3.1 – Eq. S 3.4

$$R = \frac{\sum_{i=1}^{n} F_i}{I} \qquad \text{Eq. S 3.1}$$

$$S = \sum_{i=1}^{n} F_i \qquad \text{Eq. S 3.2}$$

$$\Delta S = \sqrt{\sum_{i=1}^{n} (\Delta F_i)^2} \qquad \text{Eq. S 3.3}$$

$$\Delta R = R\sqrt{(\frac{\Delta S}{S})^2 + (\frac{\Delta I}{I})^2} \qquad \text{Eq. S 3.4}$$

Where F_i and I are the virus titer in the i^{th} fraction of elution step and Initial sample, respectively. Similarly, ΔF_i and ΔI are related to standard deviation of the virus titers in related samples.

Chapter IV

Sterile Filtration of Oncolytic Viruses: An Analysis of Effects of Membrane Morphology on Fouling and Product Recovery

Authors: Shabnam Shoaebargh, Ian Gough, Maria Fe Medina, Adam Smith, Joris van der Heijden, Brian Lichty, John Bell, David R. Latulippe

Published in Journal of Membrane Science, 2018, Vol. 548, 239-246

4.1. Abstract

Oncolytic viruses (OVs) are an emerging class of bio-therapeutics that have attracted significant interest due to their inherent specificity for targeting malignant tissues in cancer immunotherapy. One of the main challenges in many OVs manufacturing processes is the dead-end sterile filtration step that is highly desirable from a safety and regulatory perspective. The primary issue is the severe membrane fouling, as indicated by a dramatic and uncontrollable transmembrane pressure (TMP) increase in constant flux experiments, and low recovery of the desired final product. While previous studies have mostly focused on selective retention or removal of viruses during the production of smaller biologics, this study is the first to obtain quantitative data for the fouling propensity of microfiltration filters and recovery of viral vectors in a sterile filtration

process. The performance of four 0.2/0.22-micron commercial sterile filters was evaluated in constant flux filtration tests with a promising OV candidate (Rhabdovirus Maraba). Among the tested sterile filters, two-layered sterile filters (i.e. Fluorodyne EX EDF and MiniSart Plus) indicated slower transmembrane pressure (TMP) increase along with a higher filtered viral volume as well as higher total viral recovery (i.e. lower titer loss). The measured TMP profiles were analyzed by blocking models with the results indicating that the fouling was best described using standard or intermediate blocking models. These results provide important insights into the development of effective sterile filtration membranes and processes that are critically needed for the large-scale production of OVs.

4.2. Introduction

Oncolytic viruses (OVs) are a new promising class of bio-therapeutics for the treatment of cancer. Many types of viruses have been proposed as viral vectors and depending on the class of virus from which an OV was derived, it will have different modes of therapeutic action including the ability to selectively infect and lyse tumor cells; additionally, they can promote an anti-tumor immune response and thus function as an *in situ* vaccine.[1] In 2015, the US Food and Drug Administration (FDA) approved the first ever OV-based therapy, Imlygic® (talimogene laherparepvec) was approved for the local treatment of melanoma lesions.[2] OVs are currently being tested in a variety of phase I, II, and III clinical trials, both on their own and in combination with other cancer therapies – Pexa-Vec is entering into a Phase III clinical trial for the treatment

of liver cancer.[3] A recent review paper reported that patients were being recruited into 40 different clinical trials in 2016 alone.[4]

The production and purification of OVs must be done under good manufacturing practice (GMP) conditions in order to adhere to strict regulatory specifications including the removal of product related impurities (e.g. endotoxins, host cell proteins, nucleic acids) and process related impurities (e.g. Benzonase, an engineered endonuclease – often used to degrade residual nucleic acids, etc.); the US FDA has a recommendation on the ratio of total number of virus particles to number of infectious particles.[1,5] Cesium chloride density-gradient ultracentrifugation is the most common preparative method for the small scales of OVs that are sufficient for phase I clinical trials. However, that method is not scalable to address the demands for clinical trials involving greater number of patients and full-scale production, and thus alternative downstream purification processes are actively being developed.[6]

The commercial success of OVs is critically dependent on solving the considerable operational and technical challenges associated with 'large-scale' OV purification processes. Those challenges are partly due to the larger size of OVs compared to traditional bio-therapeutic molecules. For example, vesicular stomatitis virus (VSV) is a bullet-shaped,[7] enveloped virus that is approximately 70 nm in diameter and 170 nm in length;[8] in comparison, the hydrodynamic diameters of monoclonal antibodies, a major class of recombinant therapeutic proteins, is in the range of 10 to 12 nm.[9] The Rhabdovirus Maraba, a serotype of VSV, has recently been shown to be a promising OV candidate.[10] The large size of OVs is a particular concern for the final sterile filtration step that immediately precedes vialing and storage of the final product.

Sterility could be obtained by terminal sterilization or using aseptic processing.[5] Terminal sterilization for products that can't be sterilized by dry heat or irradiation is achieved using a normal-flow (i.e. direct-flow) membrane filter with a rated pore size of 0.2 μm (or smaller) that has been validated for the removal of a challenge microorganism such as *Brevundimonas diminuta* (*B. diminuta*).[5]

A detailed and comprehensive understanding of the performance of sterile filtration membranes (e.g. fouling behavior, virus transmission) is critically needed to ensure the commercial success of OVs. While there have been numerous previous studies of using membranes to selectively retain viruses or virus-like particles and allow smaller bio-therapeutic molecules (e.g. recombinant proteins) to pass through the membrane,[11–14] there are relatively few ones on the transmission of viruses through membranes. An early set of studies by Cliver and colleagues [15–17] primarily focused on the filtration performance of different enteroviruses (diameter ~ 30 nm) with a large number of membrane types for the detection of viruses in environmental samples. A limited set of results were presented for the filtration performance of a type 1 Lang Reovirus;[15] interestingly, a different serotype of Reovirus, type 3 Dearing, is currently being studied as a potential OV in clinical trials.[1] In another study, Reeves and Cornetta, developed a serial filtration system for the production of clinical retroviral vectors.[18] In a very recent work, the passage of soft pathogens such as bacteria (e.g. *B. diminuta*) and bacteriophages through custom-made polyethersulfone (PES) membranes were studied.[19]

In this study, the performance of four commercially available sterile filtration membranes from three different manufacturers was evaluated using pre-purified

batches of the Rhabdovirus Maraba. A key criterion in selecting the four membranes was that they were available in both a small 'lab-scale' syringe filter format (to be used for this study) and a large 'process-scale' format (to be used for larger-scale applications). For example, the Fluorodyne EX EDF membrane (Pall) is available in a syringe filter format with approximately 3 cm^2 of membrane area, a mini capsule design with 230 cm^2 of membrane area, and a pleated filter cartridge with 5000 cm^2 of membrane area; according to the manufacturer the latter two are for processing volumes in the tens of liter and hundreds of liters range, respectively. Constant flux filtration tests were conducted at various conditions with the membrane fouling determined via continuous measurement of the transmembrane pressure (TMP). The severity of membrane fouling has been shown to affect the efficiency of filtration processes through product loss, decrease in membrane permeability, and frequent membrane replacements.[20,21] In order to develop a detailed understanding of the fouling process, the measured TMP profiles were compared to standard blocking models based on pore blockage, intermediate pore blockage, pore constriction, and cake formation.

4.3. Experimental

4.3.1. Rhabdovirus Source and Characterization

Three batches of purified Rhabdovirus Maraba (hereafter referred to as Batch A, B, and C) were prepared at the Biotherapeutic Manufacturing Centre at the Ottawa Hospital Research Institute. The purification process includes harvesting, clarification, and membrane-based purification steps to achieve a final batch volume of 150 ml in a pH 7.4 buffer solution containing 10 mM HEPES, 150 mM NaCl, and 4% sucrose. The

purified batches of viral vectors were immediately stored at -80^{o}C, courier expressed overnight to McMaster University, and again stored at -80^{o}C.

The average virus titer for Batches A, B, and C was determined to be $4.7\pm0.9 \times 10^{9}$, $2.2\pm0.9 \times 10^{10}$, and $1.5\pm0.6 \times 10^{10}$ plaque forming unit (PFU) per mL using the procedure described below. VERO cell lines (prepared at the McMaster Immunology Research Centre) were propagated in alfa-Minimum Essential Medium (α-MEM, Thermofisher) supplemented with 8% fetal bovine serum (Gibco, Life Technologies) and 1% L-Glutamine (prepared at the McMaster Immunology Research Centre) in an incubator at 37 °C and 5% CO_2. VERO cells were seeded at 8×10^{5} cells on 60 mm titer plates to achieve the desired cell density. A serial dilution of the viral samples in alfa-MEM media were prepared to assess the virus sample titer. Twenty-four hours after seeding, cells were infected with 100 µl of the last three serially-diluted viral samples followed by rocking the plates every 15 min. After viral adsorption, 3 mL of agarose overlay (1:1 of 1% agarose and 2× supplemented Minimum Essential Medium-F11) were added to the plates. The number of formed plaques were counted the following day. A reference virus sample was included in each plaque assay analysis. Virus total titer (PFU) was calculated based on the total filtered volume of virus solution for each of the sterile filters. The total protein concentration in each batch was determined using the bicinchoninic acid (BCA) assay (Pierce) as per the manufacturer's instructions.

Virus samples were imaged using a JOEL 1200 EX TEMSCAN transmission electron microscope (TEM) equipped with an AMT digital camera. To prepare the viral sample for TEM imaging, a small drop (~5 µL) of the viral sample was pipetted onto a paraffin film (Parafilm), covered with a formvar-carbon coated copper grid, negative

stained by placing the grid on a drop of 2% uranyl acetate, and then left to air dry. The TEM was operated at an accelerating voltage of 80 kV and magnification factors in the range of 150,000 to 300,000.

The size distribution of the Rhabdovirus Maraba sample was determined using dynamic light scattering (DLS) via a ZetaSizer NanoZS instrument (He-Ne red laser, 633 nm, Malvern Instruments, Malvern, UK). The position of the laser attenuator was at 173° relative to the laser source to ensure backscattering detection. A high viral titer (i.e. greater than 10^9 PFU/mL) was required due to the sensitivity limitation of the instrument.[22,23]

4.3.2. Characterization of Rhabdoviral vector preparations

The individual prepared batches of Rhabdovirus Maraba (hereafter referred to as OV solution) were initially characterized using TEM. Multiple images were analyzed for each batch and a representative image of an individual virus particle from Batch A is shown in panel a of Fig. 4.3. The average width and length of the individual viruses that were imaged were 73 ± 4 nm and 167 ± 48 nm, respectively. All of the TEM images showed that other unidentified smaller particles were also present in the prepared batches. Some of the TEM images showed large aggregates of viral particles, see panel b of Figure 3 for an example; however, it is possible that the fixing of the sample to the SEM grid confounded our ability to identify the actual amount of virus aggregate in solution. Thus, as shown in panel c of Fig. 4.3, DLS analysis was used to determine the relative intensity-based size distribution for the same OV solution (i.e. Batch A). Three distinct peaks with different size distribution ranges were detected. The size range for

the half peak height of the first peak was 20 to 28 nm and it is our hypothesis that this represents aggregated protein particles in solution. According to the BCA assay, the protein concentration of the OV solution was approximately 500 µg/mL. The size range for the half peak height of the second peak was 85 to 130 nm which is in agreement with the dimensions of the individual virus particles as measured by TEM and reported in the literature. The size range for the half peak height of the third peak was 350 to 600 nm and it is our hypothesis that this represents the aggregated viral particles in solution. It is worth noting that the DLS intensity results are biased toward the large aggregated particles due to higher scattered light compared to the smaller particles [24,25]. However, the raw intensity-based data is preferred to volume- or number-based data due to the assumptions in the transformation of data from intensity to volume or number, especially for non-spherical particles.

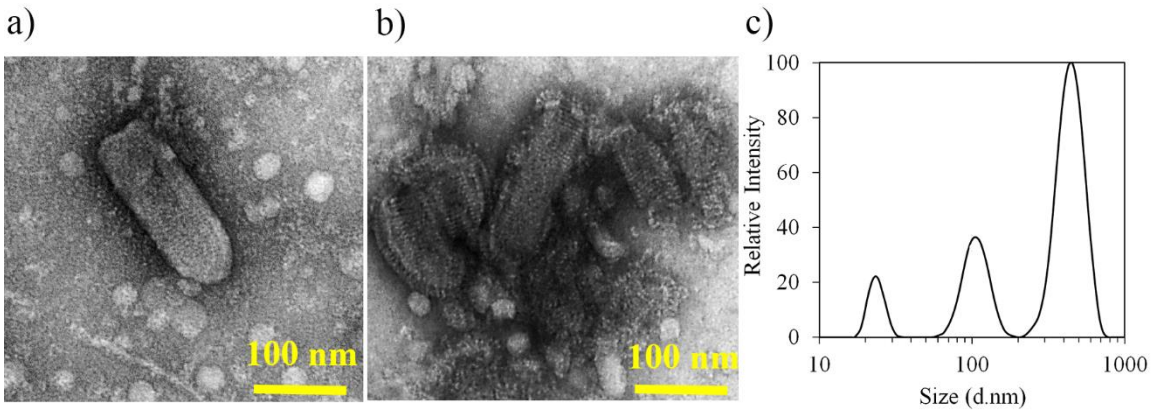

Fig. 4.1 Characterization results for the Rhabdoviral vector sample; Panel (a): TEM image of a single virus from Batch A at ×200 000 magnification; Panel (b): TEM image of aggregated virus from Batch C at ×250 000 magnification; Panel (c): DLS results for Batch A.

4.3.3. Sterile Filtration Membranes

As shown in Table 4.1, four microfiltration syringe filters, with 0.2 or 0.22 µm pore size ratings, from three different manufacturers were used in this study. They were chosen partly on the basis of their different physico-chemical characteristics but mostly because the same membrane is also commercially available in larger 'process-scale' modules. Two of the filters (Durapore and MiniSart NML) contain just the sterile filtration membrane while the other two (MiniSart Plus and Fluorodyne EX EDF) have an extra 'pre-filter' material on top of the sterile filtration membrane.

Scanning electron microscopy (SEM) images of the membranes were obtained using a Vega II LSU (Tescan) instrument. The membranes and pre-filter materials were physically extracted from each syringe filter module, individually mounted on specimen carriers, and gold sputtered for 80 seconds under vacuum conditions at a current of 20 mA. As shown in Figure 4.1, the SEM images of the top membrane surface showed a considerable difference in the pore structure and morphology. The cross-section images shown in Fig. S 4.1 were obtained by first freeze-fracturing the membrane using liquid nitrogen and then following the same sample preparation procedure described above; the thickness of the membrane layers reported in Table 4.1 were obtained from the cross-section SEM images.

Table 4.1 Physical properties of the sterile syringe filters evaluated in this study

Manufacturer	Filter name	Number of layers	Materials	Pore size[a] (µm)	Area (cm^2)	Thickness[b] (µm)
EMD Millipore	Durapore	1	PVDF[*]	0.22	4.5	116±3
Sartorius	MiniSart NML	1	SFCA[†]	0.2	6.5	145±2
	MiniSart Plus	2	GF/SFCA[‡]	1.2/0.2	5.3	494±17/139±6
Pall Corporation	Fluorodyne EX EDF	2	PES/PVDF[ψ]	0.2/0.2	2.8	208±7/81±2

[*] Polyvinylidene fluoride
[†] Surfactant free cellulose acetate
[‡] Glass fiber / Surfactant free cellulose acetate
[ψ] Polyethersulfone / Polyvinylidene fluoride
[a] Specified by membrane manufacturer
[b] Determined via SEM characterization (refer to Figure S1 for additional details)

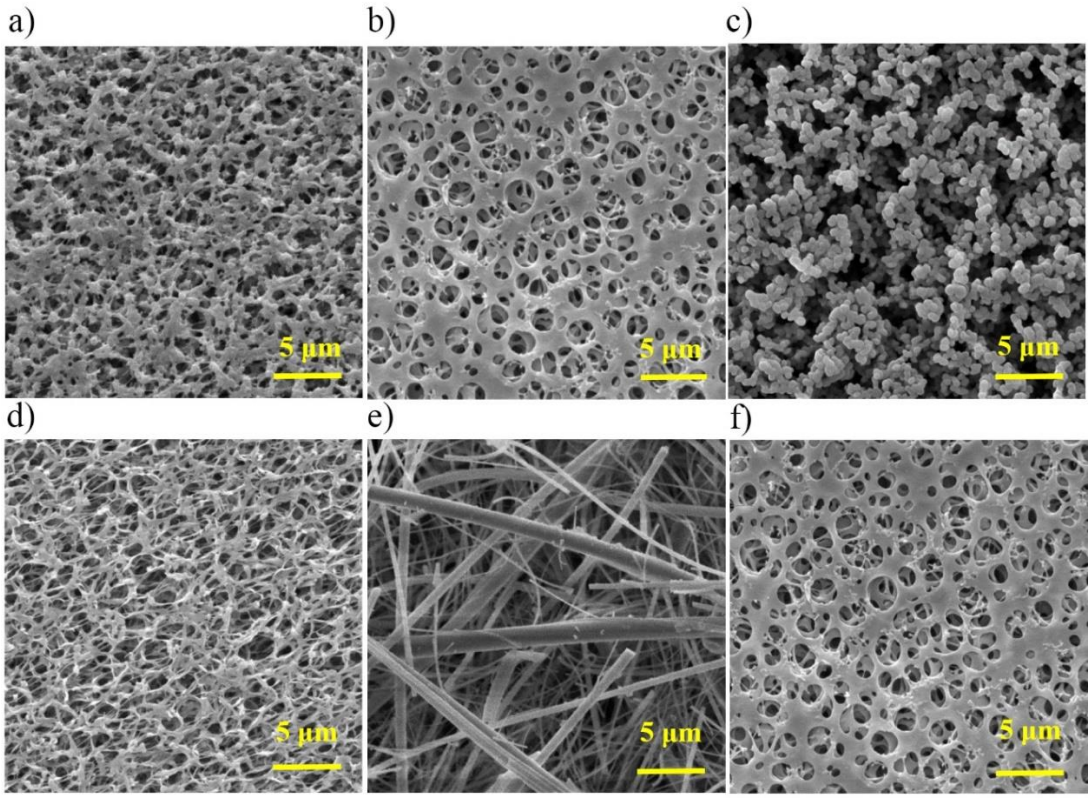

Fig. 4.2. Scanning electron micrographs (×8000 magnification) of the top surface of the layers of the four microfiltration membranes that were used in this study:

Durapore 0.22 μm single layer PVDF membrane is shown in panel a; MiniSart NML 0.2 μm single layer SFCA membrane is shown in panel b; Fluorodyne EX EDF membrane 0.2 μm top PES layer is shown in panel c; Fluorodyne EX EDF membrane 0.2 μm bottom PVDF layer is shown in panel d; MiniSart Plus membrane 1.2 μm top GF layer is shown in panel e; MiniSart Plus membrane 0.2 μm bottom SFCA layer is shown in panel f.

4.3.4. Virus Sterile Filtration Experiments

A schematic diagram of the constant flux filtration setup is shown in Fig. 4.2. Two Teflon reservoirs with a capacity of 50 mL each were used for the feed and filtrate reservoirs. A Masterflex L/S peristaltic pump (Cole-Parmer) with disposable L/S 14 silicone tubing was used to set the filtrate flux; the TMP was monitored via a pressure transducer connected to a KrosFlo Digital Pressure Monitor (SpectrumLab). The entire setup was located and operated in a biosafety cabinet (Class II, Type A2) in order to comply with biosafety regulations and thus all experiments were conducted at ambient temperature (22 ± 3 °C).

A virus-free pH 7.4 buffer solution containing 10 mM HEPES (Gibco, Life Technologies), 150 mM NaCl (Reagent grade, Bioshop), 4% sucrose (Ultrapure, Bioshop), was prepared to match that of the Rhabdovirus solution and filtered through a 0.2 μm PES sterile filter (Nalgene, Thermo Scientific). Before the filtration experiment, each syringe filter was pre-conditioned by passing a minimum of 30 mL of the virus-free buffer first in the 'normal' orientation (i.e. front to back) followed by the 'reverse' orientation (i.e. back to front). Then, the hydraulic permeability of the native (i.e. unused) membrane ($L_{P,0}$) was determined from the plot of filtrate flux (J_v) as a function of TMP according to Eq. 4.1:

$$L_p\left[\text{mL.min}^{-1}.\text{cm}^{-2}.\text{kPa}^{-1}\right]=\frac{J_v\left[\text{mL.min}^{-1}.\text{cm}^{-2}\right]}{\text{TMP [kPa]}} \qquad \text{Eq. (4.1)}$$

Each sterile filtration experiment included the following six stages:

I. Filtration of approximately 30 ml of the virus-free buffer at a constant flux of 0.3 $\text{mL.min}^{-1}.\text{cm}^{-2}$; according to Table 1, the syringe filters have slightly different active membrane areas and thus the required flow rate varied from 0.85 mL.min^{-1} (for the Fluorodyne EX EDF syringe filter) to 1.6 mL.min^{-1} (for the MiniSart NML syringe filter).

II. The reservoirs and silicone tubing were emptied of virus-free buffer and then filled with approximately 50 mL of thawed Rhabdoviral vector solution. The filtration experiments were conducted at a constant filtrate flux of 0.3 $\text{mL.min}^{-1}.\text{cm}^{-2}$ and run until either the volume of solution was depleted or the TMP reached 103 kPa (since the peristaltic pump could not maintain the desired flux value at TMP conditions greater than 135 kPa).

III. The reservoirs and silicone tubing were emptied and re-filled with virus-free buffer and the post-filtration hydraulic permeability ($L_{P,III}$) was determined by measuring the TMP values at various filtrate flux settings.

IV. The syringe filter was flipped over so it was in a ‘reverse’ orientation and approximately 15 mL of virus-free buffer was passed through the membrane (at the same flux of 0.3 $\text{mL.min}^{-1}.\text{cm}^{-2}$) and the reversed orientation hydraulic permeability ($L_{P,IV}$) was determined by measuring the TMP values at various filtrate flux settings.

V. The syringe filter was flipped back to its 'normal' orientation and the hydraulic permeability ($L_{P,V}$) was determined again using virus-free buffer by measuring the TMP values at various filtrate flux settings.

VI. The reservoirs and silicone tubing were emptied of virus-free buffer and then re-filled with a ~5% sodium hypochlorite solution (i.e. household bleach) that was passed through the membrane (at the same flux of 0.3 $mL.min^{-1}.cm^{-2}$) to wash the syringe filter filtration setup and clean the membrane.

To avoid any potential contamination, any non-disposable parts (i.e. fittings and reservoirs) were immersed in a 0.5 M sodium hydroxide solution, rinsed with excessive water, and autoclaved before performing the next filtration experiment.

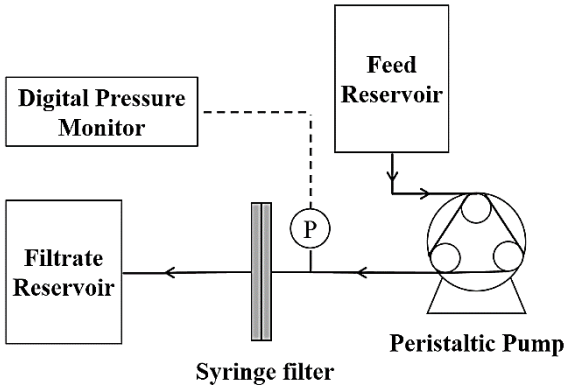

Fig. 4.3. Sterile filtration setup (not to scale); the reader is referred to section 4.3.3 for details on the components.

4.4. Results and Discussion

4.4.1. Sterile filtration of Rhabdoviral vectors

The TMP profiles during filtration of OV solution (Batch A) through each of the four microfiltration membranes is shown in panel a of Fig. 4.4. All four membranes

exhibited a continuous increase in TMP; note that the TMP profile for the MiniSart Plus membrane appears as a succession of small step changes due to the resolution limitation of the pressure transducer. Although all four filters were rated with 0.2 or 0.22 µm pore sizes, there were considerable differences in the filtration performance. For example, at a throughput (filtrate volume per membrane area) of 0.02 m, the TMP required to achieve the desired filtrate flux was 76, 23, 4, and 3 kPa for the Durapore, MiniSart NML, Fluorodyne EX EDF, and MiniSart Plus filters, respectively. Also, the filtration experiment with the MiniSart Plus membrane had to be stopped because it depleted the entire 45 mL volume of OV solution, whereas the other three were stopped when the TMP limit of 103 kPa was reached. As was previously reported for the filtration of protein solutions,[24] the membrane properties (including membrane material, membrane thickness, pore structure, and pore morphology) have a great impact on the performance of the sterile filtration step. In order to make a quantitative comparison of the filtration performance, the initial fouling rate where the TMP increases linearly with filtrate volume [20,21] was calculated for each membrane; the criteria for linearity was an R^2 value greater than 0.95. The results in Figure 4a gave initial fouling rate values of 3.01 and 1.04 $kPa.mL^{-1}$ for the Durapore and MiniSart NML membranes. While the Fluorodyne EX EDF membrane gave an initial fouling rate of 0.48 $kPa.mL^{-1}$, it was the MiniSart Plus membrane whose initial fouling rate of 0.11 $kPa.mL^{-1}$ was an order of magnitude lower than those obtained for the single-layer membranes. Both single-layer membranes had much higher initial fouling rates than the double-layered membranes. The factor of four difference between the Fluorodyne EX EDF and MiniSart Plus results is most likely due to differences in the pre-filter properties (see Fig. 4.1, Fig. S 4.1, and Table 4.1). In order to demonstrate the significance of the pre-filter layer, subsets of

filtration experiments were conducted with the Fluorodyne EX EDF syringe filter in the 'normal' orientation (with the pre-filter PES layer in front of the PVDF membrane) and the 'reverse' orientation (with the PVDF membrane in front of the pre-filter PES layer). As shown in Fig. S 4.2, the TMP profile in the reverse orientation had a much more dramatic increase with filtrate volume. It is assumed that the pre-filter layer captured the large virus aggregates before they reached the membrane surface and thus decreased the fouling rate. A previous study reported similar observations when the filtration of a model protein using Millipore Viresolve 180 membrane was compared for the 'skin-side up' and 'skin-side down' membrane orientations.[26]

A comparison of the total amount of active virus in the collected filtrate is shown in panel b of Fig. 4.4. The results are shown as a box-and-whisker plot to show the distribution of results for the triplicate measurements that each included two dilution series of the filtrate sample; the maximum and minimum of all measurements for the total viral titer (using plaque assay) along with the median of the measurements shown as the horizontal line inside the box. The median of the total titer measurements of the filtered Rhabdoviral solution using Durapore, MiniSart NML, Fluorodyne EX EDF, and MiniSart Plus were 9.5×10^9, 1.8×10^{10}, 1.3×10^{10}, 4.5×10^{10} PFU, respectively. For comparison, the percent recovery using the Durapore, MiniSart NML, and Fluorodyne EX EDF filters were 5%, 11%, and 7% respectively. Sentence about MiniSart Plus was 21% - but artificially low because experiment was stopped early. These differences are mostly due to the volume of the filtered virus rather than the concentration of the filtered virus. For example, the Durapore filter filtered 10 mL at 9.5×10^8 PFU/mL while the MiniSart Plus filter filtered 45 mL at 1.0×10^9 PFU/mL. Comparing the viral titer of the initial sample and the collected filtered viral samples

demonstrated that except for the Fluorodyne EX EDF, the rest of the filters resulted in a very similar titer of the filtered viral solution which we could hypothesized that due to the consistency of the initial sample (Batch A), the loss might be associated partially with the large aggregated particles that were excluded from the viral stream through the filters. However, it could be hypothesized that double-layered filters (e.g. Fluorodyne EX EDF) could result in higher titer loss due to increased probability of the entrapment of viral particles thorough the layers compared to single layered filters. On the other hand, when it comes to filtration of viral solutions for longer times or larger volumes, mechanical disruption of the viral particles moving through the fouled membranes could be a major factor contributing to viral titer loss too.[18] By comparing the total titer results (Fig. 4.4b), the filters with double layers, not unexpectedly, could run for longer time.

The three batches of OV solutions were obtained from three separate production runs at the Biotherapeutics Manufacturing Centre. The TMP profiles obtained for Batch A and Batch B with the Fluorodyne EX EDF and MiniSart Plus membranes are compared in Fig. 4.5. For both filters, the filtration experiments with Batch B gave consistently higher TMP values than Batch A at the same filtration volume. This behavior is likely due to the higher average titer of Batch B ($2.2\pm0.9\times10^{10}$ PFU/mL), which was approximately five times greater than that of Batch A ($4.7\pm0.9\times10^{9}$ PFU/mL); a similar trend was also reported by Reeves and Cornetta.[18] Overall, it was promising to observe that the MiniSart Plus membrane gave the best performance, in terms of lowest TMP values and highest total filtrate titer for both batches of OV solutions.

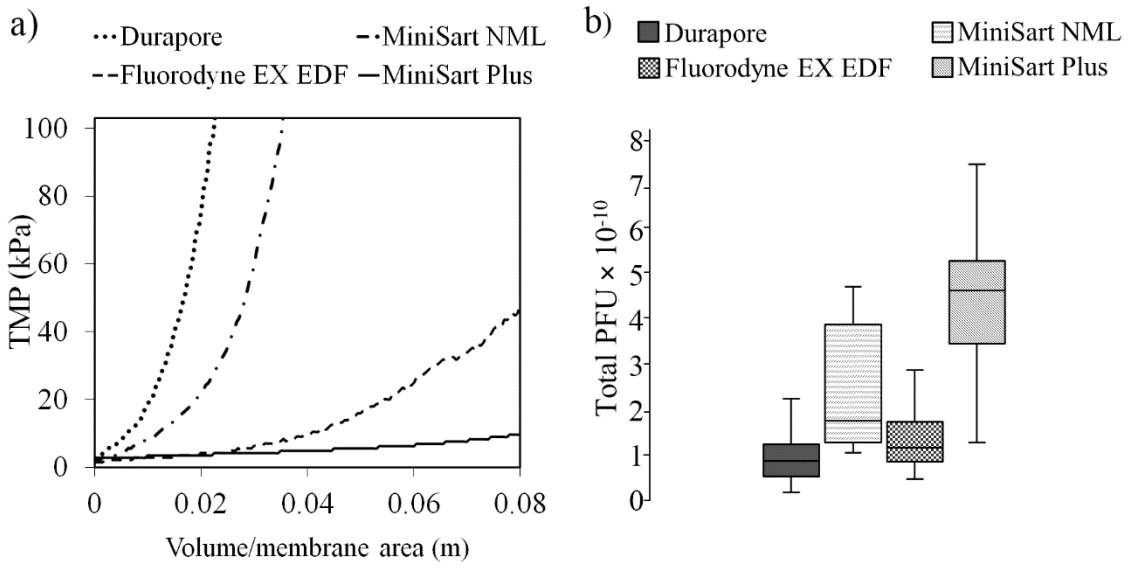

Fig. 4.4 Comparison of filtration performance of the four microfiltration membranes with OV solution (Batch A). Transmembrane pressure profiles at a constant filtrate flux of 0.3 $mL.min^{-1}.cm^{-2}$ are shown in panel a. Box and whisker plots of the filtrate total titer values are shown in panel b.

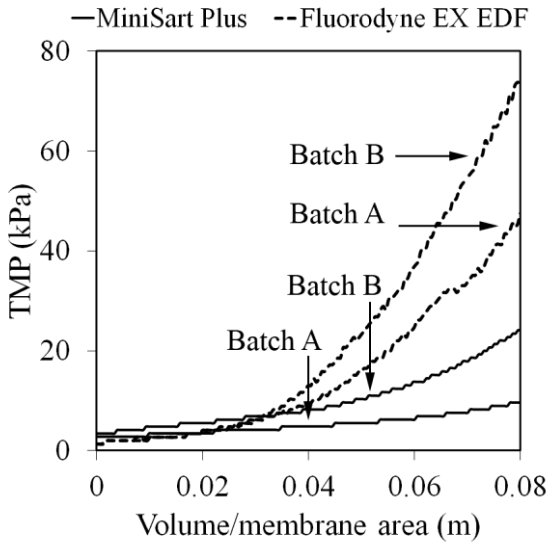

Fig. 4.5. Comparison of transmembrane pressure profiles as function of throughput (filtrate volume per membrane area) for two different batches (A and B) of OV solution using Fluorodyne EX EDF and MiniSart Plus syringe filters – Batch A results are same as those reported in Fig. 4a.

4.4.2. Analysis of results using membrane blocking models

Various models of membrane fouling that rely on different mechanisms of pore blocking have been proposed to describe the TMP rise that occurs during constant flux filtration studies. The four conventional fouling models are outlined below:[27]

- The complete blocking model (Eq. 4.2) is based on particles depositing on the membrane surface and completely blocking the membrane pores.

$$\frac{TMP(t_0)}{TMP(t)} = 1 - K_b t \qquad \text{Eq. 4.2}$$

where $TMP(t_0)$ is the TMP reading during Stage I for filtration of the virus-free buffer at a constant flux of 0.3 $mL.min^{-1}.cm^{-2}$, K_b is the apparent complete blocking rate constant (s^{-1}), and t is the filtration time.

- The standard blocking model (Eq. 4.3) is based on particles accumulating on the inside of the pore structure and restricting the available pore area.

$$\left[\frac{TMP(t_0)}{TMP(t)}\right]^{1/2} = 1 - \frac{K_s J_v t}{2} \qquad \text{Eq. 4.3}$$

where K_s is the apparent standard blocking rate constant (m^{-1}).

- The intermediate blocking model (Eq. 4.4) is based on a combination of directly blockage of the membrane pores by particles and accumulation of particles on top of the already deposited foulants.

$$\ln\left(\frac{TMP(t)}{TMP(t_0)}\right) = K_i J_v t \qquad \text{Eq. 4.4}$$

where K_i is the apparent intermediate blocking rate constant (m^{-1}).

- The cake formation model (Eq. 4.5) is based on particles depositing on the membrane surface to form a permeable layer with additional resistance to flow.

$$\frac{TMP(t)}{TMP(t_0)} = 1 + K_c J_v^2 t \qquad \text{Eq. 4.5}$$

where K_c is the apparent cake formation rate constant ($s.m^{-2}$).

In order to determine the suitability of each model, the continuous TMP profiles in Fig. 4.4 for the two best performing filters were translated into the discrete symbols were shown in the two panels of Fig. 4.6 by first converting the x-axis values from throughput (filtrate volume per membrane area) to time units and then calculating the average TMP value for each two-minutes intervals. Note that for the results reported below, there was no significant difference if shorter time intervals were used to compare the experimental results to the blocking models.

The best-fit modelling of the results for the Fluorodyne EX EDF membrane is shown in panel a of Fig. 4.6. It is readily apparent that the intermediate blocking model (with best-fit constant K_i = 44.1 m^{-1}) clearly provided the best fit to the experimental results over the entire duration of the filtration experiment. However, the model did over-predict the experimental result by approximately 25% at the longest filtration time. The complete and standard blocking models had a reasonably good agreement at very low filtration times (i.e. less than 8 mins) but were clearly unsuitable for longer filtration times. Our hypothesis is that the presence of aggregated virus particles (as shown in DLS results in Fig. 4.2) caused partial blockage of the pores in the pre-filter layer (0.2 μm rated PES) of the membrane. An alternative explanation is that aggregates deposited on the membrane surface and acted as nucleation sites for further deposition events.[28,29]

Previous studies have used confocal microscopy with fluorescently-labeled bacteriophage to observe their position within the internal structure of virus-filtration membranes;[13,30] however this approach would be considerably challenging to adopt for OV solutions given the inherent bio-safety requirements.

The best-fit modelling of the results for the MiniSart Plus membrane is shown in panel b of Fig. 4.6. The very gradual rise in TMP that was measured made it more difficult to evaluate the suitability of the different blocking models. Either the complete model (with best-fit constant $K_b = 4.8\times10^{-4}$ s^{-1}), standard model (with best-fit constant $K_s = 12.0$ m^{-1}), or intermediate model (with best-fit constant $K_i = 15.7$ m^{-1}) showed good agreement with the experimental data at filtration times less than 20 minutes.

However, at the longer filtration times, the complete model did over-predict the experimental result by approximately 40%. In order to conclusively determine whether the standard or intermediate blocking models is best suited for the MiniSart membrane, it would be necessary to repeat the experiments and run for longer filtration times – however, the primary challenge was the limited availability of OV solution. It is interesting to note that the suitability of the four blocking models was consistent for different batches of OV solution. For example, as shown in Fig. S 4.3, the best-fit agreement to the TMP profiles for Batch B were again the intermediate model (K_i = 52.0 m^{-1}) for the Fluorodyne EX EDF membrane and either the standard model (K_s = 15.9 m^{-1}) or intermediate model ($K_i = 23.4$ m^{-1}) for the MiniSart Plus membrane.

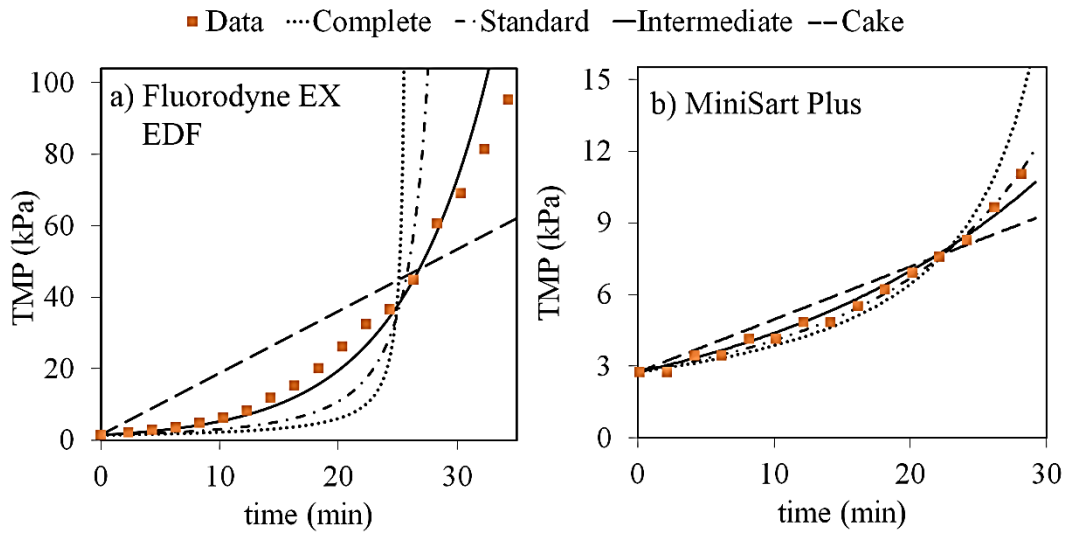

Fig. 4.6. Comparison of best-fit curves from the four blocking models described in the text and experimental transmembrane pressure profiles for filtration of Rhabdoviral vector solution (Batch A) at a constant filtrate flux of 0.3 mL.min^{-1}.cm^{-2} through the Fluorodyne EX EDF (panel a) and MiniSart Plus (panel b) membranes.

4.4.3. Evaluation of fouling reversibility

The performance of the two double-layered membranes before, during, and after filtration of the OV solution (Batch A) are compared in greater detail in Fig. 4.7. The two panels on the left show the TMP profile during the entire test (composed of six different stages as marked by the vertical dashed lines) that was completed for each type of syringe filter; the top left panel is for the Fluorodyne EX EDF membrane and the bottom left panel is for the MiniSart Plus membrane. A comparison of the results from the four hydraulic permeability measurements that were completed at different points during the filtration test is shown in the two panels on the right; again, the top right panel is for the Fluorodyne EX EDF membrane and the bottom right panel is for the MiniSart Plus membrane. The hydraulic permeabilities of the native membrane (i.e.,

unfouled, $L_{p,0}$) were quite similar with values of 0.16 and 0.11 mL.min^{-1}.cm^{-2}.kPa^{-1} for the Fluorodyne EX EDF and MiniSart Plus membranes, respectively. During Stage I (filtration of 30 mL of virus-free buffer at a constant flux of 0.3 mL.min^{-1}.cm^{-2}), there was no detectable change in the TMP. The results for Stage II (filtration of OV solution at a constant flux of 0.3 mL.min^{-1}.cm^{-2}) are the same as those originally shown in Fig. 4.4, thus the reader is referred to the detailed discussion of the results in Section 4.4.2. The magnitude of the TMP rise during Stage II appears to be well correlated with the change in hydraulic permeability that was observed during Stage III. For the Fluorodyne EX EDF membrane, the post-filtration hydraulic permeability ($L_{P,III}$) was 98% lower than that for the native membrane ($L_{P,0}$). In comparison, for the MiniSart Plus membrane, the post-filtration hydraulic permeability ($L_{P,III}$) was 70% lower than that for the native membrane ($L_{P,0}$). During Stage IV, virus-free buffer was passed through the membrane after it was installed in a 'reverse' orientation (i.e. back-to-front) in order to evaluate the potential to remove any accumulated particles/foulants from the membrane surface.[20,24] The effect of this strategy was membrane specific as the Fluorodyne EX EDF membrane showed no statistical change in the hydraulic permeability while the MiniSart Plus membrane had a 30% increase in hydraulic permeability of Stage IV compared to Stage III. This improvement in membrane performance is likely due to the different structure of the pre-filter layer above each membrane; however, additional work is needed to confirm this hypothesis and will be the focus of an upcoming study. It was interesting to note that during Stage VI, when the sodium hypochlorite solution (~5%) was passed through each membrane at flux of 0.3 mL.min^{-1}.cm^{-2}, there was a sudden and dramatic decrease in the required TMP. For example, the TMP for the Fluorodyne EX EDF dropped from 77.2 kPa to 4.1 kPa

following the introduction of the first few milliliters of sodium hypochlorite solution. This phenomenon is likely due to the lysing of the trapped particles in the membrane structure and subsequent passage through the membrane.[31]

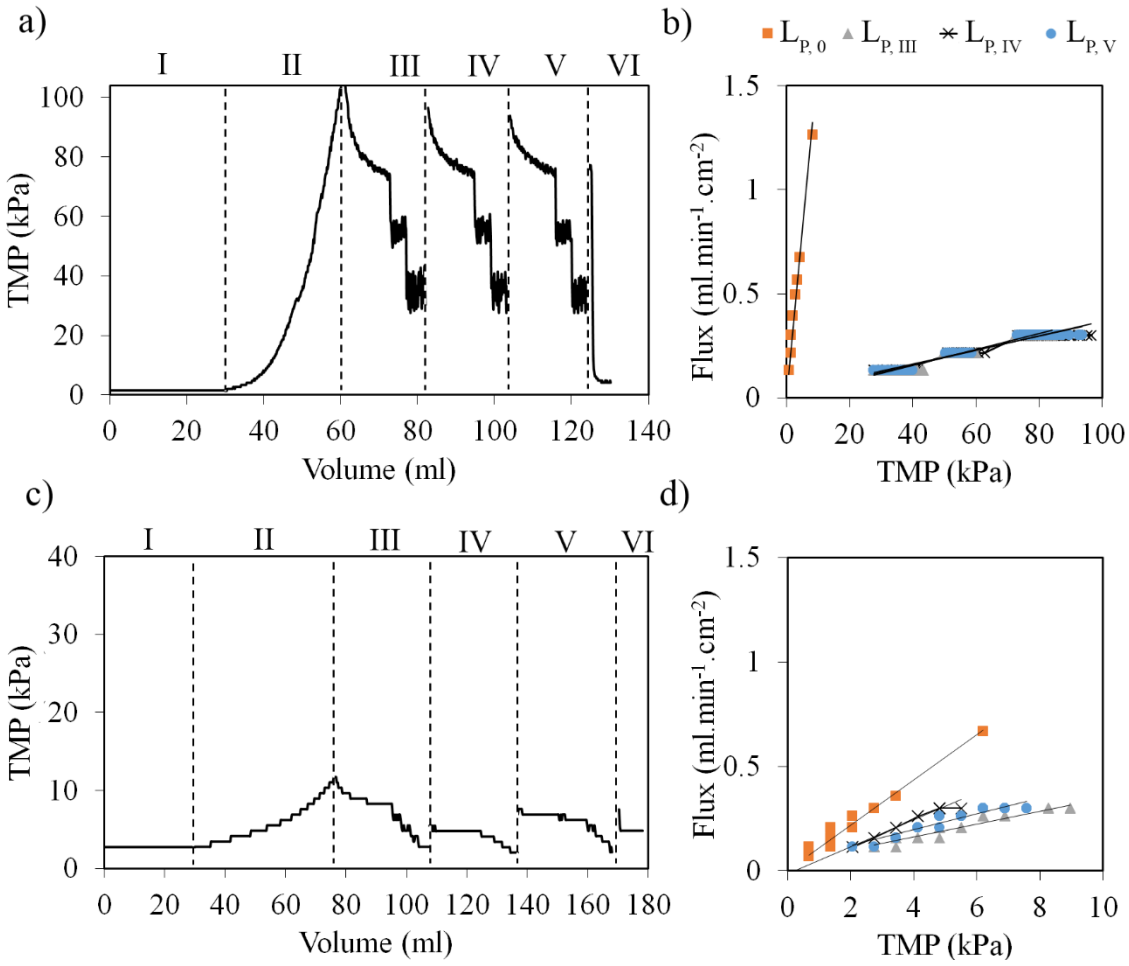

Fig. 4.7. Comparison of microfiltration membrane performance before, during, and after the sterile filtration tests. The two panels on the left (a and c) compare transmembrane pressure profiles during the pre-filtration of virus-free buffer (stage I), filtration of the OV solution (stage II), and three subsequent hydraulic permeability tests (stages III, IV, and V). The two panels on the right (b and d) compare the results from the four separate hydraulic permeability tests; note that Stage IV was conducted with the syringe filter in the reverse orientation. The two top panels (a and b) correspond to the Fluorodyne EX EDF filter; the two bottom panels (c and d) correspond to the MiniSart Plus filter.

4.5. Conclusions

The results presented in this study clearly show the importance of membrane morphology on the fouling behavior and product recovery during sterile filtration of oncolytic viruses, a promising class of bio-therapeutics for the treatment of cancer. During constant flux filtration experiments with Rhabdovirus Maraba solutions, the one-layer sterile filter membranes (Durapore and MiniSart NML) had TMP profiles that were significantly different than the two-layer sterile filter membranes (Fluorodyne EX EDF and MiniSart Plus). This behavior is likely due to the presence of virus aggregates in the feed solution, which are effectively trapped in the pre-filter layer of the two-layer membranes. The best performance was obtained with the MiniSart Plus membrane – it was able to filter the entire 45 mL volume of feed solution with the final TMP being well below the limit of 103 kPa. For the other three membranes, the filtration experiments had to be stopped when this TMP limit was reached. The titer results showed that the two-layer membranes resulted in a higher amount of virus in the filtrate stream, however this difference is mostly due to the higher volume of collected filtrate. There were slight differences in the TMP profiles for the different batches of feed Rhabdovirus Maraba solution which was attributed to the difference in titer amounts. Of the various models that have been previously developed to describe membrane fouling, both the standard blocking and intermediate blocking models were able to fit the experimental TMP data for the MiniSart Plus membrane. Finally, the severity of membrane fouling was evaluated by performing hydraulic permeability measurements after switching the orientation of the syringe filters. Overall the effects were membrane specific as the Fluorodyne EX EDF membrane showed no statistical

change in hydraulic permeability while the MiniSart Plus membrane had a 30% increase in hydraulic permeability.

While there have been numerous previous studies of using virus filtration membranes (pore sizes ~ 20 to 40 nm) to selectively retain viruses as potential impurities in the production of bio-therapeutics, this study is the first to obtain quantitative data for the fouling propensity of membranes (pore sizes ~ 0.2 to 0.22 µm) during the sterile filtration of viral vector products. The four membranes that were used in this work are available in large 'process-scale' formats and thus the collection of results presented herein are extremely useful for solving the current challenges associated with large-scale production of oncolytic viruses.

4.6. Acknowledgments

Funding was provided by the 'Alliance for Biotherapeutics Manufacturing Innovation' project that was supported by the Ontario Research Fund-Research Excellence program. Additional funding was provided by BioCanRx in the form of a Summer Studentship Award to Ian Gough. The authors are especially grateful to Julia Pomoransky and Chantal Lemay from Turnstone Biologics (Ottawa, ON), and Jennifer Quizi from the Ottawa Hospital Research Institute for their guidance on OV manufacturing process. From the Chemical Engineering Department at McMaster University, the authors thank Raja Ghosh and Todd Hoare for their particularly insightful contributions and Paul Gatt for fabricating the parts for the filtration setup. From the Faculty of Health Sciences at McMaster University, the authors thank Natasha Kazhdan and Uma Sankar (Department of Department of Pathology and Molecular

Medicine) and Marcia Reid (Electron Microscopy Facility) for their assistance with the experimental work.

4.7. References

1. Ungerechts, G. *et al.* Moving oncolytic viruses into the clinic: clinical-grade production, purification, and characterization of diverse oncolytic viruses. *Mol. Ther. Clin. Dev.* **3,** (2016).
2. Rehman, H., Silk, A. W., Kane, M. P. & Kaufman, H. L. Into the clinic: talimogene laherparepvec (T-VEC), a first-in-class intratumoral oncolytic viral therapy. *J. Immunother. cancer* **4,** 53 (2016).
3. SillaJen Inc.. Hepatocellular Carcinoma Study Comparing Vaccinia Virus Based Immunotherapy Plus Sorafenib vs Sorafenib Alone. *https://ClinicalTrials.gov/show/NCT02562755*
4. Lawler, S. E., Speranza, M.-C., Cho, C.-F. & Chiocca, E. A. Oncolytic viruses in cancer treatment: a review. *JAMA Oncol.* **3,** 841–849 (2017).
5. U.S. Food and Drud Administration Guidance for Industry. in *Sterile Drug Products Produced by Aseptic Processing–Current Good Manufacturing Practice* (2004).
6. Nestola, P. *et al.* Adenovirus purification by two-column, size-exclusion, simulated countercurrent chromatography. *J Chromatogr A* **1347,** 111–121 (2014).
7. Zhang, J. *et al.* Maraba MG1 virus enhances natural killer cell function via conventional dendritic cells to reduce postoperative metastatic disease. *Mol Ther* **22,** 1320–1332 (2014).
8. Ge, P. *et al.* Cryo-EM model of the bullet-shaped vesicular stomatitis virus. *Science (80-.).* **327,** 689–693 (2010).
9. Hawe, A., Hulse, W. L., Jiskoot, W. & Forbes, R. T. Taylor dispersion analysis compared to dynamic light scattering for the size analysis of therapeutic peptides and proteins and their aggregates. *Pharm. Res.* **28,** 2302–2310 (2011).
10. Pol, J. G. *et al.* Maraba Virus as a Potent Oncolytic Vaccine Vector. *Mol Ther* **22,** 420–429 (2014).
11. Pontius, F. W., Amy, G. L. & Hernandez, M. T. Fluorescent microspheres as virion surrogates in low-pressure membrane studies. *J. Memb. Sci.* **335,** 43–50 (2009).
12. Wickramasinghe, S. R., Stump, E. D., Grzenia, D. L., Husson, S. M. & Pellegrino, J. Understanding virus filtration membrane performance. *J. Memb. Sci.* **365,** 160–169 (2010).
13. Bakhshayeshi, M. *et al.* Use of confocal scanning laser microscopy to study virus retention during virus filtration. *J. Memb. Sci.* **379,** 260–267 (2011).
14. Grein, T. A., Kovacs, Z., Ebrahimi, M., Michalsky, R. & Czermak, P. Membrane supported virus separation from biological solutions. *Chemie Ing. Tech.* **85,** 1183–1192 (2013).

15. Cliver, D. O. Virus interactions with membrane filters. *Biotechnol. Bioeng.* **10,** 877–889 (1968).

16. Cliver, D. O. Factors in the membrane filtration of enteroviruses. *Appl. Microbiol.* **13,** 417–425 (1965).

17. Kostenbader Jr, K. D. & Cliver, D. O. Membrane filter evaluations using poliovirus. *J. Virol. Methods* **7,** 253–257 (1983).

18. Reeves, L. & Cornetta, K. Clinical retroviral vector production: step filtration using clinically approved filters improves titers. *Gene Ther* **7,** 1993–1998 (2000).

19. Helling, A. *et al.* Passage of soft pathogens through microfiltration membranes scales with transmembrane pressure. *J. Memb. Sci.* **522,** 292–302 (2017).

20. Sun, X., Kanani, D. M. & Ghosh, R. Characterization and theoretical analysis of protein fouling of cellulose acetate membrane during constant flux dead-end microfiltration. *J. Memb. Sci.* **320,** 372–380 (2008).

21. Ho, C.-C. & Zydney, A. L. Transmembrane pressure profiles during constant flux microfiltration of bovine serum albumin. *J. Memb. Sci.* **209,** 363–377 (2002).

22. Langlet, J., Gaboriaud, F. & Gantzer, C. Effects of pH on plaque forming unit counts and aggregation of MS2 bacteriophage. *J. Appl. Microbiol.* **103,** 1632–1638 (2007).

23. Dika, C., Duval, J. F. L., Ly, H. M., Merlin, C. & Gantzer, C. Impact of internal RNA on aggregation and electrokinetics of viruses: a comparison between MS2 and corresponding VLPs. *Appl. Environ. Microbiol.* AEM-00407 (2011).

24. Ho, C.-C. & Zydney, A. L. Effect of membrane morphology on the initial rate of protein fouling during microfiltration. *J. Memb. Sci.* **155,** 261–275 (1999).

25. Murdock, R. C., Braydich-Stolle, L., Schrand, A. M., Schlager, J. J. & Hussain, S. M. Characterization of nanomaterial dispersion in solution prior to in vitro exposure using dynamic light scattering technique. *Toxicol. Sci.* **101,** 239–253 (2008).

26. Syedain, Z. H., Bohonak, D. M. & Zydney, A. L. Protein fouling of virus filtration membranes: Effects of membrane orientation and operating conditions. *Biotechnol. Prog.* **22,** 1163–1169 (2006).

27. Iritani, E. A review on modeling of pore-blocking behaviors of membranes during pressurized membrane filtration. *Dry. Technol.* **31,** 146–162 (2013).

28. Maa, Y. & Hsu, C. C. Membrane fouling in sterile filtration of recombinant human growth hormone. *Biotechnol. Bioeng.* **50,** 319–328 (1996).

29. Loh, S. *et al.* Interplay among membrane properties, protein properties and operating conditions on protein fouling during normal-flow microfiltration. *J. Memb. Sci.* **332,** 93–103 (2009).

30. Dishari, S. K. *et al.* Effects of solution conditions on virus retention by the Viresolve® NFP filter. *Biotechnol. Prog.* **31,** 1280–1286 (2015).

31. Rutala, W. A. & Weber, D. J. Guideline for disinfection and sterilization of

prion-contaminated medical instruments. *Infect. Control Hosp. Epidemiol.* **31,** 107–117 (2010).

4.8. Supplementary Material

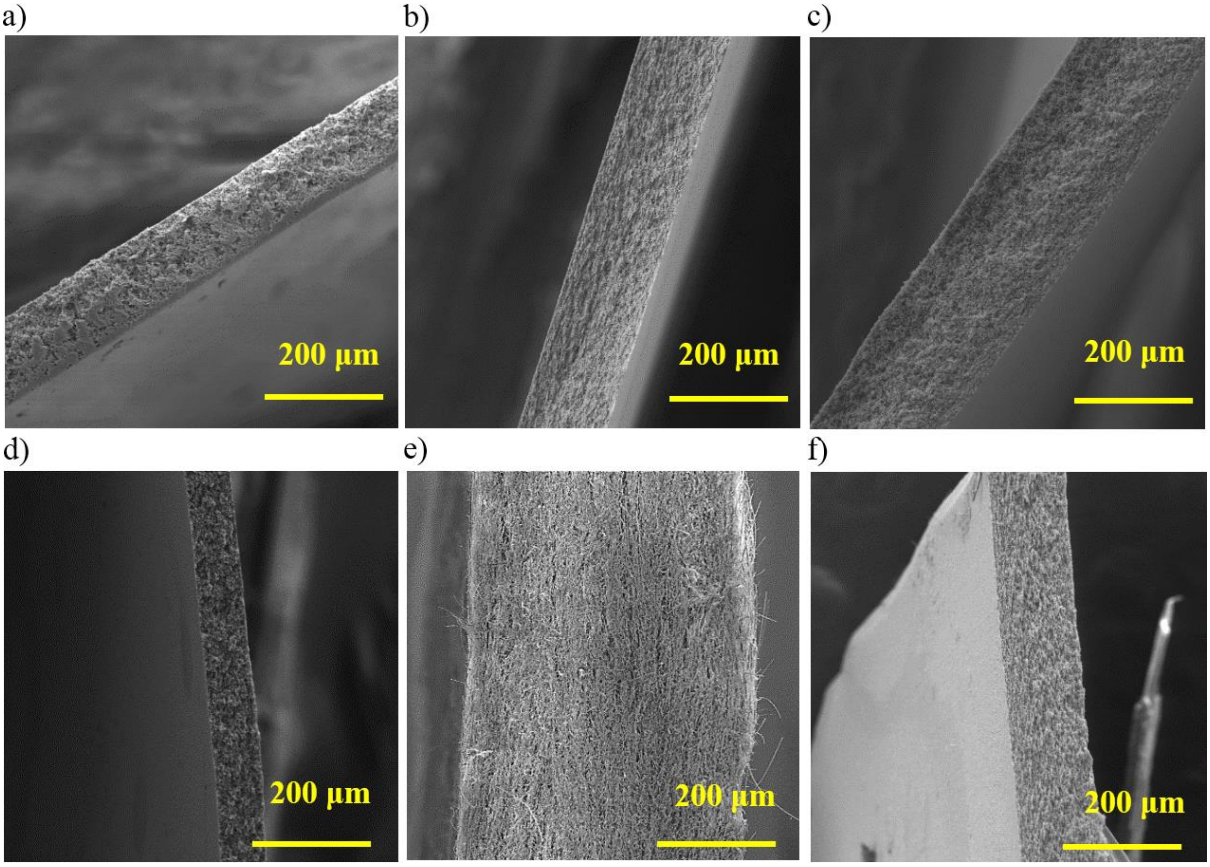

Fig. S 4.1. Scanning electron micrographs (×300 magnification) of the cross section of the layers of the four microfiltration membranes that were used in this study: Durapore 0.22 µm single layer PVDF membrane is shown in panel a; MiniSart NML 0.2 µm single layer SFCA membrane is shown in panel b; Fluorodyne EX EDF membrane 0.2 µm top PES layer is shown in panel c; Fluorodyne EX EDF membrane 0.2 µm bottom PVDF layer is shown in panel d; MiniSart Plus membrane 1.2 µm top GF layer is shown in panel e; MiniSart Plus membrane 0.2 µm bottom SFCA layer is shown in panel f.

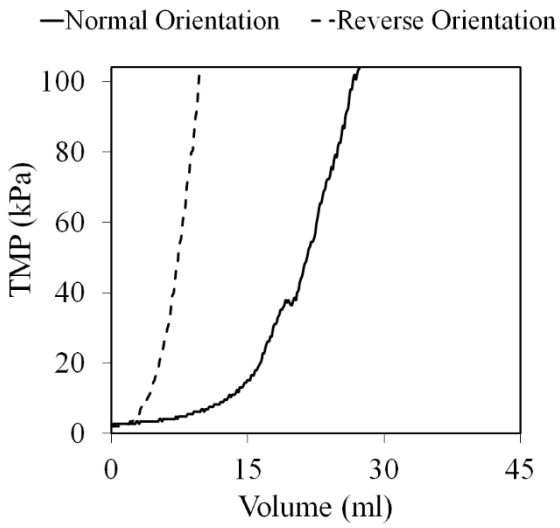

Fig. S 4.2. Comparison of transmembrane pressure profiles for filtration of OV solution (Batch C) at a constant filtrate flux of 0.3 $mL.min^{-1}.cm^{-2}$ using the Fluorodyne EX EDF syringe filter in normal orientation (i.e., PES/PVDF) and reverse orientation (i.e., PVDF/PES).

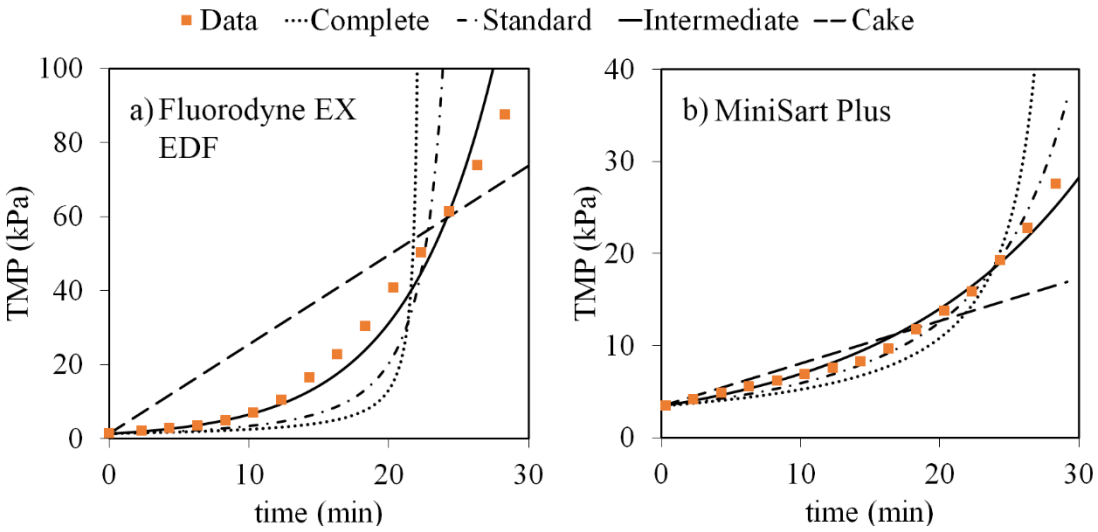

Fig. S 4.3. Comparison of best-fit curves from the four blocking models described in the text and experimental transmembrane pressure profiles for filtration of Rhabdoviral vector solution (Batch B) at a constant filtrate flux of 0.3 mL.min^{-1}.cm^{-2} through the Fluorodyne EX EDF (panel a) and MiniSart Plus (panel b) membranes.

Chapter V

Probing the effect of stabilizers on the aggregation of oncolytic viruses via a microscale filtration process

Authors: Shabnam Shoaebargh, Evan Wright, Matthew Csordas, Maria Fe Medina, Brian Lichty, David R. Latulippe

In preparation for submission in Biotechnology and Bioengineering

5.1. Abstract

Oncolytic viruses (OVs) are a class of cancer therapies that are currently undergoing clinical trials and on their way to full regulatory approval. One inevitable part of OV manufacturing is a membrane-based process with a major challenge of membrane fouling and consequent product loss. A small-scale microfiltration setup was developed allowing for constant flux microfiltration using a low volume of the virus solution (< 3mL) while measuring transmembrane pressure (TMP) online. Using this setup, the effects of different additives including various proteins (bovine serum albumin and alpha-lactalbumin) and organic polymers (polyethylene glycol and polyvinylpyrrolidone) on filtration of the oncolytic Rhabdovirus vector were screened. Results demonstrated that tested proteins decreased fouling rate and increased the virus recovery. An addition of 5% bovine serum albumin (BSA) to the virus solution

decreased the TMP readings about 4-times while increasing the virus recovery about 6-times (~59%) compared to microfiltration of the virus run with no additive (~9%). In contrast, the organic polymers could not imitate the effects of the protein additives. Moreover, the membrane surface was coated with BSA protein. The results demonstrated that the coated membrane increased the virus recovery to about 42%, comparable to the case of the virus solution run with BSA additive (~59%). Scanning electron microscopy images revealed a lower surface fouling happened for the coated membrane.

5.2. Introduction

Global interest in improved manufacturing methods for virus particles is growing, due to promising outcomes of clinical trials of virotherapy and gene therapy. However, manufacturing of viruses is suffering from tremendous virus losses happening mostly through downstream processing (DSP). One inevitable part of DSP is membrane-based processes, associated with a major challenge of membrane fouling, an undesirable phenomenon caused by adsorption or deposition of particles inside pores or on membrane surface.[1] Membrane fouling leads to a decrease in the efficiency of filtration processes, a dramatic increase of transmembrane pressure (TMP) or flux decline, which all adversely decrease membrane permeability, require frequent membrane replacements, and consequently lead to dramatic loss of valuable virus product.[2,3] Virus loss through membrane-based processes could be due to inactivation or physical disruption of virus particles,[4] specific or non-specific virus particle adsorption,[5,6] aggregated virus particles and complexes with impurities,[7] and virus particle

entrapment in the membrane pores.[4,8] When particles and membrane pore size are at the same order, the transport is not just dependent on pore size, but also depends on particle-particle interactions as well as particle-membrane interactions.[9] Different factors such as virus size and shape,[10] virus surface structure [11] and charge,[12] virus hydrophobicity [13] along with membrane material, membrane surface structure and charge [14,15] would determine possible interactions and consequent degree of loss.[16,17]

To alter fouling propensity of membrane, the surface has been modified by improving characteristics such as hydrophilicity, charge, and roughness.[18] Biomimetic membranes modified with active enzymes,[19] albumin,[20] chitosan and gelatine,[21] and polyethylene glycol [22] have been tested for micro/ultrafiltration of proteins such as human prion protein [22] and platelet.[20] On the other hand, a couple of papers examined membrane antifouling agents such as beef extract,[23,24] calf or bovine serum,[6,23] and glycine [24] for their ability to improve virus recovery. These 'coating' agent act by covering the surface of the membrane without blocking the membrane pores. One of the first studies demonstrated that enteroviruses loss was minimized by incorporation of serum or gelatine in the virus solution as well as coating the membrane surface.[6] The effects of the 'coating' agents has been mostly studied in cross-flow ultrafiltration, where the virus particles were supposed to be retained.[23] Few works have focused on virus recovery from dead-end microfiltration process. On the other hand, all the referred works were tested on non-enveloped waterborne viruses such as enteroviruses [6,23] and adenovirus [17] or phages.[24]

Another main cause of membrane fouling, and consequent virus loss is the aggregation of virus particles, mediated by various biophysical interactions in the

solution. Virus aggregates might cause full membrane pore blockage or internal fouling based on the pore size. Furthermore, deposited aggregated particles on the membrane surface could serve as nucleation sites for further virus particles attachment.[24] Aggregated virus particles also affect bio-distribution following *in vivo* administration, resulting in unwanted inflammatory immune responses, and may even cause reduced vector infection efficiency.[25] It is well accepted that aggregation of the virus particles is totally undesirable. Therefore, one potent solution for decreasing or controlling membrane fouling rate would be destabilizing aggregated virus particles while stabilizing virus monomeric particle. Additives that have been tested for their effects on virus particle aggregation include sugars such as glycerol [26,27] and sucrose,[28] surfactants such as polysorbate 80,[7] different salts [29] such as sodium chloride and magnesium sulfate, proteins,[10] amino-acids,[29] and polymers such as dextran [30] and chitosan.[28] In a study by Kissmann et al.,[28] sucrose (20% w/v), trehalose, and chitosan (0.5% w/v) were capable of thermally stabilizing Norwalk virus-like particles (VLPs). However, Wright et al. [29] have shown that sucrose didn't prevent adeno-associated virus type 2 (AAV2) aggregation at the maximum tested concentration of 5% w/v. For deposition of viruses on mica, bovine serum albumin [10] and glycerol (3%) [26] were effective for disaggregation of Tobacco Mosaic virus particles and AAV2, respectively. However in another study, 5% glycerol did not prevent AAV2 aggregation caused by dilution [29] while a high concentrations of 25% was successful in preventing aggregation.[27] These studies demonstrate that additives perform differently for various virus types as well as different applications.

When evaluating additives for virus formulation and aggregation prevention, it is common to use an accelerated thermal degradation process coupled with spectroscopic

analysis.[31] Other methods which have been used to assess the extent of aggregation include dynamic light scattering,[28,29] sedimentation velocity,[32] and size exclusion chromatography.[33] While these methods can give an indication of the long-term stability of virus particle in the formulation and the state of aggregation of a virus, they do not reflect the interplay between a virus, an additive, and a membrane surface. On the other hand, by assessing additives using a microscale filtration process the results will directly reflect the membrane performance during downstream processing. Thus, a small-scale sterile filtration setup was designed allowing for online TMP measurement at constant flux microfiltration of a low volume of virus solution.

Our team has previously developed a sterile filtration setup to evaluate different commercial sterile filters for microfiltration of an oncolytic virus.[34] Although the setup was very useful for screening various sterile syringe filters, a high volume (up to 100 mL) was required to conduct duplicate testing of just one filtration condition.[34] Also, we were unable to specify the size of the membrane area to test and were therefore dependent on the available sizes of various commercial syringe filters provided by the manufacturer. To this end, we designed a membrane filtration setup with a membrane holder that will allow comparisons of different type of membranes with the same effective area. This setup also allowed us to reduce the effective membrane area to test, thereby decreasing the amount of virus required to perform the filtration tests (less than 3 mL). Therefore, the current small-scale sterile filtration setup allowed for filtration of a low volume of virus solution. Although the focus of the referred studies was non-enveloped waterborne viruses, this work studied sterile filtration of enveloped Rhabdovirus with an initial high concentration ($>10^9$ infectious particle per mL). As a matter of fact, virus particles were the product and recovery of virus particles from

filtration step was desired. Using this setup, effects of additives including various biomolecules (bovine serum albumin, alpha-lactalbumin) and polymers (Polyethylene glycol and Polyvinylpyrrolidone) on membrane fouling were monitored and possible correlations with virus recovery were investigated.

5.3. Experimental

5.3.1. Material

Poly (ethylene glycol) (PEG20, 23.7 kDa and PEG40, 41.5 kDa), Polyvinylpyrrolidone (PVP40, 40 kDa), and Alpha-Lactalbumin (α-LA, from chicken egg white, 14.2 kDa), were purchased from Sigma-Aldrich. Polydispersity index of PEG20 and PEG40 were 1.19 and 1.30, reported by manufacturer. Bovine serum albumin (BSA, heat-shock isolated fraction V, biotechnology grade, purity >98%, 66.4 kDa), sodium chloride (NaCl, Biotechnology grade, purity >99.5%), and sucrose (Biotechnology grade, purity >99.5%) were purchased from BioShop and used without any further purification. Protein solutions were prepared freshly by dissolving a proper weight percentage (%w/v) in the formulation buffer, 10 mM HEPES ((Gibco, Life Technologies)), 4% sucrose (Bioshop), 150 mM NaCl (BioShop) at pH 7.4, followed by sterile filtration using 0.2 µm Acrodisc® syringe filter with PES membrane, depending on the sample volume size. No stirring was used during the dissolution of the additives solutions to avoid inducing aggregates formation, only gentle rocking was used. Durapore PVDF membrane (0.22 µm, pre-cut 13 mm membranes), MiniSart Plus with glass fiber/surfactant-free cellulose acetate layers (GF/SFCA: 1.2 µm/0.2 µm, 28 mm syringe filter), Fluorodyne EX EDF with polyether-sulfone/polyvinylidene

fluoride layers (PES/PVDF: 0.2 µm/0.2 µm, 29 mm syringe filter) were purchased from Millipore-Sigma, Sartorius, and Pall, respectively.

5.3.2. Rhabdoviral Vector Source and Infectivity Assay

Two batches (referred to Batch A and B) of semi-purified Rhabdoviral vector expressing green fluorescent protein (GFP) was kindly provided by Biotherapeutic Manufacturing Center at Ottawa Hospital Research Institute, for which purification process included harvesting, clarification and membrane filtration with the final volume of 400 mL in the formulation buffer (10 mM HEPES, 4% sucrose, 150 mM NaCl at pH 7.4). The virus batch was stored at -80ºC upon arrival, thawed on next day and aliquoted into 5 mL per falcon tube and stored at -80ºC for further experiments.

Infectivity of virus samples was examined using 50% tissue culture infective dose ($TCID_{50}$) assay. Vero cells were seeded at 5×10^4 cells per well in 'flat-bottom' 96-well plate (Corning®, USA). Next day, serial dilutions of virus samples with 5-times dilution factor were prepared in DMEM (supplemented by 8% FBS) in 'round-bottom' 96-well plate (Corning®, USA). Six wells were allocated per dilution, and a total of 8 dilutions were plated ($10^{-4.9}$ to $10^{-9.8}$); therefore, two virus samples could be tested in one plate. Cell infection was obtained by dispensing 100 µl of serially diluted virus sample on Vero cells (with >90% confluence), followed by incubation at 37 °C and 5% CO_2 for 48 hours. The cytopathic effect caused by the virus infection was detected by visualizing GFP expression using Typhoon Trio$^+$ scanner (GE Healthcare) equipped with Blue 488 nm/520 BP 40 laser. The infectious titer was calculated using Spearman-Karber method according to Eq. (5.1).

$$\log_{10}^{TCID_{50}} = x_{p=1} + \frac{1}{2}d - d\sum_{x_{p=1}}^{x_{\min}} p_x \qquad \text{Eq. (5.1)}$$

Where d is $\log_{10}^{dilution}$, $x_{p=1} = \text{argmin}_x (p_x = 1)$, and p is proportion of positive wells.

To better capture variations in the assay, an extra step of the calculation was implemented based on making combinations of 4 wells out of 6 infected wells for the $TCID_{50}$ titer calculation which ended up having a total number of 15 different combinations from each sample. The reported $TCID_{50}$ values in this chapter as well as standard deviations were the average and standard deviation of 15 above-mentioned combinations. Every virus infectivity measurement was repeated at least two times, and the average and standard deviation were reported, and error bars for the virus infectivity were generated using propagation of errors.

5.3.3. Small-scale microfiltration

5.3.3.1. Experimental Set-up

A small-scale dead-end sterile filtration setup was designed aiming at reducing the utilized virus solution volume per experiment to overcome the most important shortcoming in our previous process design.[34] The schematic of the setup was shown in Fig. 5.1. The setup allowed for filtration of the virus solution at a constant flux of 0.3 $mL.min^{-1}.cm^{-2}$ using Harvard Apparatus syringe pump (PHD Ultra-injector) while simultaneously monitoring changes in the transmembrane pressure (TMP) using Omega USB pressure transducer (PX409, Omega Engineering, Stamford, CT) and data collection by Omega Digital Transducer Application software (Version 2.2.1). The key

design part was the membrane housing, a commercial membrane holder (Cole-Parmer) made of polycarbonate with a diameter of 13 mm and effective area of 0.5 cm^2. The pre-cut Durapore membranes (13 mm) from Millipore-Sigma was used for small-scale filtration experiments unless using other type of membranes was stated.

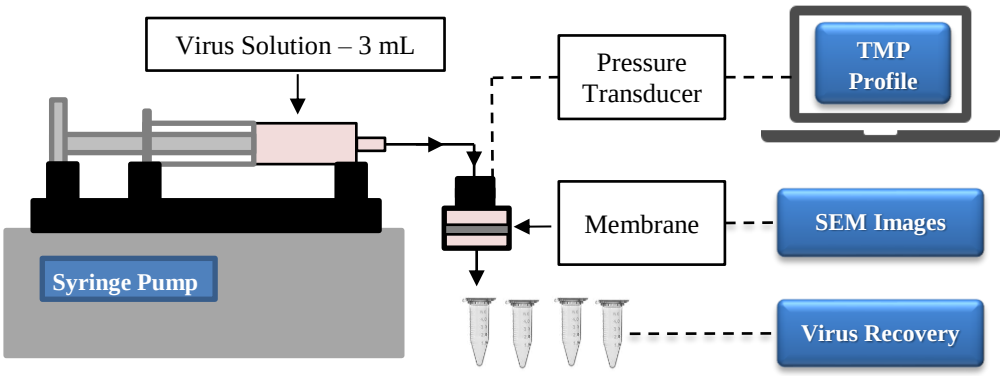

Fig. 5.1 Schematic of small-scale sterile filtration setup

5.3.3.2. Sterile Filtration of Virus Solution

Prior to sterile filtration experiment, the Durapore PVDF 0.22 µm membrane was fully wetted to eliminate any trapped bubble inside the holder. The hydraulic permeability of the native membrane was measured from the slope of flux versus TMP [34] in the flux range of 0.1 $mL.min^{-1}.cm^{-2}$ up to 12 $mL.min^{-1}.cm^{-2}$ to cover both low- and high-pressure reading ranges. Furthermore, the recorded permeability of the native membrane was always compared to the average permeability of the membrane to ensure similar permeability values, with a maximum 5% deviation. The whole setup including the holder, membrane, fittings, and tubing were autoclaved prior to use. The entire experiment was conducted in a biosafety cabinet (Class II, Type A2) to comply with biosafety regulations.

Two sets of sterile filtration experiments were designed; one set of experiments was referred to 'additive test', conducted by addition of 0.5 mL of additives solution (dissolved in the formulation buffer) to 2.5 mL of the virus solution. The ratio of the additive to the virus solution was 1:5 and always kept the same. The total volume of the virus solution prior to microfiltration was always 3 mL. The control virus run (i.e. virus alone) consisted of 0.5 mL of the formulation buffer without any additive with 2.5 mL of the virus stock solution. The list of tested additives is summarized in Table 5.1. The additives were selected in a way that we have a combination of charged and uncharged materials at different size ranges as well as different groups (e.g. proteins and polymers).

The other set of experiments was referred to 'coating test', where 3 mL of BSA solution with the concentration of 5% w/v was first passed through the filter prior to filtration of the virus alone solution. Later, the control virus run, 2.5 mL of the virus stock with 0.5 mL of formulation buffer, was filtered through the coated membrane.

2.5 mL of the virus solution was filtered and four 500 µl samples were collected sequentially and referred to S1, S2, S3, and S4. The remaining 500 µl was taken as an initial sample. The recovery of the virus through microfiltration run was defined as Eq. (5.2).

$$\%\text{Recovery}=\frac{\text{Virus infectivity of pooled sample of S1-S4 } (\text{ID}_{50}.\text{mL}^{-1})}{\text{Virus infectivity of initial virus sample } (\text{ID}_{50}.\text{mL}^{-1})}\times 100 \quad \text{Eq. (5.2)}$$

The sterile filtration run was stopped at either the TMP reached 70 kPa or 2.0 mL of virus solution was filtered. Moreover, repeated measurements were conducted under

identical experimental conditions. To avoid any bacterial growth, additives solutions were prepared fresh before the experiment.

Table 5.1 List of examined additives

Group	Name	Molecular Weight (kDa)	Concentration (%w/v)
Proteins	BSA	66.4	1.25, 2.50, 5.00
	α-LA	14.2	
Polymers	PEG20	23.7 *	1.25
	PEG40	41.5 *	
	PVP40	40 ǂ	

*Determined by manufacturer using GPC-SEC analysis

ǂ Reported by manufacturer

5.3.4. Virus Concentration Analysis

The concentration of the virus solution was quantified using a qViroX platform (Izon Science, Christchurch, New Zealand) along with Izon Control Suit software (Version 3.3.2). The working principle of the instrument is based on Tunable Resistive Pulse Sensing (TRPS) method. The formulation buffer was used as an electrolyte and for preparing dilutions of the virus samples and calibration beads. The diluted samples were vortexed and sonicated for 30 seconds (FisherScientific) prior to measurement. The tunable nanopore (NP200, Izon) with 200 nm pore size was purchased from FroggaBio Inc. and mounted on the instrument followed by calibration of the nanopore's stretch. The formulation buffer (75 µl) was pipetted into the lower well first and then 40 µl of the sample was dispensed to the upper well, with great care to not to introduce bubble to the wells. Continuous passage of particles with the rate of 500-1500

particles per min was targeted by adjusting the nanopore stretch (43-47 mm), transmembrane voltage (0.3-0.5 mV), and applied pressure (4-13 cm H_2O), while taking care to keep the noise level as low as possible (<12 pA).[35] A pressure was implemented for minimizing the effects of the virus particle's surface charge on its passage through the pores, while multi-pressure measurements were conducted to obtain a more precise measurement of the virus concentration. Followed by the sample measurement run, a calibration beads run (CPC200, mean 210 nm, concentration: 1×10^{12} particle per mL) were performed under the exact conditions of the sample run. Between two measurements, the cell was thoroughly washed with formulation buffer until achieving a stable baseline with no particle transmission. It is worth noting that the cell was cleaned by diluted Bleach solution (10%) whenever it was needed. Later, the same software was used for analyzing data and obtaining virus size distribution and concentration.

5.3.5. Dynamic Light Scattering

The size distribution of additives in the formulation buffer was determined using DLS method using Zetasizer NanoZS instrument (Malvern Instruments, UK), equipped with He-Ne red laser (633 nm). To ensure backscatter detection, the attenuator was fixed at 173° relative to the source laser and its position was automatically optimized by the instrument. The number of sub-runs was automatically determined (always > 10 sub-runs) with conducting at least six main measurement cycles. In this work, the average and standard deviation of performed runs were reported.

The additive solutions were made at stock concentration of 1.25%w/v in the formulation buffer, followed by filtration with 0.2 µm Acrodisc® syringe filter (Pall). It is worth noting that the syringe filters wetted with the formulation buffer beforehand. The viscosity of each additive solution was measured using Vibro Viscometer (Malvern Pananalytical), and the data was plugged into Zetasizer software (version 7.13, Malvern) to compensate for effects of viscosity on hydrodynamic size. The stock solution was diluted with the formulation buffer whenever lower concentrations were needed.

5.3.6. Scanning Electron Microscopy

After microfiltration run, the Durapore PVDF membrane was taken out of the holder, rinsed with DNase-RNase free water (500 µl) to remove loosely bonded particles, followed by staining with 500 µl of 2% Glutaraldehyde buffered in Cacodylate for 30 minutes. Later, the membrane was rinsed twice with DNase-RNase free water to remove residuals of the fixative and left to be air-dried. It should be noted that the staining procedure was conducted right after completing the sterile filtration experiment. The control was native membrane gone through the staining procedure. The entire procedure was conducted in a biosafety cabinet (Class II, Type A2) to comply with biosafety regulations.

Scanning electron microscopy (SEM) images of the membrane were taken using Vega II LSU (Tescan) instrument under vacuum with accelerating voltage of 10 kV at a magnification factor of 4000. Prior to taking SEM images, the stained membrane samples were mounted on specimen carriers and gold sputtered for 40 seconds under vacuum at the current of 20 mA. It is worth noting that 4-6 different images were taken

from one membrane to avoid localization and consequent errors. Later, the taken SEM images were analyzed by ImageJ software (National Institutes of Health, http://rsb.info.nih.gov/ij, version 1.52a) using 'Color Threshold' option with threshold method of 'Default' and color of 'Red' used to highlight the pores by means of 'Brightness' panel.

5.4. Results and Discussion

5.4.1. Stock Virus Filtration

Filtration performance of the sterile filters were examined and compared to the results from the previous setup, shown in Fig. 5.2. For this experiment, the syringe filters from the manufacturers were cracked, membranes were taken out, and cut to fit the holder (13 mm). As shown in Fig. 5.2, the trend of each membrane's performance using either previous or current setup design were similar. In our previous work,[34] a high volume of virus solution (15-45 mL) was required to perform a run depended on the type of syringe filter. Therefore, 2-6 experiments could be conducted with 100 mL of virus solution. However, using the current small-scale setup, more than 30 tests could be done using the same amount of virus solution (100 mL), which is an ideal option for screening different formulation buffers and their components. The results demonstrated that Durapore PVDF membrane had the highest fouling potency, displaying dramatic change in TMP readings during filtration of a very low volume of virus solution. This property makes Durapore PVDF a perfect option for our objective of screening the effect of additives on filtration of the virus solution.

A set of experiments was designed to test the effects of virus concentration on the Durapore PVDF membrane performance and consequently TMP profile, and results were shown in Fig. 5.3. Infectivity of the stock virus solution (i.e. no dilution) from Batch A was $(2.5\pm0.3)\times10^{9}$ $ID_{50}.mL^{-1}$. The virus solution was diluted 1:1 and 1:5 with the formulation buffer. The 1:1 and 1:5 dilution resulted in virus concentration of $(1\pm0.3)\times10^{9}$ $ID_{50}.mL^{-1}$ and $(1.8\pm0.8)\times10^{8}$ $ID_{50}.mL^{-1}$, respectively. The results indicated that the virus concentration could dramatically affect the TMP profile, where higher dilution resulted in the lower TMP profile (Fig. 5.3).

To confirm that the reduction in TMP is not simply due to the presence of virus aggregates, the virus solution was filtered sequentially through a Durapore PVDF membrane and the permeated virus solution was collected. Prior to the second filtration, the tubing and membrane were discarded, and replaced with clean unused units. The collected filtered virus solution was again filtered through another fresh Durapore PVDF membrane. The result indicated no significant TMP changes for the second filter (shown in Fig S 5.1). Samples were taken from the filtrate of each filtration run and the amount of infectious virus was examined. The virus titer of the permeate from the first filtration step was $(2.0\pm0.5)\times10^{8}$ $ID_{50}.mL^{-1}$, which means that the transmitted virus through the first filter was about 10% of the total infectious virus particles in the initial sample. The latter result is in a good agreement with results shown in Fig. 5.3, where 1:5 dilution of the stock virus solution also caused no significant changes in TMP profile.

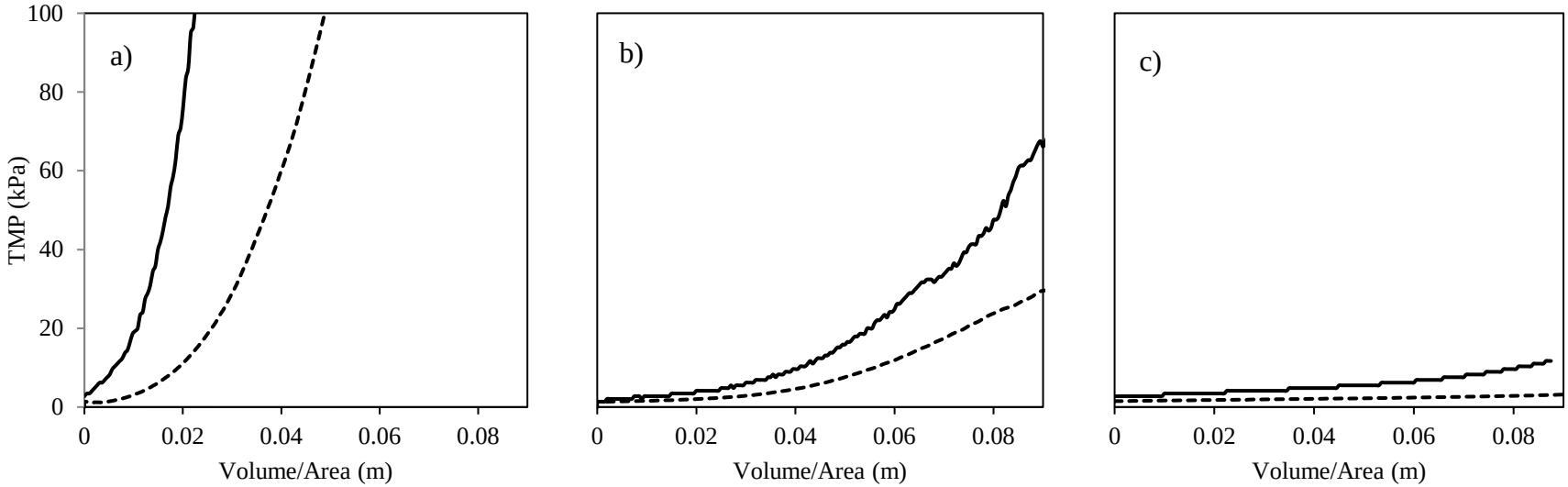

Fig. 5.2 Comparing fouling behavior of various filters using the previous setup [34] (solid line) and the current setup (dashed line) through sterile filtration of Rhabdovirus solution; a) Durapore, PVDF 0.22 µm; b) Fluorodyne EX EDF, PES/PVDF 0.2 µm/0.2 µm; c) MiniSart Plus, GF/CA 1.2 µm/0.2 µm. Initial virus infectivity of the feed was $(4.7\pm0.9)\times10^{9}$ PFU.mL^{-1} and $(2.3\pm0.2)\times10^{9}$ ID_{50}.mL^{-1} in the previous work (described in Chapter 4)[34] and the current work (Batch A), respectively.

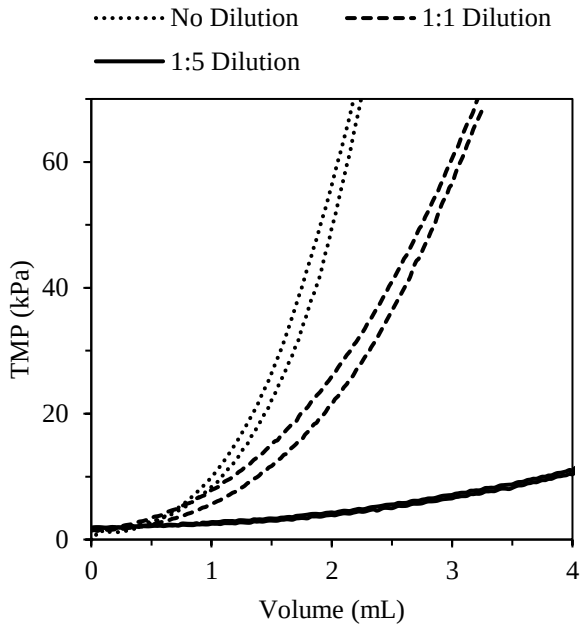

Fig. 5.3. Virus concentration effects on TMP profile. Infectivity of the stock virus solution (i.e. No dilution) from Batch A was $(2.5\pm0.3)\times10^{9}$ $ID_{50}.mL^{-1}$ while infectivity of 1:1 and 1:5 dilutions were $(1\pm0.3)\times10^{9}$ $ID_{50}.mL^{-1}$ and $(1.8\pm0.8)\times10^{8}$ $ID_{50}.mL^{-1}$, respectively.

5.4.2. Virus Solution Additives

Freshly made protein solutions were added individually to the virus solution at different final concentrations (% w/v) and filtered through Durapore PVDF membrane. Fig. 5.4 a and b demonstrated TMP profiles of virus solution with BSA and α-LA additives. It is well accepted that the slope of the increase in TMP profile is referred to membrane fouling rate.[34] Membrane fouling rate was lower for the runs with protein addition compared to the control virus run (0% additive). Increasing BSA concentration in the virus solution resulted in lower TMP pressure readings. However, 1.25% and 2.5% α-LA resulted in similar TMP profile while increasing α-LA more than 2.5% demonstrated inverse result although it is still lower than TMP of the control virus run.

The effects of different additives on virus recovery through the Durapore PVDF membrane was shown in Fig. 5.4c. The virus recovery was defined as the number of infectious virus particles that passed through the membrane relative to the initial number of infectious particles in the virus solution (Eq. 5.2). As shown, increasing the concentration of added BSA also increased the recovery of virus particles, from 9%±1% when no additive was added, to 59%±9% when 5% BSA was added to the virus solution. Moreover, addition of 1.25% and 2.5% α-LA resulted in similar virus recovery of about 40% (Fig. 5.4c). However, increasing α-LA concentration to 5% was detrimental as it decreased virus recovery (28%±4%) compared to the virus recovery when 2.5% of α-LA was added. (18%±4%). Similarly, increasing α-LA concentration to 5% also resulted in a higher TMP profile (Fig 5.4b). Interestingly, addition of either 2.5% BSA or 2.5% α-LA resulted in similar TMP profiles as well as similar virus recoveries. It is worth noting that the initial virus infectivity didn't change by addition of either BSA or α-LA (Data not shown).

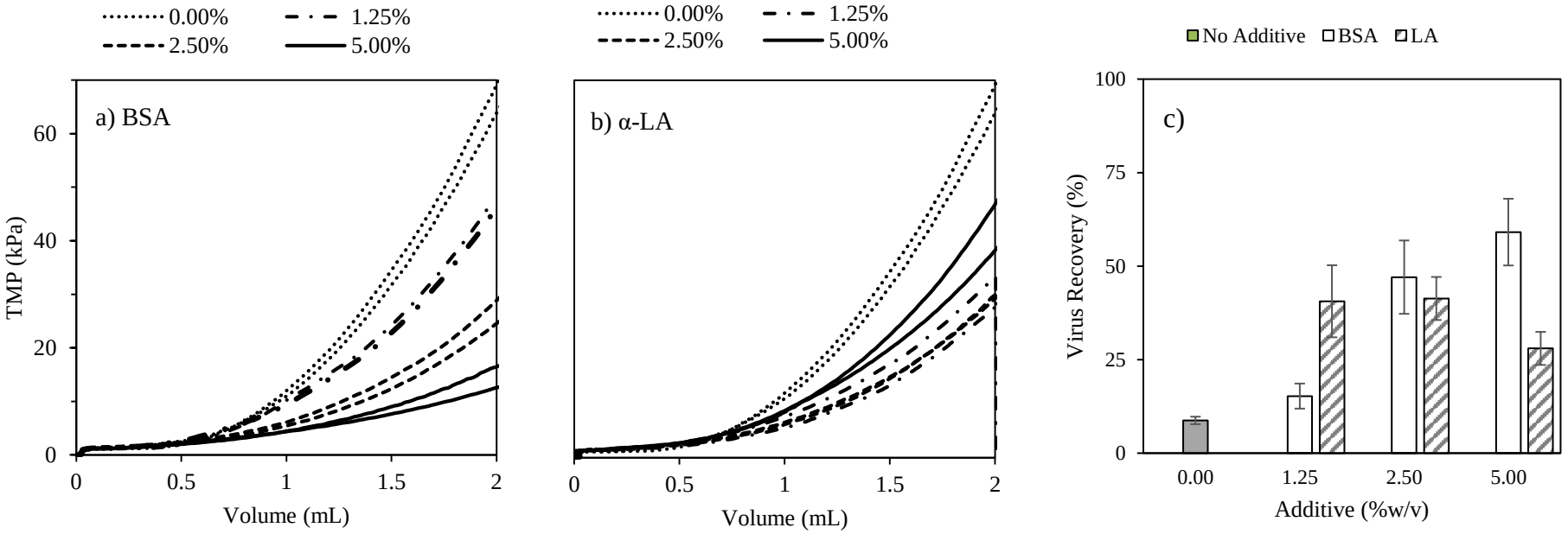

Fig. 5.4 Comparison of filter performance through sterile filtration of the virus solution without and with protein additives at various concentrations. TMP profiles with BSA and α-LA are shown in panel a and b, respectively. Virus recovery results are shown in panel c. Initial virus infectivity of the control virus run was $(2.6\pm0.2)\times10^{9}$ $ID_{50}.mL^{-1}$. The collected filtrates (S1-S4) of each run pooled and later examined for the virus infectivity.

To further investigate the role of additives during virus filtration, different polymers were tested (Table 5.1). The effects of polymer molecular weight and polymer structure could be investigated by comparing the results of PEG40 versus PEG20, and PEG40 versus PVP40, respectively. The TMP profile of the virus solutions with added polymer are shown in Fig. 5.5a. PVP40 and PEG20 demonstrated lower TMP profiles comparable to the virus solutions with added proteins while addition of PEG40 didn't show any significant change in TMP profile. However, virus recovery with addition of polymers was lower in comparison to protein additives, with less than 25% recovered infectious virus. In addition, adding polymers to the virus solution caused an initial drop in the virus titer (on average ~50%) while with the protein additives (BSA and α-LA) this behavior was not observed. It is worth to mention that Hirasaki et al.[35] examined the effect of PEG 400 Da (max. 2%w/v) and serum albumin (max. 5%w/v) on infectivity of bacteriophage ϕX174, and reported no change in the phage infectivity. Presumably, the molecular weight of the polymer is an important factor affecting the virus titer.

Additives are exerting their effect by interacting with the membrane surface and/or virus particle surface. The membrane material, PVDF, itself is hydrophobic but has been modified by the manufacturer to increase hydrophilicity, likely by grafting polymerizable monomers such as hydroxyalkyl acrylate or methacrylate, showing hydroxyl functions.[36] Durapore PVDF was reported to have a zeta potential value of -19.5 mV at pH 7.0,[37] indicating having negative charge at our solution condition. The virus particles were also negatively charged, tested by an anionic column chromatography (CIM QA, 6 µm pore size) with results showing less than 1% infective

virus particle in the flow through (not shown here). BSA and α-LA have isoelectric points of 4.9 [37,38] and 5.1,[39] and consequently were both negatively charged in our solution. PEG and PVP are neutral (i.e. uncharged) polymers; however, PVP behaves as a negatively charged polyelectrolyte in water at pH 7.4, owning to its resonating structure.[40] Badoga et al. [40] demonstrated that the zeta potential of PVP (360 kDa) was changed from +4.2 mV to -10.4 mV by changing pH from 2.0 to 7.4. All the above facts raise the question that how additives were able to interact with either virus particles or the membrane surface in case all the materials were negatively charged.

Organic polymers such as PEG and PVP are made of monomers with either nuetral or negative charge, which could not result in a sufficient interaction between the polymer and the membrane surface. However, due to convective flow and abundant amount of the polymers in the virus solution, there is a chance that polymers were forced to deposit one the membrane surface and fill constricted pores, and consequently easing the virus transmission. In contrast, a biomolecules such as BSA have been shown to have positive, negative, and hydrophobic patches, even though the overall charge of the biomolecule is negative.[10,39] This feature could be one main difference between proteins and organic polymers, which might enable the interaction between protein and PVDF membrane surface. Hetrogenous (i.e. asymmetric) charge distribution of proteins plays a significant role on the orientation of the protein molecule as it is interacting with the membrane surface.[10,39,41] When a protein is forced to be close proximity to the membrane surface by convective flow, the soft biomolecule changes its orientation to maximize the short-range attraction with the membrane surface (PVDF) while minimizing the long-range repulsion.[39] Jachimska et al. [39] demonstrated that BSA

biomolecules mediated the attachment of fluorescent latex particles to mica, while all components possessed a negative charge. In another example, Silva et al. [41] demonstrated that the positively charged BSA adsorbed onto polycation-treated surface. The resulting protein layer on the membrane surface from this first interaction minimized virus particle interaction with the membrane surface. In addition, the interacted proteins with the virus surface could provide a steric hindrance, similar to fibre or spikes, preventing virus-virus and virus-membrane interactions.[11] One interesting study was reported by Mesthrige et al. [10] that demonstrated that BSA biomolecules disaggregated Tobacco Mosaic Virus by interacting with the virus surface via hydrophobic patches while both TMV and BSA were negatively charged.

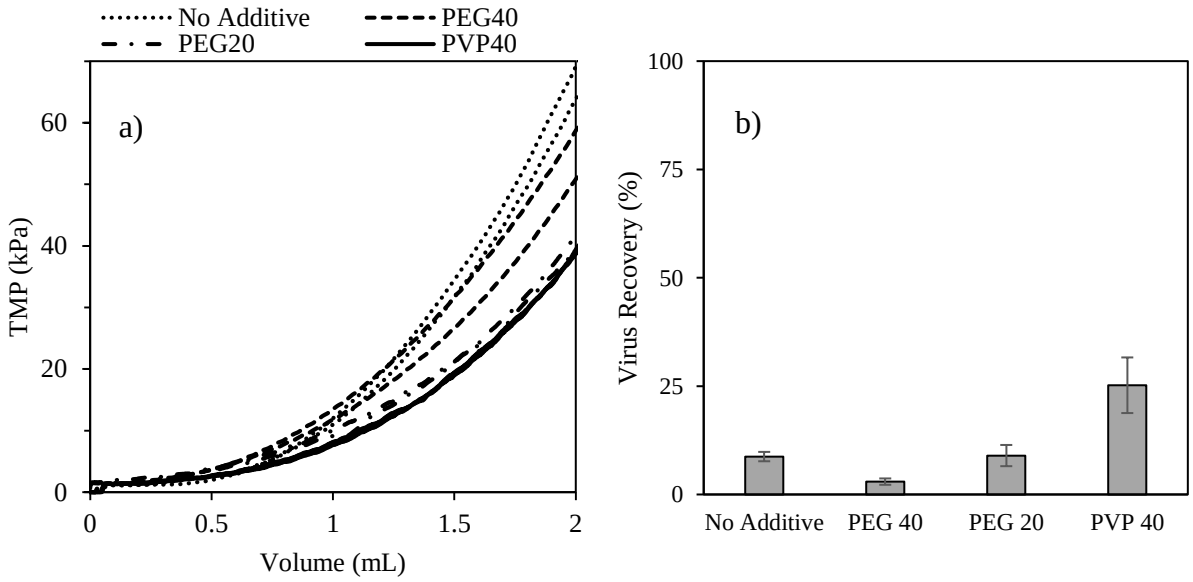

Fig. 5.5 Comparison of filter performance through sterile filtration of the virus solution without and with polymer additives at concentration of 1.25%w/v. TMP profiles with PEG20, PEG40, and PVP40 are shown in panel a. Virus recovery results are shown in panel c. Initial virus infectivity of the control virus run was (2.6±0.2)×109 $ID_{50}.mL^{-1}$. The collected filtrates (S1-S4) of each run pooled and later examined for the virus infectivity.

To find out more about additives interactions with virus and membrane surfaces, hydrodynamic size of additives and concentration of the virus particles with additives were examined. The hydrodynamic size of additives in the formulation buffer was shown in Table 5.2. The results are in good agreement with literature.[30,42,43] As shown, even though the polymers have molecular weights smaller than BSA, they have a larger hydrodynamic radius size. Interestingly, the additives with smaller hydrodynamic size, BSA and α-LA, resulted in higher virus recoveries and lower TMP profiles with no titer drop upon addition of additive to the virus solution. Similarly, a study by Armstrong et al.[30] on aggregation of Red Blood Cells (RBCs) demonstrated that additives with hydrodynamic radius less than 4 nm inhibit RBCs aggregation while additives with hydrodynamic radius higher than 4 nm induced RBCs aggregation.[30]

Table 5.2 Hydrodynamic radius of studied additives in the formulation buffer

Additive	**Hydrodynamic Radius (nm)**
BSA	3.82±0.04
α-LA	1.94±0.03
PEG20	4.16±0.33
PEG40	5.35±0.48
PVP40	5.18±0.18

The concentration of the virus solution after addition of the additives were investigated by using the qViroX instrument and TRPS technique. The control virus solution (0.5 mL of the formulation buffer added to 2.5 mL of virus solution) had $(8.7\pm2.0)\times10^{9}$ virus particle (VP) per mL. The number of the virus particles in the virus

solution after addition of proteins, BSA and α-LA, were $(1.1\pm0.9)\times10^{10}$ VP.mL^{-1} and $(1.1\pm0.2)\times10^{10}$ VP.mL^{-1}, respectively. In addition, protein additives didn't change the initial infectious virus titer. However, addition of the polymer to the virus solution demonstrated adverse effects on the virus titer. The observed decrease in the virus infectivity after addition of polymers may be due to a) virus particles were aggregated and consequently precipitated after addition of polymers; b) polymers interacting with the virus particle surface resulted in lower infection efficiency in the cells. The results from particle concertation analysis revealed that the number of the particles in the solution after addition of PEG20 and PEG40 were low compared to the concentration of the control virus solution. Addition of PEG40 to the virus solution caused the lowest virus particle concentration, $(3.3\pm2.0)\times10^{9}$ VP per mL. It could be concluded that PEG20 and PEG40 caused virus particles to aggregate and consequently precipitate during the preparation of the virus solution with these additives. Interestingly, the number of the virus particles in the virus solution after addition of PVP40 was $(8.4\pm1.0)\times10^{9}$ VP.mL^{-1}, similar to the virus particle number in the control virus solution. On the other hand, PVP40 addition caused about 50% drop in the virus titer, $(1.2\pm0.5)\times10^{9}$ ID_{50}.mL^{-1}. This result suggested that the interaction of PVP40 with the virus envelop decreased infection efficiency of the virus particles. One possible explanation is that the negatively charged PVP40 interacted with the positively charged P2-like peptide from the glycoprotein spikes on the virus envelop, which is responsible for triggering the virus fusion into host cell,[44] shielded the peptide, and consequently lower the virus infection efficiency.

5.4.3. Coated Membrane Surface

Another strategy to minimize interactions between virus particle and membrane surface is modification of the membrane surface. A test was designed to check on the role of BSA during filtration either combined with virus particles as an additive, or as an agent to coat the membrane surface. As a negative control, the virus sample was filtered on its own without the presence of additives through native (i.e. uncoated) membrane. The results are shown in Fig. 5.6. When the virus solution was filtered through the coated membrane with 5% BSA, the TMP profile decreased by about 48% compared to the TMP of the virus alone sample, highlighting the effects of surface modification by BSA (Fig. 5.6a). However, addition of 5% BSA to the virus solution prior to filtration resulted in an even lower TMP profile (~ 28%). As shown in Fig. 5.6b, the pattern of the virus recovery as a function of the collected filtrates were varied for different cases. The virus recovery for the virus control run (i.e. virus alone) and virus with BSA additive displayed a parabolic pattern with one maximum and decreasing in the later samples. The S1, the first collected filtrate (500 µl), always demonstrated the lowest virus recovery, most possibly because of the fact that the membrane was pre-wetted, Thus, that sample would definitely be diluted with the hold-up liquid in the membrane holder. Another interesting point is that the control virus run displayed the highest virus titer in the third sample (S3), while the virus run with BSA additive had the highest titer in the second sample (S2). The latter result simply demonstrated how interaction between virus particles and membrane reduces the virus transmission through the membrane. Thus, in the absence of additives, the virus particles that pass through the membrane first were presumably coating the membrane, allowing the

remainder the virus particles in solution easier transmission through the membrane. In a study by Kong et al.,[45] it was shown that repetitive filtration of DNA through PVDF membrane increased the DNA transmission. According to our result, one possible explanation could be that DNA was covering the membrane surface in the previous passes, and consequently lowering the interction of DNA with membrane surface and increasing its transmission. Using the BSA coating method, the virus titer in the samples after S1 had similar range with no statistically significant differences, in contrast to the control virus run as well as BSA added virus solution.

Initial virus stock from Batch B had 232±29 $\mu g.mL^{-1}$ of total protein. During the virus control run, about 60% of the total protein were lost, either because of interactions with the membrane, non-specific deposition, and/or entrapment. During the control virus run on the coated membrane, a high amount of the protein was in the collected filtrate due to washing off the coated proteins by the virus solution. The S1 had the highest protein amount (100%) while decreasing in later ones, 66% (S2), 14% (S3), and 9% (S4). The S4 still had about 700 $\mu g.mL^{-1}$ of the total protein. Nevertheless, as shown in Fig. 5.6b, there wasn't any significant change in the virus titer as comparing S2, S3, and S4.

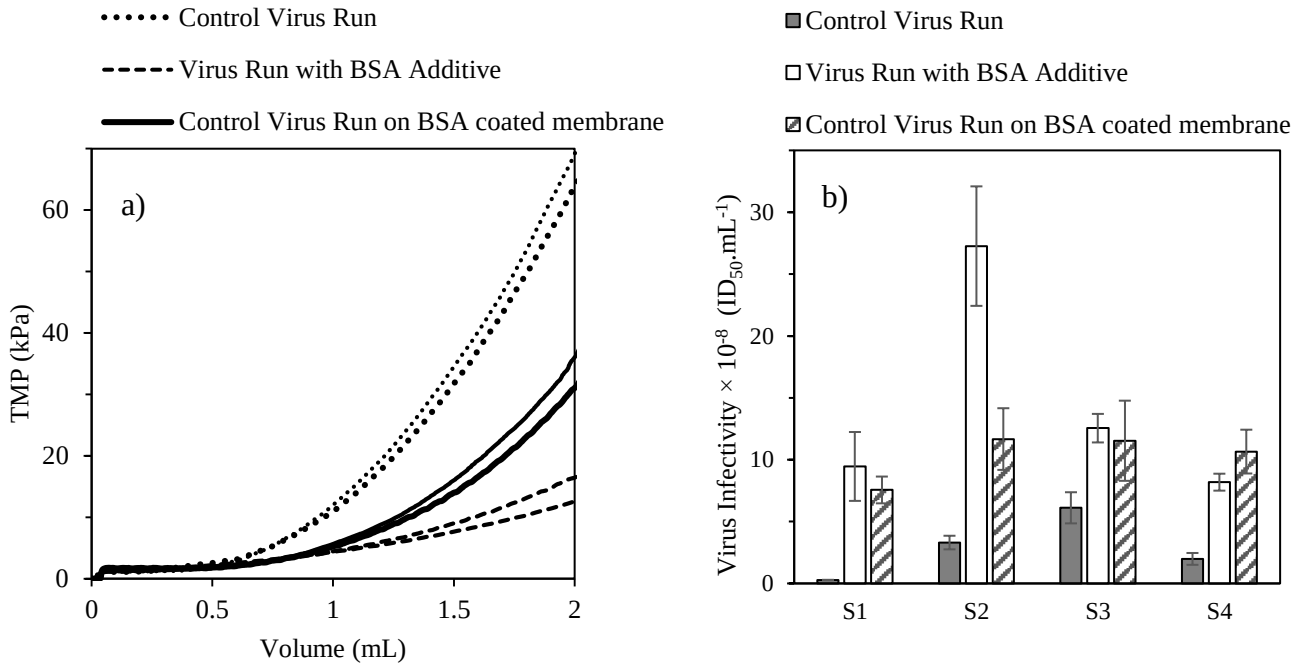

Fig. 5.6 A comparison of the a) filtration performance and b) virus infectivity of the collected filtered samples (S1, S2, S3, and S4) for the control virus run (i.e. virus alone), the virus run with BSA additive (5.00%), and the control virus run on BSA coated membrane. Initial virus infectivity was $(2.6\pm0.2)\times10^{9}$ $ID_{50}.mL^{-1}$.

After filtration, all the membranes were collected and SEM images of the membranes were taken (Fig. 5.7 a-d, top panel). The observed membrane surface fouling was the highest in the control virus run followed by the virus run with BSA additive, and the least surface fouling was in the control virus run on the coated membrane. The SEM images revealed that coating the membrane by BSA reduced deposition of the particles on the membrane surface. The SEM images were further analyzed by Image J software (National Institutes of Health, http://rsb.info.nih.gov/ij). The membrane images processed using this software are shown in Fig. 5.7 e-h bottom panel, wherein available pores (i.e. non-covered pores) were colored red. The percentage of the available area was calculated based on the area of the non-covered pores over the total area of the taken image. At least four different SEM images were taken from different parts of one membrane, analyzed by the software and averaged results were reported. The percentage of the available areas were 25%±2%, 2%±1%, 8%±2%, and 12%±3% for the membranes after 5% BSA run (i.e. only BSA in the virus-free formulation buffer), the control virus run, the virus run with 5% BSA additive, and the control virus run on BSA coated membrane. Based on SEM images, one might conclude that surface fouling was predominant in case of the control virus run (i.e. virus alone) and the virus run with BSA additive (Fig. 5.7 b/f and c/g) in contrast to the coated membrane by BSA (Fig. 5.7 d/h). However, TMP profile of the control virus run on the pre-blocked membrane was higher relative to BSA added virus solution, suggesting that the fouling might occur mainly inside the pores (Fig. 5.6a and Fig. 5.7 d/g). The latter hypothesis of internal pore blocking, couldn't be checked by means of SEM. This behavior could be explained by considering that coating of the membrane was applied by just running BSA solution through the membrane (5%w/v for 3 mL); hence, the surface of the membrane, which was mainly exposed to the flow, might be covered with BSA much better than pore walls. Brink et al. [46] also observed that coating surface of microfilters (polypropylene

and polysulfone) by β-lactoglobulin, methylcellulose, and polyvinyl methyl ether didn't prevent internal pore blockage during microfiltration of protein solutions; the coating was achieved by passive adsorption, by immersing membrane in the protein solution prior to microfiltration. The authors had a similar explanation of the limited access of additives into inside pores to cover the pore walls due to diffusion limitations.[46]

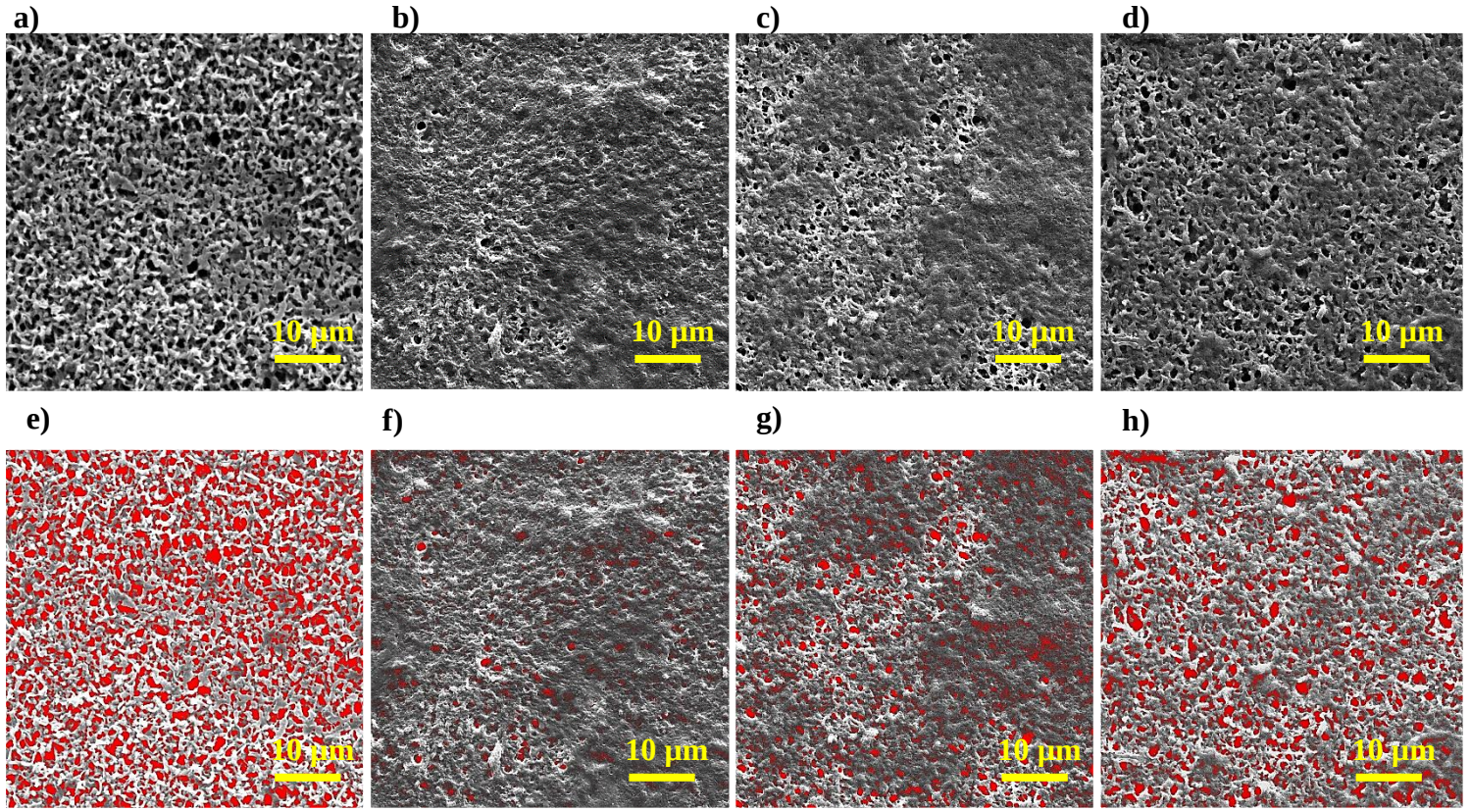

Fig. 5.7. Scanning electron micrographs (×4000 magnification) of the membrane after sterile filtration runs (a-d); analyzed SEM images using Image J software; pores were highlighted with a red color (e-h); a/e) BSA run (i.e. BSA coated membrane), b/f) control virus run (no additive), c/g) virus run with BSA additive (5%), d/h) control virus run on BSA coated membrane

5.4.4. TMP Versus Virus Recovery

To better analyze the data, we calculated the ratio of TMP $_{Additive}$/TMP $_{Control}$ (Fig. 5.S2). The resulting graph revealed a relatively stable ratio in the rapid fouling phase, where more than 1 mL was filtered, and the ratio was reached to plateau. The average of this ratio for each point at the plateau phase (> 1 mL) was used to compare TMP profiles and effect of additives on fouling rate. In this chapter, the averaged result was denoted as "plateau TMP $_{Additive}$/TMP $_{Control}$" for an easier reference. This ratio was plotted against the virus recovery and shown in Fig. 5.8. As expected, there is a correlation between performance of the membrane and the virus recovery. Lower ratios resulted in higher virus recoveries.

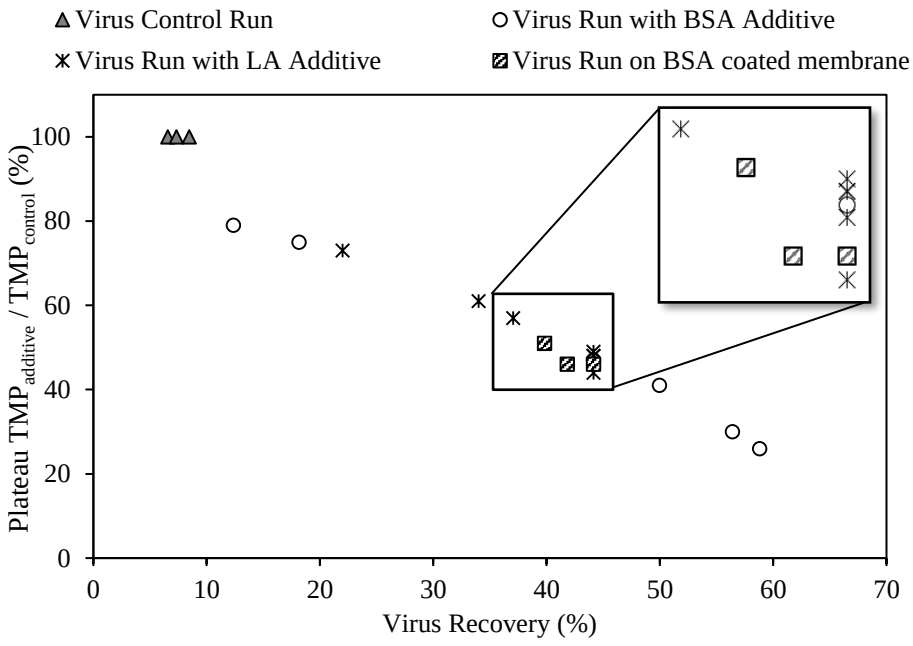

Fig. 5.8. Percentage of plateau $TMP_{additive}/TMP_{control}$ as a function of the virus recovery (%). Initial virus infectivity was $(2.6\pm0.2)\times10^{9}$ $ID_{50}.mL^{-1}$.

5.5. Conclusions

Our results in this chapter demonstrated that using protein additives and modifying membrane surface with proteins improved the virus transmission through the membrane. By comparing the results of different additives, we theorize that effects of proteins (i.e. BSA and α-LA) on the virus recovery and membrane performance was superior due to their intrinsic feature of being soft biomolecule. The availability of different patches on protein surface enabled the interactions with both the membrane and virus particle surface, and consequently improved virus transmission through membrane. Remarkably, coating membrane surface with BSA prior to virus run resulted in comparable virus recovery (~42%) to BSA added virus solution (~59%). It is common practice during virus filtration steps to wet the membrane with buffer to maximize recovery of the filtered virus solution, and ultimately total number of recovered virus particles. Our results show that using buffer alone is not sufficient, and that addition of protein additives or pre-blocking the membrane will ensure even higher virus recovery. In this paper, we tested the effects of BSA and different polymers as additives. However, the technology for the creation of permanently modified bio-based membranes is available [47] and the availability of such membranes can potentially improve virus recovery from the filtration step during virus manufacturing. Biomimetic surfaces could therefore be developed to modify surfaces of sterilizing filters intended for virus stream filtration and this will be our future work.

Moreover, the strong correlation between TMP profile readings with the initial virus concentration and the virus recovery emphasized that TMP profile could be a useful operational measurement, an indication of membrane performance and consequent

virus recovery. Therefore, defining a new index for virus microfiltration processes based on TMP profiles is suggested, similar to the idea of Silt Density Index and Modified Fouling Index Ultrafiltration for measuring fouling propensity of reverse osmosis feed water. In addition, results from this work could be easily and more accurately applied to microfiltration process optimization, leading to increased process yield, due to the analogies between the test setup and actual downstream processing unit operations.

5.6. Acknowledgments

Funding was provided by the 'Alliance for Biotherapeutics Manufacturing Innovation' project that was supported by the Ontario Research Fund – Research Excellence program (RE07-092). The authors thank Adam Smith, Joris van der Heijden, and John Bell from the Biotherapeutics Manufacturing Center at the Ottawa Hospital Research Institute for providing the virus sample and their insight into the work. From McMaster University, Karen Mossman for providing access to qViroX instrument, Susan Collins for training qViroX instrument, Marcia Reid (Electron Microscopy Facility) for her assistance with SEM apparatus, and Biointerfaces Institute for providing access to DLS and Vibro Viscometer instrument.

5.7. References

1. Ghosh, R. *Principles of bioseparations engineering*. (World Scientific Publishing company, 2006).
2. Ho, C.-C. & Zydney, A. L. Transmembrane pressure profiles during constant flux microfiltration of bovine serum albumin. *J. Memb. Sci.* **209,** 363–377 (2002).
3. Mulder, M. Polarisation phenomena and membrane fouling. in *Basic Principles of Membrane Technology* 416–464 (Springer, 1996).
4. Wickramasinghe, S. R., Kalbfuss, B., Zimmermann, A., Thom, V. & Reichl, U. Tangential flow microfiltration and ultrafiltration for human influenza A virus concentration and purification. *Biotechnol. Bioeng.* **92,** 199–208 (2005).
5. Mocé-Llivina, L., Jofre, J. & Muniesa, M. Comparison of polyvinylidene fluoride and polyether sulfone membranes in filtering viral suspensions. *J. Virol. Methods* **109,** 99–101 (2003).
6. Cliver, D. O. Factors in the membrane filtration of enteroviruses. *Appl. Microbiol.* **13,** 417–425 (1965).
7. Konz, J. O., Lee, A. L., Lewis, J. A. & Sagar, S. L. Development of a purification process for adenovirus: controlling virus aggregation to improve the clearance of host cell DNA. *Biotechnol Prog* **21,** 466–472 (2005).
8. Gesan-Guiziou, G., Wakeman, R. J. & Daufin, G. Stability of latex crossflow filtration: cake properties and critical conditions of deposition. *Chem. Eng. J.* **85,** 27–34 (2002).
9. Ghosh, R. & Cui, Z. F. Fractionation of BSA and lysozyme using ultrafiltration: effect of pH and membrane pretreatment. *J. Memb. Sci.* **139,** 17–28 (1998).
10. Wadu-Mesthrige, K., Pati, B., McClain, W. M. & Liu, G.-Y. Disaggregation of Tobacco Mosaic Virus by Bovine Serum Albumin. *Langmuir* **12,** 3511–3515 (1996).
11. Wong, K., Mukherjee, B., Kahler, A. M., Zepp, R. & Molina, M. Influence of inorganic ions on aggregation and adsorption behaviors of human adenovirus. *Environ. Sci. Technol.* **46,** 11145–11153 (2012).
12. Dika, C., Duval, J. F. L., Ly, H. M., Merlin, C. & Gantzer, C. Impact of internal RNA on aggregation and electrokinetics of viruses: a comparison between MS2 and corresponding VLPs. *Appl. Environ. Microbiol.* AEM-00407 (2011).
13. Langlet, J., Gaboriaud, F., Duval, J. F. L. & Gantzer, C. Aggregation and surface properties of F-specific RNA phages: Implication for membrane filtration processes. *Water Res.* **42,** 2769–2777 (2008).
14. Reichl, U. & Wolf, M. W. Downstream processing of cell culture-derived virus particles. *Expert Rev. Vaccines* **10,** 1451–1475 (2011).

15. Morenweiser, R. Downstream processing of viral vectors and vaccines. *Gene Ther.* **12,** S103 (2005).

16. Shi, H., Pasco, E. V & Tarabara, V. V. Membrane-based methods of virus concentration from water: a review of process parameters and their effects on virus recovery. *Environ. Sci. Water Res. Technol.* **3,** 778–792 (2017).

17. Shannon, M. A. *et al.* Science and technology for water purification in the coming decades. in *Nanoscience And Technology: A Collection of Reviews from Nature Journals* 337–346 (World Scientific, 2010).

18. Rana, D. & Matsuura, T. Surface Modifications for Antifouling Membranes. *Chem. Rev.* **110,** 2448–2471 (2010).

19. McDaniel, C. S. *et al.* Molecular Healing of Polymeric Materials, Coatings, Plastics, Elastomers, Composites, Laminates, Adhesives, and Sealants by Active Enzymes. U.S. Patent Application 12/696,651, filed August 19, 2010.

20. De Queiroz, A. A. A., Barrak, É. R., Gil, H. A. C. & Higa, O. Z. Surface studies of albumin immobilized onto PE and PVC films. *J. Biomater. Sci. Polym. Ed.* **8,** 667–681 (1997).

21. Dai, Z.-W., Nie, F.-Q. & Xu, Z.-K. Acrylonitrile-based copolymer membranes containing reactive groups: Fabrication dual-layer biomimetic membranes by the immobilization of biomacromolecules. *J. Memb. Sci.* **264,** 20–26 (2005).

22. Balakrishnan, B., Kumar, D. S., Yoshida, Y. & Jayakrishnan, A. Chemical modification of poly (vinyl chloride) resin using poly (ethylene glycol) to improve blood compatibility. *Biomaterials* **26,** 3495–3502 (2005).

23. Winona, L. J., Ommani, A. W., Olszewski, J., Nuzzo, J. B. & Oshima, K. H. Efficient and predictable recovery of viruses from water by small scale ultrafiltration systems. *Can. J. Microbiol.* **47,** 1033–1041 (2001).

24. Tartera, C., Araujo, R., Michel, T. & Jofre, J. Culture and decontamination methods affecting enumeration of phages infecting Bacteroides fragilis in sewage. *Appl. Environ. Microbiol.* **58,** 2670–2673 (1992).

25. Braun, A., Kwee, L., Labow, M. A. & Alsenz, J. Protein aggregates seem to play a key role among the parameters influencing the antigenicity of interferon alpha (IFN-α) in normal and transgenic mice. *Pharm. Res.* **14,** 1472–1478 (1997).

26. Wang, P. *et al.* Glycerol facilitates the disaggregation of recombinant adeno-associated virus serotype 2 on mica surface. *Colloids Surfaces B Biointerfaces* **60,** 264–267 (2007).

27. Xie, Q., Hare, J., Turnigan, J. & Chapman, M. S. Large-scale production, purification and crystallization of wild-type adeno-associated virus-2. *J. Virol. Methods* **122,** 17–27 (2004).

28. Kissmann, J. *et al.* Physical stabilization of norwalk virus-like particles. *J.*

Pharm. Sci. **97,** 4208–4218 (2008).

29. Wright, J. F. *et al.* Identification of factors that contribute to recombinant AAV2 particle aggregation and methods to prevent its occurrence during vector purification and formulation. *Mol. Ther.* **12,** 171–178 (2005).

30. Armstrong, J. K., Wenby, R. B., Meiselman, H. J. & Fisher, T. C. The hydrodynamic radii of macromolecules and their effect on red blood cell aggregation. *Biophys. J.* **87,** 4259–4270 (2004).

31. Ausar, S. F., Foubert, T. R., Hudson, M. H., Vedvick, T. S. & Middaugh, C. R. Conformational stability and disassembly of Norwalk virus-like particles effect of pH and temperature. *J. Biol. Chem.* **281,** 19478–19488 (2006).

32. Floyd, R. & Sharp, D. G. Viral aggregation: effects of salts on the aggregation of poliovirus and reovirus at low pH. *Appl Env. Microbiol* **35,** 1084–1094 (1978).

33. Vajda, J., Weber, D., Brekel, D., Hundt, B. & Müller, E. Size distribution analysis of influenza virus particles using size exclusion chromatography. *J. Chromatogr. A* **1465,** 117–125 (2016).

34. Shoaebargh, S. *et al.* Sterile filtration of oncolytic viruses: An analysis of effects of membrane morphology on fouling and product recovery. *J. Memb. Sci.* **548,** 239–246 (2018).

35. Hirasaki, T., Yokogi, M., Kono, A., Yamamoto, N. & Manabe, S. Removal and determination of dispersion state of bacteriophage φX174 in aqueous solution by cuprammonium regenerated cellulose microporous hollow fiber membrane (BMM®). *J. Memb. Sci.* **201,** 95–102 (2002).

36. Momtaz, M., Dewez, J.-L. & Marchand-Brynaert, J. Chemical reactivity assay and surface characterization of a poly(vinylidene fluoride) microfiltration membrane ("Durapore DVPP"). *J. Memb. Sci.* **250,** 29–37 (2005).

37. Bowen, W. R. & Gan, Q. Properties of microfiltration membranes: Adsorption of bovine serum albumin at polyvinylidene fluoride membranes. *J. Colloid Interface Sci.* **144,** 254–262 (1991).

38. Kelly, S. T. & Zydney, A. L. Protein fouling during microfiltration: Comparative behavior of different model proteins. *Biotechnol. Bioeng.* **55,** 91–100 (2000).

39. Jachimska, B. & Pajor, A. Physico-chemical characterization of bovine serum albumin in solution and as deposited on surfaces. *Bioelectrochemistry* **87,** 138–146 (2012).

40. Badoga, S., Pattanayek, S. K., Kumar, A. & Pandey, L. M. Effect of polymer–surfactant structure on its solution viscosity. *Asia-Pacific J. Chem. Eng.* **6,** 78–84 (2011).

41. A Silva, R., Urzúa, M., F S Petri, D. & L Dubin, P. *Protein Adsorption onto Polyelectrolyte Layers: Effects of Protein Hydrophobicity and Charge*

Anisotropy. *Langmuir : the ACS journal of surfaces and colloids* **26,** (2010).

42. Li, Y., Yang, G. & Mei, Z. Spectroscopic and dynamic light scattering studies of the interaction between pterodontic acid and bovine serum albumin. *Acta Pharm. Sin. B* **2,** 53–59 (2012).
43. Gokarn, Y. R., McLean, M. & Laue, T. M. Effect of PEGylation on Protein Hydrodynamics. *Mol. Pharm.* **9,** 762–773 (2012).
44. Da Poian, A. T., Carneiro, F. A., & Stauffer, F. Viral membrane fusion: is glycoprotein G of rhabdoviruses a representative of a new class of viral fusion proteins? *Brazilian J. Med. Biol. Res.* **38,** 813–823 (2005).
45. Kong, S., Titchener-Hooker, N. & Levy, M. S. Plasmid DNA processing for gene therapy and vaccination: Studies on the membrane sterilisation filtration step. *J. Memb. Sci.* **280,** 824–831 (2006).
46. Brink, L. E. S., Elbers, S. J. G., Robbertsen, T. & Both, P. The anti-fouling action of polymers preadsorbed on ultrafiltration and microfiltration membranes. *J. Memb. Sci.* **76,** 281–291 (1993).
47. Akashi, N. & Kuroda, S. Protein immobilization onto poly (vinylidene fluoride) microporous membranes activated by the atmospheric pressure low temperature plasma. *Polymer (Guildf).* **55,** 2780–2791 (2014).

5.8. Supplementary Material

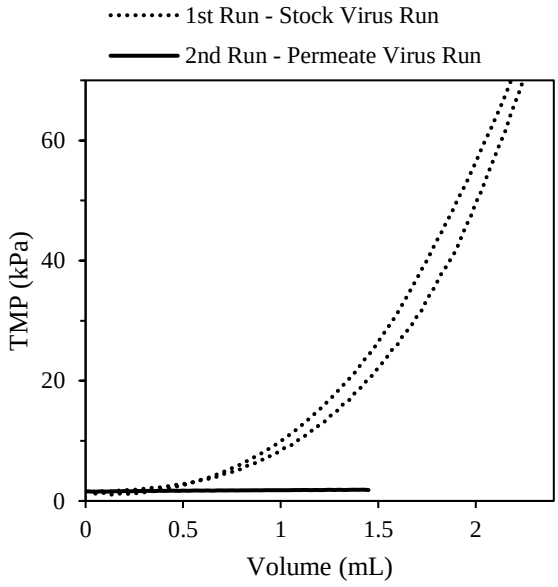

Fig. S5.1 TMP profile as a function of filtered Rhabdovirus solution (Batch A) with the titer of $(2.5\pm0.3)\times10^{9}$ $ID_{50}.mL^{-1}$ and the permeated virus solution (i.e. filtrate from the stock virus run) with titer of $(2.0\pm0.5)\times10^{8}$ $ID_{50}.mL^{-1}$

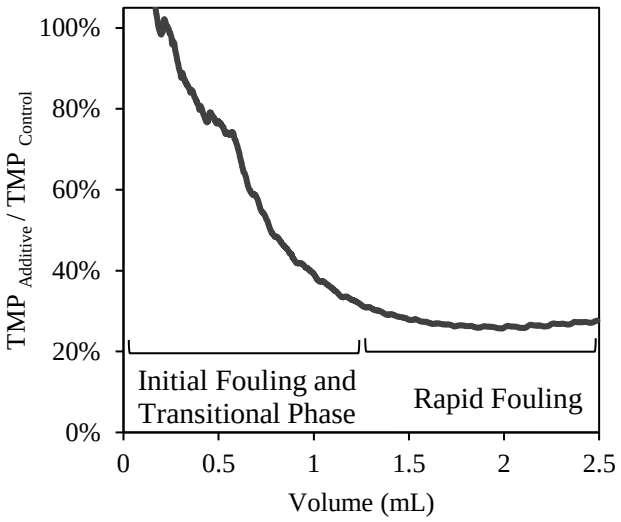

Fig. S 5.2 Ratio of TMP $_{Additive}$ (TMP readings of the virus solution with additive) over TMP $_{Control}$ (TMP readings of the control virus solution run) as a function of filtered volume.

Chapter VI – Conclusions and Recommendations for Future Work

6.1. Conclusions

The experimental results in Chapter III provide the first data in support of the viability of using a monolithic chromatography process to purify oncolytic Rhabdovirus. An extensive amount of work was done to produce Rhabdoviral vectors, establish assays and detectable limits (e.g. infectivity assay, total protein, and DNA assays), characterize the virus feed (e.g. size distribution, contaminant levels, virus titer), and to study long-term virus stability at different storage conditions and short-term virus stability at different buffer conditions. Furthermore, the influence of column pore size on the monolithic anion-exchange column's performance for QA functional groups was also investigated.

When a pore size of 2 or 6 µm was used in conjunction with both stepwise and linear-gradient elution, the monolithic anion-exchange column produced low Rhabdoviral vector recovery. It was concluded that this behavior was largely attributable to the irreversible interaction between the negatively charged Rhabdovirus envelope and the positively charged QA functional groups in the column. Interestingly, the monolithic column with a 6 µm pore size enabled noticeable host cell protein removal during the flow-through (>60%). Next, monolithic hydrophobic interaction chromatography with OH functional groups (CIM OH) and a 6 µm pore size was evaluated for a range of different experimental conditions, including AS salt concentration (1.5-2.0 M), pH

level (7.4 and 8.0), and additive (glycerol). It was found that increasing the concentration of AS (from 1.5 M to 2.0 M) as well as increasing the working pH (from 7.4 to 8.0) improved the virus recovery from the column – in average the virus recovery was more than 60% of the infectious particles. Moreover, remarkable removal of host cell protein (>70%) and DNA (>80%) was observed in the flow-through using monolithic hydrophobic interaction column (6 µm). It should be noted that this significant amount of DNA removal was achieved without having nuclease digestion step. For the first time, it was shown that glycerol mediates the elution of the virus from the hydrophobic column while also stabilizing the virus particles. Significantly, this interaction enabled high infectious-virus recovery from the monolithic hydrophobic interaction column. In the presence of glycerol, the virus recovery from monolithic hydrophobic interaction column (CIM OH) increased from 67±19% to 77±17% at pH 7.4 and from 84±11 % to 97±20% at pH 8.0.

The experimental work in Chapters IV and V focused on the sterile filtration of oncolytic Rhabdovirus. In Chapter IV, a custom-built sterile filtration setup was used to evaluate the performance of four commercial sterile filters: Durapore (EMD Millipore), Fluorodyne EX EDF (Pall Corporation), MiniSart NML (Sartorius), and MiniSart Plus (Sartorius). In addition, SEM was used to study the structure and morphology of each filter. The primary criterion for selecting these four filters was their availability for use in both a small, “lab-scale” format (i.e. a syringe filter with a membrane area of approximately 3 cm^2) as well as a large, “process-scale” format of approximately 5,000 cm^2. Constant flux filtration tests were conducted using a

peristaltic pump, with membrane fouling being determined via continuous measurement of the TMP.

The results from chapter IV demonstrated that membrane morphology influences fouling behavior and virus recovery during filtration. An analysis of the virus-titer levels in the filtrates from the different membranes revealed that the two-layer membranes (Fluorodyne EX EDF and MiniSart Plus) produced a higher amount of virus in the filtrate stream. For example, the MiniSart Plus, with GF as a prefilter (1.2 µm) and SFCA as the main sterile filter (0.2 µm), had the highest infectious-virus recovery rate at 4.5×10^{10} PFU, or about 21% of the initial feed. However, this difference was mostly due to the two-layered filters' ability to filter higher volumes of virus solution. Similarly, the tested commercial filters were able to produce filtrates with similar virus concentrations (~1×10^{9} PFU per mL), but they showed a distinctive tendency towards membrane fouling. For example, the TMP readings when using Durapore membrane were increased dramatically and hit the defined maximum TMP (103 kPa) after filtering less than 10 mL of the Rhabdovirus solution; in contrast, the MiniSart Plus was able to filter more than 45 mL of the virus solution without a significant change in TMP readings.

To evaluate the severity of the membrane fouling, hydraulic-permeability measurements were performed in the "normal orientation" (i.e. front-to-back) after a wash in the "reversed orientation" (i.e. back-to-front). The obtained measurements showed no statistical change in hydraulic permeability for the Fluorodyne EX EDF while a 30% increase in hydraulic permeability for the MiniSart Plus. Furthermore, blocking models were used to analyze the TMP profiles, with the results indicating that

fouling mainly adhered to the standard and/or intermediate blocking models. This result indicates that fouling mainly occurs due to pore blockage and/or pore restriction. Overall, these results provide insights into the development of effective sterile filtration membranes that are critical for large-scale OV production.

The primary challenge of the work in Chapter IV was the need for large volumes of the virus solution for each test (15-45 mL depending on the tested filter type); as such, virus-solution availability was one of this work's limitations. In order to obviate this limitation, a custom-built small-scale microfiltration setup was developed in Chapter V. The main advantage of this setup was that it only required a few milliliters of virus sample for each filtration test, and it was used to evaluate two methods for improving sterile filtration: inhibiting/controlling virus aggregation by adding stabilizers, and membrane surface modification. The microfiltration membrane used in these tests was selected based on the results from Chapter IV, which indicated that the Durapore PVDF membrane was most prone to fouling. Thus, this membrane was ideal for screening the effects of different additives on virus-particle stabilization during filtration.

Various additives were selected from biomolecules and polymers at different molecular size ranges, namely BSA (66.5 kDa), α-LA (14.5 kDa), PEG (20 and 40 kDa), and PVP (40 kDa). The goal of the tests in Chapter V was to increase the transmission of virus particles through the membrane (i.e. virus recovery) while also reducing membrane fouling. The latter can be monitored by tracking TMP readings through the microfiltration run, with lower TMP readings indicating a lower membrane fouling rate. The results demonstrated that proteins performed best for this purpose. For example, the addition of BSA to the Rhabdoviral solution decreased the TMP reading about 4-

times and increased virus recovery about 6-times compared to microfiltration tests with no additive. Next, organic polymers were tested. The results revealed that adding polymers to the virus solution produced an initial drop in titer, which was a phenomenon that was not observed when protein was added.

Later, the Durapore membrane surface was coated by passing the BSA solution. To compare the effectiveness of BSA, a control virus solution was filtered through the coated membrane, which produced a comparable virus recovery (~42%) to the virus solution containing BSA (~59%), thus demonstrating the potential of bio-based membrane-surface modifications for virus-filtration applications. Interestingly, SEM images revealed that the surface-modified membrane (with BSA) exhibited lower fouling compared to the runs with the control virus and the virus with the BSA additive.

Moreover, a strong correlation between virus recovery and the TMP profile reading was observed, which indicated that the TMP profile can be a useful operational measurement. Therefore, the defining of a new index based on the TMP profiles for virus-oriented microfiltration processes is recommended. This index is envisioned as being similar to the Silt Density Index[1] and the Modified Fouling Index Ultrafiltration,[2] which are both used for measuring the fouling propensity of reverse-osmosis feed water.

6.2. Future Works and Recommendations

Future studies should be designed to obtain additional insights into both the fundamental phenomena controlling virus aggregation and the effective applications of DSP technologies for virus purification. A brief summary of some suggested directions for future investigations is provided below.

- High salt concentration can induce virus-particle aggregation, which in turn can affect the column's performance and efficiency. As described by Gagnon et al.,[3] this phenomenon produces significant variations in preparative-scale and large-scale HIC. One technique is called "Continuous Online Dilution,"[3] which entails gradually mixing the sample solution and stock salt solution online while being applied to the column. This method reduces the target particles' residence time in the high-salt binding condition to the lowest possible degree, thus reducing the chance of aggregation formation, and consequently improving the column's performance and yield. Moreover, this method also allows the user to control the amount of time the target particles as exposed to the salt solution, which is hard to do when dealing with off-line sample preparation for HIC.[3]

- In addition, it is recommended that the required salt concentration in the binding condition be lowered, specifically when attempting to scale-up the purification method with a hydrophobic interaction column. To this end, it may be fruitful to examine other available hydrophobic interaction columns with stronger ligands, such as phenyl, to decrease the salt concentration required for binding. One

commercially available option is the Monolithic CIM C4 with a low density of butyl functional groups. It is worth noting that, if the hydrophobic interaction between the target virus and the column matrix becomes too strong, recovery will be low due to conformational changes. Therefore, effect of the functional group's chemistry and salt concentration, as well as salt type, should be optimized with regards to the target virus.

- As discussed in Section 2.1.2, membrane adsorbers have similar advantages as monolithic columns, such as convective mass transfer, high flow rates, and short processing time. Therefore, another suggestion would be examining hydrophobic interaction membrane adsorber such as Sartobind® Phenyl (a strong HIC column) to compare with the performance of monolithic hydrophobic interaction column. Important factors to compare would be the binding condition (mainly required salt concentration), the virus recovery, and contaminants removal (e.g. host cell proteins and nucleic acids).

- In Chapter V, the effects of adding different amounts of proteins (BSA and α-LA) and polymers (PVP40, PEG20, and PEG40) to the Rhabdovirus solution were examined, with the results revealing a strong correlation between virus recovery and increased TMP. The small-scale setup could be a useful alternative method for studying how additives affect virus recovery and membrane fouling, as the results will directly reflect the membrane's performance during downstream processing. Therefore, a wide range of additives, such as the ones examined by Kissmann et al.[4] and Armstrong et al.[5] (Table 2.8), and other potent biomolecules could be tested

using this setup. In addition, the effects of various salt concentrations, pH values, and experimental conditions, such as different membrane materials, could also be tested. One potentially interesting starting point would be to investigate lysozyme (14.4 kDa). Since lysozyme is a protein with a high IEP (10.5-11[6]), its inclusion would cause all the proteins in the working solution to be positively charged. Moreover, given the drop in the virus titer that was observed upon the addition of polymers, it is strongly suggested that polymers with smaller molecular weights be examined, as these molecules will also have a smaller hydrodynamic size.

- The other method that was proposed for achieving higher virus recovery was surface modification (Chapter V). One method of increasing the feasibility of using coated membranes in virus applications is to incorporate permanent bio-based surface modifications, which can be implemented by attaching proteins or peptides to the membrane surface via chemical bonding. In Chapter V, it was also shown that pore blockage, and not surface fouling, was the reason why the TMP was higher when the virus was run through the coated membrane than it was for the runs with the virus with BSA additive (Fig. 5.6a and Fig. 5.7). Thus, the use of proteins to modify membrane surface is a promising alternative, however, an optimized method of surface modification should be developed to achieve proper surface coverage.

- It is recommended to measure the zeta potential of Rhabdovirus particles. Zeta potential measurement of viruses such as human Ad 40,[7] and MS2, GA, Qb and SP phages [8] was previously reported. Generally, zeta-potential measurement is

combined with size distribution analysis to study particle aggregation/disaggregation. Zeta-potential data allows the behavior of virus particles to be studied using DLVO theory, which accounts for attractive and repulsive energies, such as electrostatic and hindrance repulsion, and van der Waals attraction.[7] Following the introduction of additives, the zeta potential of the virus particles can be measured, and DLVO theory and energy diagrams can be used to explain their behavior in terms of aggregation/disaggregation or increased/decreased transmission through the membrane (mentioned in Chapter V). It is worth noting that electrolyte concentration should be as low as possible while measuring zeta potential of biologics since interaction and deposition of biologics on electrodes could cause over-heating in the cell. Measuring zeta potential of the virus particle was one of this thesis' main goals; unfortunately, there was a limited access to the required instruments, (Zetasizer, Malvern) due to dealing with BSL2 agent, and these experiments could not be completed.

6.3. References

1. ASTM Standard, Standard test method for silt density index (SDI) of water. *D19* **8,** 4107–4189 (2007).

2. Salinas-Rodriguez, S. G., Amy, G. L., Schippers, J. C. & Kennedy, M. D. The Modified Fouling Index Ultrafiltration constant flux for assessing particulate/colloidal fouling of RO systems. *Desalination* **365,** 79–91 (2015).

3. Gagnon, P., Eric, G. & Torgny, L. Large-Scale Process Development for Hydrophobic Interaction Chromatography, Part I--Gel Selection and Development of Binding Conditions. LC GC Magazine-Magazine of Separation Science-Liquid. in *Chromatography Gas Chromatography* **13,** 318–327 (LC-GC, 1995).

4. Kissmann, J. *et al.* Physical stabilization of norwalk virus-like particles. *J. Pharm. Sci.* **97,** 4208–4218 (2008).

5. Armstrong, J. K., Wenby, R. B., Meiselman, H. J. & Fisher, T. C. The hydrodynamic radii of macromolecules and their effect on red blood cell aggregation. *Biophys. J.* **87,** 4259–4270 (2004).

6. Forciniti, D., Hall, C. K. & Kula, M. R. Protein partitioning at the isoelectric point: influence of polymer molecular weight and concentration and protein size. *Biotechnol. Bioeng.* **38,** 986–994 (1991).

7. Shi, H., Xagoraraki, I., Parent, K. N., Bruening, M. L. & Tarabara, V. V. Elution Is a Critical Step for Recovering Human Adenovirus 40 from Tap Water and Surface Water by Cross-Flow Ultrafiltration. *Appl. Environ. Microbiol.* **82,** 4982 LP-4993 (2016).

8. Langlet, J., Gaboriaud, F., Duval, J. F. L. & Gantzer, C. Aggregation and surface properties of F-specific RNA phages: Implication for membrane filtration processes. *Water Res.* **42,** 2769–2777 (2008).